Seminario
Avances en Espectro-radiometría
Resúmenes ponencias

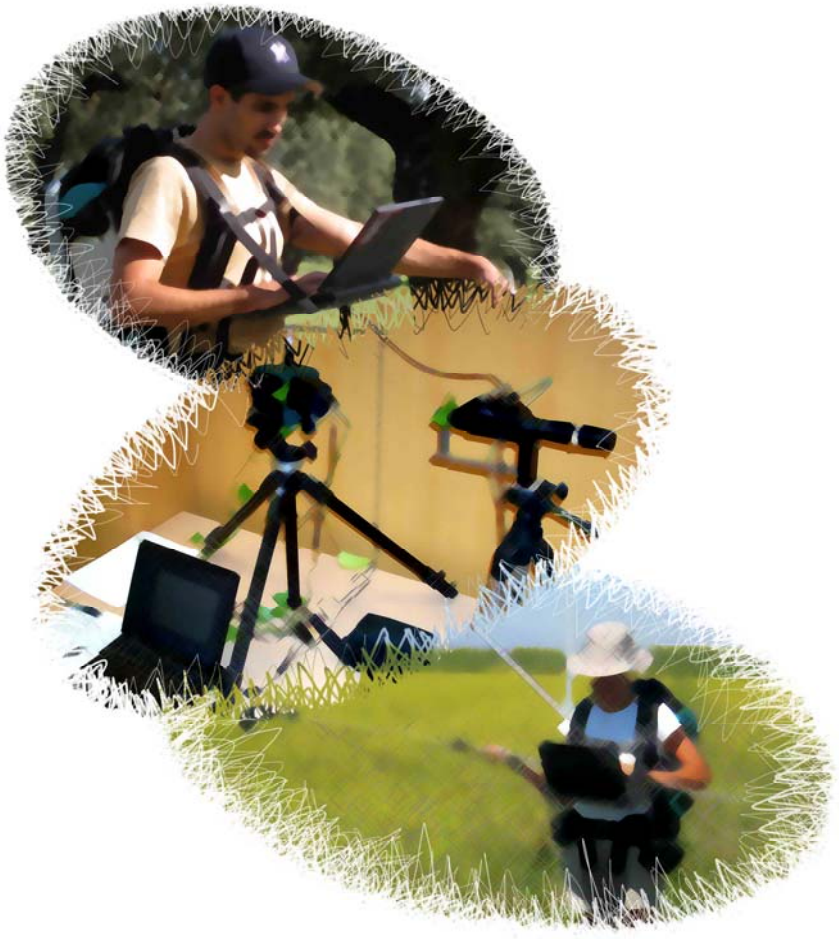

3-4 Diciembre 2009

Centro de Ciencias Humanas y Sociales (CCHS-CSIC)

CSIC
Consejo Superior de Investigaciones Científicas

SpecLab
Laboratorio de Espectro-radiometría y Teledetección Ambiental

CCHS

Programa del Seminario

Jueves. 3 de Diciembre

9:00-10:30 Inscripción participantes y entrega de documentación.

10:30-10:50 Café de bienvenida.

10:50-11:00 Acto de apertura y presentación del Seminario
Eduardo Manzano. Director del Centro de Ciencias Humanas y Sociales
F. Javier Martínez. Jefe del grupo de Investigación GITIG
M. Pilar Martín. Coordinadora del Comité organizador del Seminario

11:00-12:00 *Field Spectroscopy and its role in Earth Observation*
E. J. Milton (University of Southampton)

12:00-13:00 *Medidas de reflectividad y transmisividad (esferas de integración) y su aplicación en modelos de transferencia radiativa*
Pablo J. Zarco-Tejada (IAS-CSIC)

13:00-14:00 *Radiometría de Campo para calibración de Imágenes Aeroportadas*
Marcos Jiménez (INTA)

14:00-15:00 Comida (Restaurante del CCHS)

15:00-16:00 Sesión promocional empresas y visitas Laboratorio SpecLab

16:00-17:00 *Instrumentos disponibles en el mercado. Análisis comparativo*
Ángela De Santis (INSA)

17:00-17:30 Café

17:30-18:30 *Aspectos prácticos en la adquisición de datos de radiometría: aplicaciones terrestres y acuáticas*.
Angela De Santis (INSA) y José Antonio Domínguez (CEDEX)

18:30-19:30 Aplicaciones en España

- **18:30-18:40** Experiencias en Radiometría de Campo
  Magalí Odi Lara (IDR)
- **18:40-18:50** Actividades del Laboratorio de Espectro-radiometría y teledetección ambiental (SpecLab)
  M. Pilar Martín Isabel (CCHS-CSIC)
- **18:50-19:00** La geología espectral: ¿cómo puede ser automática?
  Asunción Riaza García (IGME)
- **19:00-19:10** Relaciones entre los productos de combustión y sus propiedades espectrales en matorrales quemados
  Raquel Montorio Llovería (Univ. Zaragoza)
- **19:10-19:20** Evaluación del contenido en ß-carotenos en la harina de cereales mediante técnicas de reflectancia espectral
  Luis F. García del Moral Garrido (Univ. Granada)
- **19:20-19:30** Caracterización espectral de coberturas de vegetación en Costa Rica: misiones aerotransportadas y radiometría de campo
  Javier Bonatti (CICANUM, Costa Rica)

Viernes. 4 Diciembre

9:00-10:00 *Measurement and analysis of bidirectional reflectance data*
Juha Suomalainen(Finish Geodetic Institute)

10:00-11:00 *Sensores Infrarrojos. Instrumentación, Protocolos de medidas y Aplicaciones*
Juan Carlos Jiménez (Universidad de Valencia)

11:00-11:30 Café

11:30-12:30 *Spectral Databases. Motivations, State of the Art, Visions*
Andreas Hueni (University of Zurich)

12:30-13:30 *Espectro-Radiometría y Teledetección Hiperespectral*
Antonio Plaza (Universidad de Extremadura)

ÍNDICE

Conferencias invitadas

Field Spectroscopy, and its role in Earth Observation
E. J. Milton.....1

Medidas de reflectividad y transmisividad (esferas de integración) y su aplicación en modelos de transferencia radiativa
Pablo J. Zarco-Tejada.....5

Radiometría de Campo para calibración de Imágenes Aeroportadas
Marcos Jiménez.....23

Instrumentos disponibles en el mercado. Análisis comparativo
Ángela De Santis.....27

Measurement and analysis of bidirectional reflectance data
Juha Suomalainen, Jouni Peltoniemi y Teemu Hakala.....31

Sensores Infrarrojos. Instrumentación, Protocolos de medidas y Aplicaciones
José A. Sobrino, Juan C. Jiménez, Guillem Sòria, Juan Cuenca,
Belén Franch, Victoria Hidalgo, Rosa Oltra, Yves Julien y Cristian Mattar.....35

Spectral Databases. Motivations, State of the Art, Visions
Andreas Hueni.....37

Espectro-Radiometría y Teledetección Hiperespectral
Antonio Plaza.....41

Trabajos presentados en la sesión de aplicaciones

Experiencias en Radiometría de Campo
Magalí Odi Lara.....45

Actividades del Laboratorio de Espectro-radiometría y teledetección ambiental (SpecLab)
M. Pilar Martín Isabel.....49

La geología espectral: ¿cómo puede ser automática?
Asunción Riaza García.....53

Relaciones entre los productos de combustión y sus propiedades espectrales en matorrales quemados
Raquel Montorio Llovería.....55

Evaluación del contenido en ß-carotenos en la harina de cereales mediante técnicas de reflectancia espectral
Luis F. García del Moral Garrido.....61

Caracterización espectral de coberturas de vegetación en Costa Rica: misiones aerotransportadas y radiometría de campo
Javier Bonatti.....63

Field Spectroscopy, and its role in Earth Observation

E.J. Milton
School of Geography
University of Southampton, UK

1. Making Sense of the Scene

The world around us comprises objects arranged in complex three-dimensional forms to create the 'scene' which is illuminated by a combination of direct light from the Sun and scattered light from the sky and the surroundings. Field spectroscopy provides us with the means to measure the interaction between electromagnetic radiation (EMR) and individual objects or the whole scene. In order to use field spectroscopy effectively it is first necessary to identify the 'scene model elements'. The first part of the talk will consider what we can learn from artistic representations of natural scenes. It will conclude by highlighting the interdependence of measurement and modelling in quantitative remote sensing.

2. Principles of Field Spectroscopy

There are several reasons why, despite many efforts to recreate the outdoor environment in the laboratory, we still need to make most of our measurements out-of-doors:

- The fragility of many natural surfaces, their complexity or their ephemeral nature;
- The character of solar illumination – its intensity, spectral distribution and angular distribution;
- The spatial non-homogeneity of lamp sources;
- Because that is what we measure with an aircraft or satellite sensor.

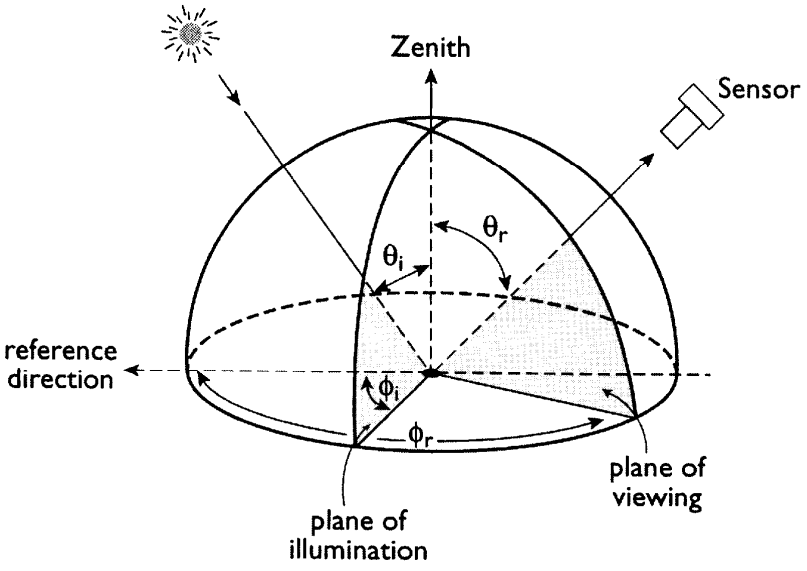

The *Bidirectional Reflectance Distribution Function (BRDF)* is an inherent property of the surface, but is is conceptual, not measureable. It is a mathematical function "relating the irradiance incident from one given direction to its contribution to the reflected radiance in another direction" (Nicodemus et al., 1977).

In the field we measure *Reflectance Factors (RF)*, which are the ratio between incoming irradiance integrated over a defined solid angle and the reflected radiance, also integrated over a defined solid angle. Schaepman-Strub et al. (2006) define several different RFs, the most important of which for our purposes is the *Hemispherical-Conical Reflectance Factor (HCRF)*.

By substituting RFs for the complete BRDF we sacrifice information on the angular distribution of irradiance, which can be important for some applications, for example the measurement of albedo ('black-sky albedo' *vs*. 'white-sky albedo'). For practical reasons, RFs are often measured using a reference panel to capture the irradiance over the sky hemisphere. In this case, the reflectance properties of the panel must be taken into account when calculating HCRF.

All physical measurements are affected by the conditions of measurement; of none is this more true than the measurement of RFs. Accurate, consistent and informative metadata are vital. Contemporary measurements of sky conditions should accompany all RFs and hand-held sunphotometers provide a simple and effective way to achieve this.

3. Methods of Field Spectroscopy

The earliest field spectroradiometers were modified laboratory instruments and were poorly suited to the field environment. Early satellite sensors had few spectral bands, so one response was the development of highly portable multiband radiometers, capable of acquiring data very rapidly. These were important in the development of remote sensing, especially in the 1980s and 1990s, and remain important in education and training.
True field spectroradiometers have evolved slowly over the past 30 years, and there is still some way to go before they are as user-friendly as other field instruments, for example hand-held GPS.

Methods may be classified according to whether the surface and the reference panel are measured sequentially with the same instrument (single-beam) or at the same time with two different instruments (dual-beam). They are also vary according to whether the surface is measured from a single direction or from multiple directions:

- Fixed geometry, single-beam
- Fixed geometry, dual-beam
- Variable geometry single/dual beam
- Proximate Field Spectroscopy

4. The role of Field Spectroscopy in Earth Observation

Field spectroscopy fulfils several roles in Earth Observation. First, it provides an effective means of teaching the physical principles of the subject, and in particular about the interactions between EMR and the environment.

Second, it provides the means to scale up from measurements of individual scene elements to pixel-sized areas. Those pixel-scale data can then be used to validate numerical models (e.g. BRDF models, scene models), to perform sensitivity analyses, to perform vicarious calibration and to correct for the effect of the atmosphere (Empirical Line Method). Spatial sampling theory (geostatistics) is key to scaling-up.

Third, field spectroscopy provides a method to study the *dynamics* of spectral reflectance; it enables us to measure the change in HCRF over time. In this respect, field spectroscopy and imaging spectrometry are complementary: imaging spectrometry provides the spatial context, but field spectroscopy provides the link with dynamic processes and change.

5. The NCAVEO Field Campaign

The talk concludes with a short slide show about a field campaign conducted in Hampshire, UK in June 2006. Field Spectroscopy was an integral part of this campaign, which was organised by the Network for Calibration and Validation in Earth Observation (NCAVEO).

Further reading

Reviews of the subject

Deering, D. W., 1989. Field measurements of bidirectional reflectance. *Theory and Applications of Optical Remote Sensing*. Asrar, G. New York, Wiley, 14-65.

Milton, E. J., 1987. Principles of field spectroscopy. *International Journal of Remote Sensing* 8, 1807-1827.

Milton, E. J., Schaepman, M., Anderson, K., Kneubühler, M. and Fox, N., 2009. Progress in Field Spectroscopy. *Remote Sensing of Environment* 113, S92-S109.

Silva, L. F., 1978. Radiation and Instrumentation in Remote Sensing. *Remote Sensing, The Quantitative Approach*. Swain, P. H. and Davis, S. M., McGraw-Hill, 21-135.

Slater, P. N., 1985. Radiometric considerations in Remote Sensing. *Proceedings of the IEEE* 73, 997-1011.

Terminology and Definitions

Nicodemus, F. F., Richmond, J. C., Hsia, J. J., Ginsberg, I. W. and Limperis, T. L., 1977. Geometrical considerations and nomenclature for reflectance, U.S. Govt. Printing Office, Washington D.C. 20402.

Schaepman-Strub, G., Schaepman, M., Painter, T. H., Dangel, S. and Martonchik, J. V., 2006. Reflectance quantities in optical remote sensing - definitions and case studies. *Remote Sensing of Environment* 103, 27-42.

Methods

Anderson, K., Milton, E. J. and Rollin, E. M., 2006. Calibration of dual-beam spectroradiometric data. *International Journal of Remote Sensing* 27, 975-986.

Anderson, K. and Milton, E. J., 2006. On the temporal stability of ground calibration targets: implications for the reproducibility of remote sensing methodologies. *International Journal of Remote Sensing* 27, 3365-3374.

Castro-Esau, K. L., Sánchez-Azofeifa, G. A. and Rivard, B., 2006. Comparison of spectral indices obtained using multiple spectroradiometers. *Remote Sensing of Environment* 103, 276-288.

Clark, R. N., Swayze, G. A., Livo, K. E., Kokaly, R. F., King, T. V. V., Dalton, J. B., Vance, J. S., Rockwell, B. W., Hoefen, T. and McDougal, R. R., 2002. Surface Reflectance Calibration of Terrestrial Imaging Spectroscopy Data: a Tutorial Using AVIRIS, U.S. Geological Survey Open-File Report, USGS Spectroscopy Lab, 41. [on-line at URL No. 3 below]

Doxaran, D., Cherukuru, N., Lavender, S. and Moore, G. F., 2004. Use of a Spectralon panel to measure the downwelling irradiance signal: case studies and recommendations. *Applied Optics* 42, 5981-5986.

Gamon, J. A., Rahman, A. F., Dungan, J. L., Schildhauer, M. and Huemmrich, K. F., 2006. Spectral Network (SpecNet) - What is it and why do we need it? *Remote Sensing of Environment* 103, 227-235.

Gu, X. F., Guyot, G. and Verbrugge, M., 1992. Evaluation of measurement errors in ground surface reflectance for satellite calibration. *International Journal of Remote Sensing* 13, 2531-2546.

Gu, X. F. and Guyot, G., 1993. Effect of diffuse irradiance on the reflectance factor of reference panels under field conditions. *Remote Sensing of Environment* 45, 249-260.

Hueni, A., Nieke, J., Schopfer, J., Kneubühler, M. and Itten, K., 2009. The spectral database SPECCHIO for improved long-term usability and data sharing. *Computers & Geosciences* 35, 557-565.

Kimes, D. S. and Kirchner, J. A., 1982. Irradiance measurement errors due to the assumption of a Lambertian reference panel. *Remote Sensing of Environment* 12, 141-149.

Kimes, D. S., Kirchner, J. A. and Newcomb, W. W., 1983. Spectral radiance errors in remote sensing ground studies due to nearby objects. *Applied Optics* 22, 8-10.

Lyapustin, A. and Privette, J., 1994. A new method of retrieving surface bidirectional reflectance from ground measurements. *Remote Sensing of Environment* 50, 303-316.

MacArthur, A., MacLellan, C. and Malthus, T. J., 2006. *What does a spectroradiometer see?* Proceedings of the Annual Conference of the Remote Sensing and Photogrammetry Society, Cambridge, UK, Remote Sensing and Photogrammetry Society,

Milton, E. J. and Rollin, E. M., 2006. Estimating the irradiance spectrum from measurements in a limited number of spectral bands. *Remote Sensing of Environment* 100, 348-355.

Peltoniemi, J. I., Kaasalainen, S., Naranen, J., Rautiainen, M., Stenberg, P., Smolander, H., Smolander, S. and Voipio, P., 2005. BRDF measurement of understorey vegetation in pine forests: dwarf shrubs, lichen and moss. *Remote Sensing of Environment* 94, 343-354.

Rundquist, D., Perk, R., Leavitt, B., Keydan, G. and Gitelson, A. A., 2004. Collecting spectral data over cropland vegetation using machine-positioning versus hand-positioning of the sensor. *Computers and Electronics in Agriculture* 43, 173-178.

Steven, M. D., 2004. Correcting the effects of field of view and varying illumination in spectral measurements of crops. *Precision Agriculture* 5, 55-72.

Thome, K. J., 2004. In-flight intersensor radiometric calibration using vicarious approaches. *Post-launch calibration of satellite sensors*. Morain, S. A. and Budge, A. M. London, Taylor and Francis, 95-102.

Websites (checked 26th November 2009)

1. http://www.fieldspectroscopy.com/
Discussion forum and resource base sponsored and moderated by ASD Inc.

2. http://www.ncaveo.ac.uk/special_topics/field_spectroscopy/
Introduction to Field Spectroscopy prepared in support of the Network for Calibration and Validation in Earth Observation.

3. http://speclab.cr.usgs.gov/PAPERS.calibration.tutorial/
USGS tutorial explaining how to use Field Spectroscopy to correct data from an imaging spectrometer (AVIRIS) for the effect of the atmosphere.

4. http://fsf.nerc.ac.uk/
Field Spectroscopy Facility – a shared pool of spectroradiometers and related instruments to support Field Spectroscopy. Funded by the UK Natural Environment Research Council.

5. http://www.techbriefs.com/component/content/article/2926
Details of NASA JPL automated ground facility for vicarious calibration of remote sensing systems.

6.http://www.geo.uzh.ch/en/units/rsl/research/spectroscopy-spectrolab/

University of Zurich, Remote Sensing Laboratories (RSL), Spectroscopy Lab.

7.http://www.optics.arizona.edu/rsg/

University of Arizona, Remote Sensing Group.

Medidas de reflectividad y transmisividad (esferas de integración) y su aplicación en modelos de transferencia radiativa

Pablo J. Zarco-Tejada
Instituto de Agricultura Sostenible (IAS)
Consejo Superior de Investigaciones Científicas (CSIC)
Alameda del Obispo, s/n
14004 - Córdoba
Tel: +(34) 957 499 280 ; +(34) 676 954 937
Fax: +(34) 957 499 252
e-mail: pzarco@ias.csic.es
http://quantalab.ias.csic.es

Resumen

Los métodos físicos de transferencia radiativa suplen las deficiencias de las relaciones estadísticas basadas simplemente en índices de vegetación, permitiendo la estimación de variables biofísicas cuantificando el efecto de la estructura de la cubierta y demás componentes como suelo o vegetación de fondo, características ópticas foliares, así como la geometría de visión en el momento de adquisición de la imagen. La teledetección hiperespectral permite la utilización de índices de vegetación de banda estrecha localizados en regiones espectrales donde dichos componentes bioquímicos se pueden estimar correctamente, como el contenido clorofílico en la región espectral de red edge (690-750 nm), contenido de agua en la región espectral de absorción del agua líquida (960 nm y 1150 nm), y el contenido de materia seca en la región entre 2000-2500 nm. El contenido clorofílico, además de la concentración de otros constituyentes bioquímicos, como contenido de agua o materia seca (celulosa, lignina, proteínas) pueden potencialmente estimarse con sensores remotos mediante inversión de modelos de transferencia radiativa, clorosis que puede ser indicador de deficiencias nutricionales. Los métodos físicos actuales de investigación para la estimación de variables bioquímicas a nivel de hoja, y biofísicas de la cubierta vegetal se basan en la unión de modelos de transferencia radiativa de hoja como PROSPECT, LEAFMOD, y LIBERTY con modelos de cubierta de simulación de la reflectancia. Modelos de cubierta de tipo geométrico como Geometrical-Optical Radiative-Transfer (GORT), FLIM, modelos turbid-medium como SAILH, su modificación GeoSAIL, y modelos 3-D de tipo Monte Carlo como SPRINT, de tipo geométrico de gran complejidad para simulación de las sombras y suelo que permiten la simulación de la reflectancia de cubiertas vegetales a partir de variables que definen la geometría y estructura de la vegetación. Para ello es crítico que los modelos físicos foliares estén validados para distintos tipos de especies y diferencias estructurales foliares, siendo necesaria la realización de medidas ópticas foliares mediante esferas integrantes que midan la reflectancia y transmitancia foliar. La presentación tratará de aspectos relacionados con la simulación foliar y a escala de cubierta mediante la conexión de modelos físicos de transferencia radiativa, y la metodología de medida de las propiedades ópticas foliares mediante esferas integrantes, tanto en hojas como en acículas.

Se adjunta artículo donde está publicada la metodología de medida de reflectancia y transmitancia mediante esfera integrante.

Available online at www.sciencedirect.com
SCIENCE DIRECT®
Remote Sensing of Environment 99 (2005) 271 – 287
Remote Sensing of Environment
www.elsevier.com/locate/rse

Assessing vineyard condition with hyperspectral indices: Leaf and canopy reflectance simulation in a row-structured discontinuous canopy

P.J. Zarco-Tejada [a,*], A. Berjón [b], R. López-Lozano [c], J. R. Miller [d], P. Martín [e], V. Cachorro [b], M.R. González [e], A. de Frutos [b]

[a] *Instituto de Agricultura Sostenible (IAS), Consejo Superior de Investigaciones Científicas (CSIC), Alameda del Obispo, s/n 14004-Córdoba, Spain*
[b] *GOA-UVA, Universidad de Valladolid, Spain*
[c] *Centro de Investigación y Tecnología Agroalimentaria de Aragón (CITA), Spain*
[d] *Department Earth and Space Science and Engineering, York University, Toronto, Canada*
[e] *Departamento de Producción Vegetal y Recursos Forestales, Universidad de Valladolid, Spain*

Received 11 June 2005; received in revised form 5 September 2005; accepted 7 September 2005

Abstract

Methods for chlorosis detection and physiological condition monitoring in *Vitis vinifera* L. through accurate chlorophyll a and b content (C_{ab}) estimation at leaf and canopy levels are presented in this manuscript. A total of 24 vineyards were identified for field and airborne data collection with the *Compact Airborne Spectrographic Imager* (CASI), the *Reflective Optics System Imaging Spectrometer* (ROSIS) and the *Digital Airborne Imaging Spectrometer* (DAIS-7915) hyperspectral sensors in 2002 and 2003 in northern Spain, comprising 103 study areas of 10×10 m in size, with a total of 1467 leaves collected for determination of pigment concentration. A subsample of 605 leaves was used for measuring the optical properties of reflectance and transmittance with a Li-Cor 1800-12 Integrating Sphere coupled by a 200 μm diameter single mode fiber to an Ocean Optics model USB2000 spectrometer. Several narrow-band vegetation indices were calculated from leaf reflectance spectra, and the PROSPECT leaf optical model was used for inversion using the extensive database of leaf optical properties. Results showed that the best indicators for chlorophyll content estimation in *V. vinifera* L. leaves were narrow-band hyperspectral indices calculated in the 700–750 nm spectral region (r^2 ranging between 0.8 and 0.9), with poor performance of traditional indices such as the *Normalized Difference Vegetation Index* (NDVI). Results for other biochemicals indicated that the *Structure Insensitive Pigment Index* (SIPI) and the *Photochemical Reflectance Index* (PRI) were more sensitive to carotenoids C_{x+c} and chlorophyll–carotenoid ratios C_{ab}/C_{x+c} than to chlorophyll content C_{ab}. Chlorophyll *a* and *b* estimation by inversion of the PROSPECT leaf model on *V. vinifera* L. spectra was successful, yielding a determination coefficient of $r^2=0.95$, with an RMSE=5.3 μg/cm^2. The validity of leaf-level indices for chlorophyll content estimation at the canopy level in *V. vinifera* L. was studied using the *scaling-up* approach that links PROSPECT and rowMCRM canopy reflectance simulation to account for the effects of vineyard structure, vine dimensions, row orientation and soil and shadow effects on the canopy reflectance. The index calculated as a combination of the *Transformed Chlorophyll Absorption in Reflectance Index* (TCARI), and the *Optimized Soil-Adjusted Vegetation Index* (OSAVI) in the form TCARI/OSAVI was the most consistent index for estimating C_{ab} on aggregated and pure vine pixels extracted from 1 m CASI and ROSIS hyperspectral imagery. Predictive relationships were developed with PROSPECT–rowMCRM model between C_{ab} and TCARI/OSAVI as function of LAI, using field-measured vine dimensions and image-extracted soil background, row-orientation and viewing geometry values. Prediction relationships for C_{ab} content with TCARI/OSAVI were successfully applied to the 103 study sites imaged on 24 fields by ROSIS and CASI airborne sensors, yielding $r^2=0.67$ and RMSE=11.5 μg/cm^2.

Keywords: Hyperspectral remote sensing; *Vitis vinifera*; Vineyards; Vine; Radiative transfer; Scaling-up; Optical index; RowMCRM

1. Introduction

Current research efforts in precision viticulture and on the temporal and spatial monitoring of *Vitis vinifera* L. show a growing interest in remote sensing methods due to its potential

* Corresponding author. Tel.: +34 957 499 280/+34 676 954 937; fax: +34 957 499 252.
E-mail address: pzarco@ias.csic.es (P.J. Zarco-Tejada).
URL: http://www.ias.csic.es/pzarco (P.J. Zarco-Tejada).

0034-4257/$ - see front matter © 2005 Elsevier Inc. All rights reserved.
doi:10.1016/j.rse.2005.09.002

for estimating vine biophysical variables such as shape, size and vigor, potential indicators of fruit quality and yield (a full review of optical remote sensing methods for vineyard monitoring can be found in Hall et al., 2002).

Successful mapping of vineyard leaf area index (LAI) using high spatial IKONOS satellite imagery was shown by Johnson et al. (2003), enabling the monitoring of plant growth for irrigation support and canopy management through temporal relationships between *Normalized Difference Vegetation Index* (NDVI) and Leaf Area Index (LAI) (Johnson, 2003). This index and other ratios were tested by Dobrowski et al. (2002; 2003) such as the *Perpendicular Vegetation Index* (PVI) and the *Ratio Vegetation Index* (RVI) derived from field data and multispectral aerial photography to estimate canopy density and dormant pruning weight prediction, suggesting consistency across growing seasons. As a result of these and other studies, broad-band multispectral remote sensing imagery of high spatial resolution shows potential applications for vineyard canopy structure characterization, leading to a successful estimation of vine canopy size, shape and row identification (Hall et al., 2003), vineyard mortality detection and missing vinestock recognition (Lagacherie et al., 2001), vineyard classification methods (Lanjeri et al., 2001), and vine canopy cover estimation for water management (Montero et al., 1999). These studies point toward the application of new techniques in viticulture based on precision agriculture, introducing methods focused on describing homogeneous management zones derived from remotely sensed biophysical variable estimates (Hall et al., 2002), connecting the within-field variability and the suggested classification of the field into different vigor classes with a potential wine quality production (Johnson et al., 2001).

Nevertheless, and despite the cited work conducted mainly with aerial photography, analogue camera systems, and digital sensors with a limited number of broad bands, little progress has been made on the remote sensing detection of vineyard physiology and condition due to the specific characteristics of the sensors needed, requiring simultaneous narrow-band capabilities and high spatial resolution. Progress on crop condition in vineyards has been made at the leaf-level studying absorptance in the visible region in the field (Schultz, 1996), and detecting phenology and grape color at harvest to gather information about berry phenolics (Lamb et al., 2004). For this reason, and due to such limited work achieved on the remote sensing of vine physiology and condition at canopy level, current research efforts are warranted toward the investigation of physical methods applied to high-spatial resolution hyperspectral remote sensing imagery to estimate leaf biochemical constituents and canopy biophysical variables to gather information related to vine status and functioning (Zarco-Tejada et al., 2003). Several studies indicate that the estimation of leaf biochemistry may be used as indicators of chlorosis due to plant stress and nutritional deficiencies caused by micro and macro elements (Fernandez-Escobar et al., 1999; Jolley & Brown, 1994; Marschner et al., 1986; Tagliavini & Rombolà, 2001; Wallace, 1991). As an example, element deficiencies such as iron and nitrogen may result in vine chlorosis and may cause a decrease of fruit yield and quality in the current and the subsequent year as fruit buds develop poorly (Tagliavini & Rombolà, 2001).

Leaf biochemistries, such as the concentration of chlorophyll a+b (C_{ab}), water (C_w), and dry matter (C_m), are indicators of stress and growth that may be estimated by empirical methods (indices) and analytical techniques (physical methods) from remote sensing data in the 400–2500 nm spectral region. Several studies demonstrate the feasibility of chlorosis detection in vegetation through C_{ab} estimation using spectroscopy and leaf optical properties (Carter & Spiering, 2002; Gitelson et al., 2003; Jacquemoud et al., 1996; le Maire et al., 2004; Sims & Gamon, 2002). Recently, several new optical indices have been proposed to relate crop physiological status with hyperspectral data through their relationship to biochemical constituent concentrations such as chlorophyll (Carter, 1994; Gitelson & Merzlyak, 1996; Vogelmann et al., 1993; Zarco-Tejada et al., 2001, 2004, 2005), carotenoids (Fuentes et al., 2001; Sims & Gamon, 2002), and water content (Gao, 1996; Peñuelas et al., 1997).

A large number of the new narrow-band optical indices that might be used with leaf and canopy hyperspectral reflectance have been tested on specific crop and forest species with success (Haboudane et al., 2002, 2004; Zarco-Tejada et al., 2001; a full review of indices can be found in Zarco-Tejada et al., 2005). Red edge reflectance indices, spectral and derivative indices, and derivative ratios have demonstrated good results for C_{ab} estimation from canopy reflectance using airborne hyperspectral data. Recently, combinations of indices based on the *Transformed Chlorophyll Absorption in Reflectance Index*, TCARI (Haboudane et al., 2002), *Modified Chlorophyll Absorption in Reflectance* MCARI (Daughtry et al., 2000), and the *Optimized Soil-Adjusted Vegetation Index*, OSAVI (Rondeaux et al., 1996), such as TCARI/OSAVI and MCARI/OSAVI, have been demonstrated to successfully minimize soil background and LAI variation in crops, providing predictive relationships for precision agriculture applications with hyperspectral imagery in closed crops (Haboudane et al., 2002) and open tree canopy orchards (Zarco-Tejada et al., 2004). Nevertheless, and despite the successful relationships obtained between specific optical indices and leaf biochemistry in closed crops, estimation of such biochemical components in vineyards at a canopy level from remote sensing requires appropriate modeling strategies accounting for its row-structure and large shadow and soil effects on the *bi-directional* reflectance (BRDF) signature. The application of previously validated leaf optical indices to discontinuous crop canopies such as *V. vinifera* L. needs extensive research with airborne hyperspectral data of optimum spatial and spectral resolution, i.e. one meter or better spatial resolution to obtain pure vine reflectance in selected spectral bands sensitive to pigment absorption. Vine row geometry leads to large variations in shadow scene proportions as a function of sun azimuth and zenith angles relative to row orientation, affecting the vegetation index and the estimated leaf biochemical constituent. It is required, therefore, that successful vine leaf-level indices are investigated at the canopy level through *scaling-up* simulation using

appropriate physical methods and very high spatial resolution. This approach (Haboudane et al., 2002; Zarco-Tejada et al., 2001, 2003) uses physical models at leaf and canopy levels to *scale-up* optical indices that are sensitive to specific biochemical constituents, therefore modeling the indices as function of canopy structure, viewing geometry and background effects.

This manuscript reports on a study of the optical properties of *V. vinifera* L. for C_{ab} estimation using narrow-band indices and radiative transfer model inversion. The work describes in detail the methods for accurate measurements of the leaf optical properties, testing the behavior of several indices for successful C_{ab} estimation. The successful leaf optical indices are proposed for *scaling-up* simulation with the *Markov-Chain Canopy Reflectance Model* (MCRM) (Kuusk, 1995a,b) with additions to simulate the row crop structure, called rowMCRM, and developed within the frame of the *Crop Reflectance Operational Models for Agriculture* (CROMA) project. The linked PROSPECT–rowMCRM model is assessed to model vineyard scene component proportions, row orientations, vineyard dimensions and background effects with high spatial resolution hyperspectral airborne imagery.

2. Airborne and field campaigns for data collection

2.1. Airborne campaigns with ROSIS and CASI hyperspectral sensors

Data acquisition campaigns were conducted in July 2002 under the European Union HySens-2002 project intended to investigate physical methods with the *Reflective Optics System Imaging Spectrometer* (ROSIS) and the *Digital Airborne Imaging Spectrometer* (DAIS-7915) airborne hyperspectral sensors to estimate leaf biochemical constituents in vineyard canopies. In July 2003 the *Compact Airborne Spectrographic Imager* (CASI) sensor was flown over Spain in collaborative research with York University (Canada) and the Spanish aerospace institute *Instituto Nacional de Técnica Aeroespacial* (INTA). Both campaigns took place in study areas of *V. vinifera* L. in *Ribera del Duero* D.O. in Northern Spain.

ROSIS imagery were acquired at 1 m spatial resolution, and calibrated to *at-sensor* radiance by the *German Aerospace Center* (DLR). CASI imagery were collected on two airborne missions, each with a specific sensor mode of operation: i) the *Mapping Mission*, with 1 m spatial resolution and 8 *user-selected* spectral bands placed in the spectrum to enable the calculation of specific narrow-band indices sensitive to pigment concentration (bands were centered at 490, 550, 670, 700, 750, 762, 775 and 800 nm with *full-width at half maximum* (FWHM) ranging between 7 and 12 nm); and the *Hyperspectral Mission*, with 4 m spatial resolution, 72 channels and 7.5 nm spectral resolution. The 12-bit radiometric resolution data collected by CASI were processed to *at-sensor* radiance using calibration coefficients derived in the laboratory by the Earth Observations Laboratory (EOL), York University, Canada. Aerosol optical depth data at 340, 380, 440, 500, 670, 870, and 1020 nm were collected using a Micro-Tops II sunphotometer (Solar Light Co., Philadelphia, PA, USA) in the study area at the time of data acquisition to derive aerosol optical depth at 550 nm. Atmospheric correction was applied to ROSIS radiance imagery using MODTRAN, whereas the CAM5S atmospheric correction model (O'Neill et al., 1997) was used for CASI imagery. Reflectance data were geo-referenced using GPS data collected onboard the aircraft. Soil reflectance spectra were used to perform a *flat-field* correction (Ben-Dor & Levin, 2000) that compensated for residual effects on derived surface reflectance estimations in atmospheric water and oxygen absorption spectral regions. Fig. 1 shows vegetation and soil spectra extracted from CASI mapping mission image on selected sites after processing to *surface reflectance*, observing the large variability in soil brightness levels, as well as the pure vine and the mixed soil+vine+shadow spectra.

Concurrent with the airborne overflights, field sampling campaigns were conducted in summer 2002 and 2003 for biochemical analysis of leaf C_{ab}, as well as to measure reflectance (R) and transmittance (T) from leaf samples to study the vine optical properties.

2.2. Study site description and leaf sampling methods

The study sites of *V. vinifera* L. used for ground and airborne collection were carefully selected from a plot network currently monitored by the local government to assure a gradient in the leaf biochemistry as sought for this study. A total of 10 fields were selected in 2002 and 14 fields in 2003 for leaf sampling collection, comprising a total of 103 study areas of 10×10 m in size. In 2002, 10 leaves per site were used for Cab sampling and reflectance and transmittance measurements. In 2003, a total of 80 leaves were sampled from each 10×10 m study area, using 50 leaves for measuring dry matter and elements N, P, K, Ca, Mg, Fe, 20 leaves for Cab determination, and 10 leaves per site for conducting reflectance and transmittance measurements. A total of 1467 leaves were used for determination of Cab on the 103 study sites comprised by the 2002 and 2003 campaigns, and 605 leaves for measuring the optical properties. Leaves used for measuring optical properties were taken to the laboratory and reflectance and transmittance measurements made on the same day to avoid pigment degradation. Dry matter was measured placing the samples in a pre-heated oven at 40 °C until a stable dry weight was reached. Structural measurements on each study site consisted of grid size, number of vines within the 10×10 m site, trunk height, vegetation height and width, and row orientation. Soil samples were collected at each site for laboratory analysis. Fig. 2 illustrates a CASI image acquired from vineyard fields, showing 15 out of the total 103 blocks of 10×10 m used for leaf sampling and ground data collection.

2.3. Leaf pigment determination by destructive sampling

The leaves from the *V. vinifera* L. sites were sampled from the top of the canopy, eliminating the small leaves indicative of low expansion. Leaves were placed in paper bags to allow tissue respiration and conservation, then stored at 4 °C prior to

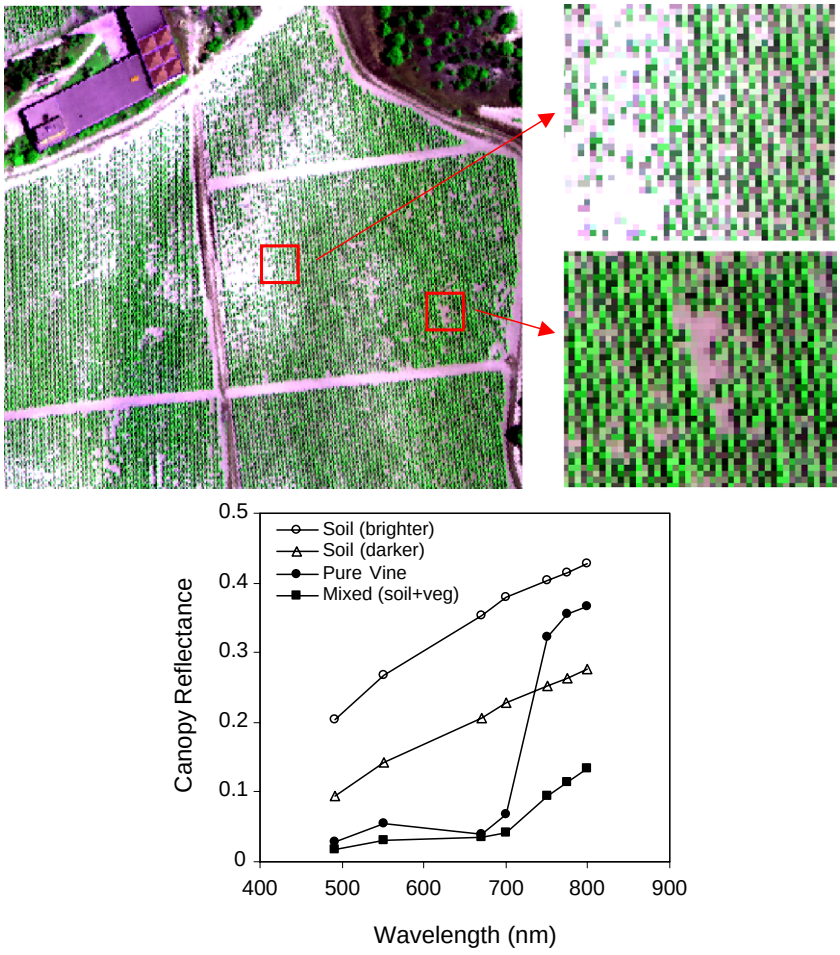

Fig. 1. Airborne CASI image collected at 1 m spatial resolution and 8 bands selected for calculation of narrow-band indices sensitive to pigment concentration. Pure vine reflectance and soil spectra extracted from the image show the within-field variability.

analysis of reflectance and transmittance, and then stored in a freezer at −8 °C prior to pigment determination. A 1.6 cm circle from each leaf sample was cut out for grinding with 4 ml acetone at 80%, and adding 8 ml acetone to a total of 12 ml in each tube. Tubes were stored in the dark at 4 °C for 48 h prior to spectrophotometer measurements. Each sample for pigment determination was filtered, placed in a cuvette and the absorbance measured between 400 and 700 nm with 2 nm fixed resolution at 1 nm interval with a Jasco V-530 UV-VIS spectrophotometer (Jasco Inc., Great Dunmow, UK). Chloro-

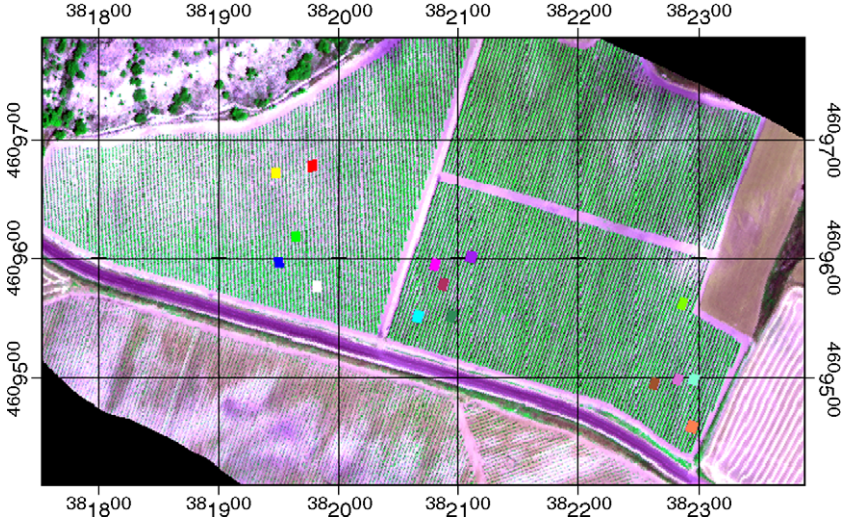

Fig. 2. Airborne hyperspectral CASI image acquired from one of the *Vitis vinifera* L. fields in this study, showing 15 blocks of 10 × 10 m selected for leaf sampling and ground data collection.

Table 1
Range of variation for the leaves sampled from the 103 study sites of *Vitis vinifera* L. used in this study

	C_a	C_b	C_{ab}	C_{x+c}	C_a/C_b	C_a/C_{x+c}	C_b/C_{x+c}	C_{ab}/C_{x+c}
Max	54.03	19.87	73.45	13.98	4.29	5.08	1.77	6.75
Min	1.74	1.25	3.40	1.39	1.05	0.74	0.33	1.06
Average	26.01	8.98	34.99	7.90	2.92	3.20	1.11	4.31

Values in μg/cm^2 (n=1467).

phyll *a* (C_a), chlorophyll *b* (C_b), and total carotenoid (C_{x+c}) concentrations were calculated using the extinction coefficients derived by Wellburn (1994) and the absorbance measured at 470, 646, and 663 nm with Eqs. (1)–(3).

$$C_a = 12.21 \cdot A_{663} - 2.81 \cdot A_{646} \quad (1)$$

$$C_b = 20.13 \cdot A_{646} - 5.03 \cdot A_{663} \quad (2)$$

$$C_{x+c} = (1000 \cdot A_{470} - 3.27 \cdot C_a - 104 \cdot C_b)/198. \quad (3)$$

These measurements resulted in a mean C_{ab} of μ=34.99 μg/cm^2, with a wide range between 3.4 and 73.45 μg/cm^2 (n=1467). Table 1 shows the range of variation of C_a, C_b, C_{ab} and C_{x+c} used later for determination of pigment content at each study site. The range of variation of the subset of 605 leaves used for optical measurements, correlation with optical indices and modelling are shown in Table 2.

2.4. Protocol for optical measurements of V. vinifera L. leaves

Reflectance and transmittance measurements of vine leaves were conducted on the subsample of 605 leaves with a Li-Cor 1800-12 Integrating Sphere (Li-Cor, Inc., Lincoln, NE, USA), coupled by a 200 μm diameter single mode fiber to an Ocean Optics model USB2000 spectrometer (Ocean Optics Inc., Dunedin, FL, USA), with a 2048 element detector array, 0.5 nm sampling interval, and 7.3 nm spectral resolution in the 350–1000 nm range. Software was designed for signal verification, adjustment of integration time, and data acquisition. An integration time of 13 ms was used for all sample measurements. Spectral bandpass characterization performed using a mercury spectral line lamp source yielded FWHM bandwidth estimates of 7.3 at 546.1 nm. Fiber spectrometer wavelength calibration was performed using the Ocean Optics HG-1 Mercury–Argon Calibration Source that produces Hg and Ar emission lines between 253 and 922 nm. Single leaf reflectance and transmittance measurements were acquired following the methodology described in the manual for the Li-Cor 1800-12 system (Li-Cor Inc., 1984) modified by Harron (2000) to correct for stray-light in the integrating sphere. For clarity, the protocol is described here with the steps required to calculate the stray-light corrected leaf hemispherical reflectance (R) and transmittance (T) using a reference target in the integrating sphere. The protocol consisted of a total of five measurements modifying the position of the collimated light, dark and white plugs in the integrating sphere to measure the transmittance signal (TSP), the reflectance signal (RSS), the reflectance internal standard (RTS), the reflectance ambient (RSA), and the dark measurement (DRK) (Table 3)). For clarity of the protocol used in this study and for future reference, a schematic view of the integrating sphere with lamp and port placement is shown in Fig. 3. Stray-light corrected reflectance and transmittance were then calculated assuming a constant center wavelength and spectral bandpass, using the set of equations described by Harron (2000) for stray-light correction in broadleaves without the requirement of sample carriers (Eqs. (4)–(8)). Another measurement protocol and a different set of equations are proposed in Harron (2000) when measuring needle samples or broad leaves smaller than the sphere sample port.

Table 2
Range of variation for the subsample of *Vitis vinifera* L. leaves used for optical measurements and correlations with optical indices

	C_a	C_b	C_{ab}	C_{x+c}	C_a/C_b	C_a/C_{x+c}	C_b/C_{x+c}	C_{ab}/C_{x+c}
Max	53.79	19.49	70.83	13.98	4.29	4.31	1.67	5.98
Min	1.74	1.25	3.40	1.39	1.05	0.96	0.35	1.50
Average	25.43	8.80	34.23	7.99	2.91	3.09	1.08	4.17

Values in μg/cm^2 (n=605).

$$R = R' \frac{GT_{fi} + \frac{R'}{R_{BaSO_4}} S_i R_w T_f}{GT_{fi} + S_i R_w T_f} \quad (4)$$

$$T = T' \left(1 + \frac{S_i R_w R T_f}{G T_{fi} R_{BaSO_4}}\right) \quad (5)$$

with R', $T'$and G given in Eqs. (6), (7) and (8),

$$R' = \frac{RSS - RSA}{RTS - RSA} R_{BaSO_4} \quad (6)$$

$$T' = \frac{TSP - DRK}{RTS - RSA} R_{BaSO_4} \quad (7)$$

$$G = (1 - W_f R_w - B_f R_{BaSO_4}) \quad (8)$$

with the following coefficients measured for the sphere used in this study,

W_f is the fraction of the sphere which is interior wall (0.968)
B_f is the fraction of the sphere which is $BaSO_4$ reference (0.009)

Table 3
Sequence of measurements with the Li-Cor 1800 integrating sphere and fiber spectrometer to enable the calculation of reflectance and transmittance with Eqs. (4)–(8) and the schematic view shown in Fig. 3

Step	Setup	Lamp	White plug	Dark plug	Sample
1	RSA	C (ON)	B	A	OUT
2	RSS	C (ON)	B	A	IN←
3	RTS	B (ON)	C	A	IN←
4	TSP	A (ON)	C	B	IN→
5	DRK	OFF	B	A	OUT

IN →: adaxial leaf surface facing sample port A.
IN ←: adaxial leaf surface facing sphere.

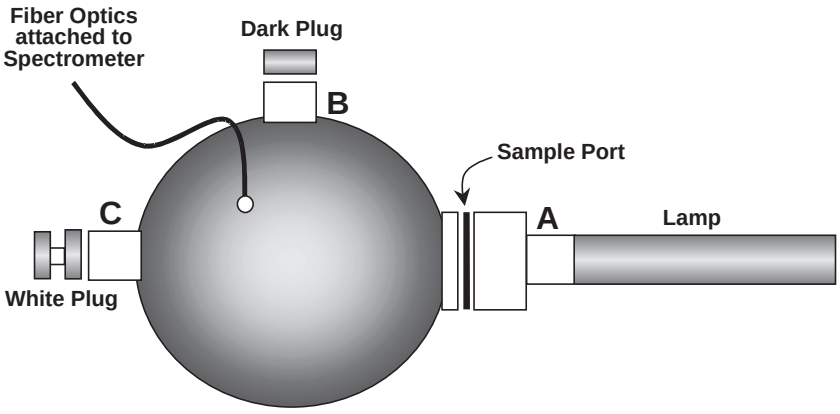

Fig. 3. Schematic view of the Li-Cor 1800-12 integrating sphere attached to an USB2000 fiber spectrometer used for reflectance and transmittance measurements.

T_{fi} is the fraction of the sphere which is target and directly illuminated (0.006)
T_f is the fraction of the sphere which is target (0.009)
S_i is the fraction of light scattered into the sphere from the illuminator (0.0001)
R_{BaSO_4} is the reflectance of the $BaSO_4$ reference (0.98)
R_w is the reflectance of sphere walls (0.9).

Experimental measurements made with the Li-Cor 1800-12 integrating sphere used in this study were employed to calculate the fraction of light scattered into the sphere from the illuminator (S_i), a function of the optical properties of the sphere and light lamp used. The S_i value obtained for the sphere used in this study was 10^{-4}, indicating that such correction factor had a very small effect on the calculated reflectance and transmittance. Nevertheless, on another integrating sphere used on this same study with different design and configuration (data not shown), the S_i correction was critical for an accurate calculation of the leaf optical properties corrected for stray-light, and therefore it has to be seriously taken into consideration in such cases. As an example of spectra measured with this methodology, Fig. 4 shows vine leaf reflectance and transmittance spectra with pigment content of 26.68 μg/cm^2, and 4 leaf reflectance measurements from leaves containing a gradient in chlorophyll concentration between 15 and 54 μg/cm^2.

3. Vegetation indices and model inversion for C_{ab} estimation in *V. vinifera* L. at the leaf-level

Leaf-level spectroscopy enables the calculation of narrow-band indices potentially related to specific light absorptions caused by leaf biochemical constituents, such as chlorophyll *a* and *b* (Carter & Spiering, 2002; Sims & Gamon, 2002; Zarco-Tejada et al., 2005), carotenoids/chlorophyll and anthocyanins/chlorophyll ratios (Fuentes et al., 2001; Gamon & Surfus, 1999; Peñuelas et al., 1995), dry matter (Fourty & Baret, 1997), and water content (Carter, 1991; Ceccato et al., 2001; Danson et al., 1992; Gao, 1996; Peñuelas et al., 1997). Several optical indices are currently used with success for C_{ab} estimation from leaf optical properties on different crop and forest species, exploiting the differences in reflectance between healthy and stressed vegetation in the visible and the red edge spectral region (Carter, 1994; Carter & Spiering, 2002; Horler et al., 1983; Vogelmann et al., 1993; Zarco-Tejada et al., 2001). A full review of these chlorophyll indices can be found in Zarco-Tejada et al. (2001, 2004, 2005) and summarized in Table 4. These indices are generally classified into visible and visible/NIR ratios, red edge indices and spectral and derivative

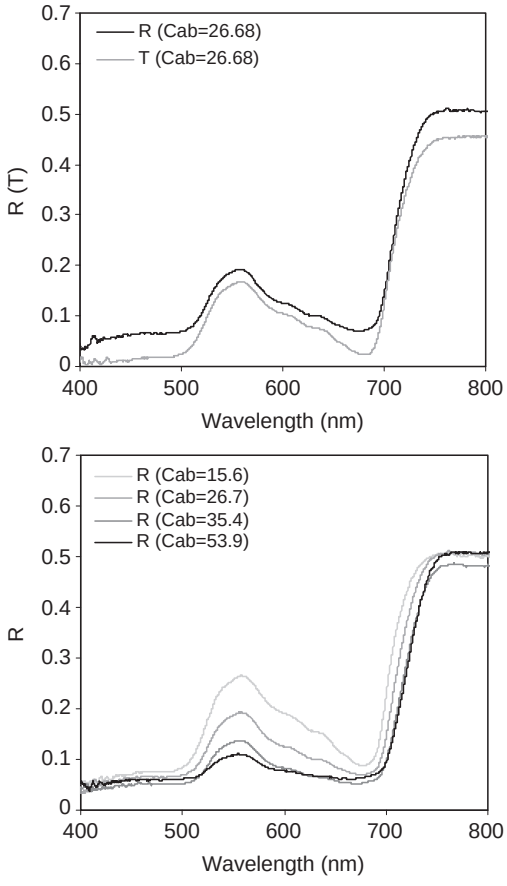

Fig. 4. Sample leaf reflectance (R) and transmittance (T) measured in a *Vitis vinifera* L. leaf with integrating sphere and protocol described in this manuscript. Destructive C_{ab} determination yielded a chlorophyll content of 26.68 μg/cm^2 (upper plot). Bottom plot shows 4 leaf reflectance measurements for vine leaves containing 15.6, 26.7, 35.4, and 53.9 μg/cm^2 respectively.

Table 4
Hyperspectral optical indices used in this study

Vegetation index	Equation	Reference
Normalized Difference Vegetation Index (NDVI)	$NDVI = (R_{NIR} - R_{red})/(R_{NIR} + R_{red})$	Rouse et al. (1974)
Simple Ratio Index (SR)	$SR = R_{NIR}/R_{red}$	Jordan (1969); Rouse et al. (1974)
Modified Simple Ratio (MSR)	$MSR = \frac{R_{NIR}/R_{red} - 1}{(R_{NIR}/R_{red})^{0.5} + 1}$	Chen (1996)
Modified Triangular Vegetation Index ($MTVI_1$)	$MTVI_1 = 1.2*[1.2*(R_{800} - R_{550}) - 2.5*(R_{670} - R_{550})]$	Haboudane et al. (2004)
Modified Triangular Vegetation Index ($MTVI_2$)	$MTVI_2 = \frac{1.5*[1.2*(R_{800} - R_{550}) - 2.5*(R_{670} - R_{550})]}{\sqrt{(2*R_{800} + 1)^2 - (6*R_{800} - 5*\sqrt{R_{670}}) - 0.5}}$	Haboudane et al. (2004)
Renormalized Difference Vegetation Index (RDVI)	$RDVI = (R_{800} - R_{670})/\sqrt{(R_{800} + R_{670})}$	Rougean and Breon (1995)
Greenness Index (G)	$G = R_{554}/R_{677}$	–
Triangular Veg. Index (TVI)	$TVI = 0.5*[120*(R_{750} - R_{550}) - 200*(R_{670} - R_{550})]$	Broge and Leblanc (2000)
Improved SAVI with self-adjustment factor L (MSAVI)	$MSAVI = \frac{1}{2}\left[2*R_{800} + 1 - \sqrt{(2*R_{800} + 1)^2 - 8*(R_{800} - R_{670})}\right]$	Qi et al. (1994)
Optimized Soil-Adjusted Vegetation Index (OSAVI)	$OSAVI = (1 + 0.16)*(R_{800} - R_{670})/(R_{800} + R_{670} + 0.16)$	Rondeaux et al. (1996)
Modified C_{ab} Absorption in Reflectance Index (MCARI)	$MCARI = [(R_{700} - R_{670}) - 0.2*(R_{700} - R_{550})]*(R_{700}/R_{670})$	Daughtry et al. (2000)
Transformed CARI (TCARI)	$TCARI = 3*[(R_{700} - R_{670}) - 0.2*(R_{700} - R_{550})*(R_{700}/R_{670})]$	Haboudane et al (2002)
Modified Chlorophyll Absorption in Reflectance Index ($MCARI_1$)	$MCARI_1 = 1.2*[2.5*(R_{800} - R_{670}) - 1.3*(R_{800} - R_{550})]$	Haboudane et al. (2004)
Modified Chlorophyll Absorption in Reflectance Index ($MCARI_2$)	$MCARI_2 = \frac{1.5*[2.5*(R_{800} - R_{670}) - 1.3*(R_{800} - R_{550})]}{\sqrt{(2*R_{800} + 1)^2 - (6*R_{800} - 5*\sqrt{R_{670}}) - 0.5}}$	Haboudane et al. (2004)
Zarco and Miller (ZM)	$ZM = R_{750}/R_{710}$	Zarco-Tejada et al. (2001)
Blue/Green and Blue/Red Pigment ndices (RGI, BGI, BRI)	$RGI = R_{690}/R_{550}$ $BGI_1 = R_{400}/R_{550}$ $BGI_2 = R_{450}/R_{550}$ $BRI_1 = R_{400}/R_{690}$ $BRI_2 = R_{450}/R_{690}$	Zarco-Tejada et al. (this study)
Simple Ratio Pigment Ind. (SRPI)	$SRPI = R_{430}/R_{680}$	Peñuelas et al. (1995)
Normalized Phaeophytinization Index (NPQI)	$NPQI = (R_{415} - R_{435})/(R_{415} + R_{435})$	Barnes (1992)
Photochemical Reflectance Index (PRI)	$PRI_1 = (R_{528} - R_{567})/(R_{528} + R_{567})$ $PRI_2 = (R_{531} - R_{570})/(R_{531} + R_{570})$ $PRI_3 = (R_{570} - R_{539})/(R_{570} + R_{539})$	Gamon et al. (1992)
Normalized Pigment Chlorophyll Index (NPCI)	$NPCI = (R_{680} - R_{430})/(R_{680} + R_{430})$	Peñuelas et al. (1994)
Carter Indices (CTR)	$CTR_1 = R_{695}/R_{420}$ $CTR_2 = R_{695}/R_{760}$	Carter (1994,1996)
Lichtenthaler Indices (LIC)	$LIC_1 = (R_{800} - R_{680})/(R_{800} + R_{680})$ $LIC_2 = R_{440}/R_{690}$ $LIC_3 = R_{440}/R_{740}$	Lichtenthaler et al. (1996)
Structure Insensitive Pigment Index (SIPI)	$SIPI = (R_{800} - R_{450})/(R_{800} + R_{650})$	Peñuelas et al. (1995)
Vogelmann Indices (VOG)	$VOG_1 = R_{740}/R_{720}$ $VOG_2 = (R_{734} - R_{747})/(R_{715} + R_{726})$ $VOG_3 = (R_{734} - R_{747})/(R_{715} + R_{720})$	Vogelmann et al. (1993); Zarco-Tejada et al. (2001)
Gitelson and Merzlyak (GM)	$GM_1 = R_{750}/R_{550}$ $GM_2 = R_{750}/R_{700}$	Gitelson and Merzlyak (1997)
Curvature Index (CUR)	$CUR = (R_{675}\cdot R_{690})/(R_{683}^2)$	Zarco-Tejada et al. (2000)

analysis indices. Other traditional indices related to vegetation structure and condition, such as NDVI or the Simple Ratio (SR), normally show low relationships with leaf biochemical constituents (Zarco-Tejada et al., 2001) and consistently show unsuccessful performance in detecting physiological stress condition.

Despite the demonstrated success of these narrow-band leaf indices for C_{ab} estimation, spectral reflectance signatures from agricultural canopies are characterized by large contributions from the soil background and LAI variation at different growth stages. In these cases, *scaling-up* methods through canopy reflectance models are needed to account for crop structure, viewing geometry and soil and shadow effects on the reflectance. The study of indices at both leaf and canopy levels demonstrates that successful indices developed at the leaf-level do not necessarily perform well at the canopy level due to the soil and structural effects mentioned (Zarco-Tejada et al., 2001, 2004). Therefore, combined indices have been proposed to minimize background soil effects while maximizing the sensitivity to C_{ab} (Haboudane et al., 2002) and LAI

(Haboudane et al., 2004) and to yield prediction relationships directly applicable to hyperspectral imagery. As an example, CARI *(Chlorophyll Absorption in Reflectance Index)* (Kim et al., 1994) was shown to reduce the variability induced on photosynthetically active radiation inferences due to non-photosynthetic materials. MCARI *(Modified Chlorophyll Absorption in Reflectance Index)* (Daughtry et al., 2000) was a modification of CARI to minimize the combined effects of the soil reflectance and the non-photosynthetic materials. SAVI *(Soil-Adjusted Vegetation Index)* (Huete, 1988) and OSAVI *(Optimized Soil-Adjusted Vegetation Index)* (Rondeaux et al., 1996) were proposed as soil-line vegetation indices that could be combined with MCARI to reduce background reflectance contributions (Daughtry et al., 2000). As a result of the development of these indices, successful C_{ab} estimation on corn agricultural canopies at different growing stages was achieved using the TCARI/OSAVI combined index in forward leaf-canopy modelling, proving its robustness due to the low sensitivity to effects caused by LAI variation and background influence (Haboudane et al., 2002). Other indices, such as the modified chlorophyll absorption ratio index (MCARI2), are discussed in depth in Haboudane et al. (2004). All these mentioned indices that can be found in Table 4 have proven different degrees of success in crop and forest species for pigment estimation at the leaf-level. Relationships between all these single and combined indices calculated from the 605 leaf R and T measurements in 2002 and 2003 campaigns (Table 4) and pigment content measurements C_a, C_b, C_{ab}, C_{x+c}, and pigment ratios C_a/C_b, C_a/C_{x+c}, C_b/C_{x+c} and C_{ab}/C_{x+c} (Table 2) were calculated using linear, exponential, and 3rd order polynomial functions to allow for both linear and non-linear relationships between indices and leaf pigment concentrations in grape leaves. The large database available of leaf optical measurements as part of this study addresses the lack of previous studies on investigating appropriate leaf optical indices in *V. vinifera* L. crop.

In addition to the generally accepted relationships existing between leaf optical indices and C_{ab}, model inversion methods using radiative transfer simulation have been successfully used to simulate leaf optical properties. Due to its extensive validation, the PROSPECT model (Jacquemoud & Baret, 1990), based on the *plate model* (Allen et al., 1969, 1970), was used in this study to simulate the leaf optical properties of *V. vinifera* L. leaves, testing the feasibility of C_{ab} estimation. Several studies demonstrate successful retrievals of pigment concentration from leaf optical properties with PROSPECT (Jacquemoud & Baret, 1990; Jacquemoud et al., 1996; le Maire et al., 2004) although limited simulation work has been conducted with extensive measurements on *V. vinifera* L leaves. The large database of leaf reflectance and transmittance spectra measured in 2002 and 2003, comprising a total of 605 measurements, were used for PROSPECT model inversion. The model inversion was performed by iterative optimization, varying input parameters N (structural parameter) from 1 to 2.5, C_{ab} between 5 and 95 μg/cm^2, C_m in the range 0.001 and 0.04 mg/cm^2, and C_w for 0.001 and 0.04 mg/cm^2, obtaining the root mean square error (RMSE) function $\xi(N)$ to be minimized using both R and T in the 400–800 nm range using Eq. (9),

$$\mathrm{RMSE} = \xi(N, C_{ab}, C_m, C_w) = \sqrt{\frac{\sum_{\lambda}\left[(R_{\mathrm{PROSPECT}} - R_m)_{\lambda}^2 + (T_{\mathrm{PROSPECT}} - T_m)_{\lambda}^2\right]}{n}} \quad (9)$$

where R_m and T_m are reflectance R and transmittance T measured from n leaf samples with the Li-Cor integrating sphere and fiber spectrometer. Estimated C_{ab} values from each R and T spectra by inversion were then compared with leaf destructive measurements of pigment concentration, and the RMSE for C_{ab} estimation from the entire database was calculated.

4. Application of leaf-level hyperspectral indices at canopy level in *V. vinifera* L. with the rowMCRM model

PROSPECT was linked to the rowMCRM model, which refers to the *Markov-Chain Canopy Reflectance Model* (MCRM) (Kuusk, 1995a,b) with additions to simulate the row crop structure. The rowMCRM model was developed within the frame of the *Crop Reflectance Operational Models*

Table 5
Nominal values and range of parameters used for leaf and canopy simulation with PROSPECT and rowMCRM for the vine study sites

PROSPECT	
Leaf parameters	Nominal values and range
Chlorophyll a+b (C_{ab})	5–95 μg/cm^2
Dry matter (C_m)	0.0035 mg/cm^2
Equivalent water thickness (C_w)	0.025 mg/cm^2
Structural parameter (N)	1.62
rowMCRM	
Canopy layer and structure parameters	Nominal values and range
Row Leaf Area Index (LAI)	1–5
Leaf Angle Distribution Function (LADF)	ε=0.95; θ_n=45° (plagiophile)
Relative leaf size (h_s)	0.083
Markov parameter (λ_z)	1.1
Leaf transmittance coefficient (t)	0.9
Leaf hair index (l_h)	0.1
Canopy height (C_H)	1.2–1.8 m
Crown width (C_W)	0.6–1.3 m
Visible soil strip length (V_s)	1.7–2.3 m
Diff. between sun azimuth and row direction (ψ)	11–95.2°
Background and viewing geometry	Nominal values and range
Soil reflectance (ρ_s)	From images (Fig. 7)
Angstrom turbidity factor (β)	0.18
Viewing geometry ($\theta_s\theta_v\ \phi$)	Calculated for each image and site

Canopy structural parameters were used in the rowMCRM model for simulation of the canopy reflectance by radiative transfer. Leaf structural parameters, and leaf biochemical parameters were used for leaf-level simulation of reflectance and transmittance using PROSPECT.

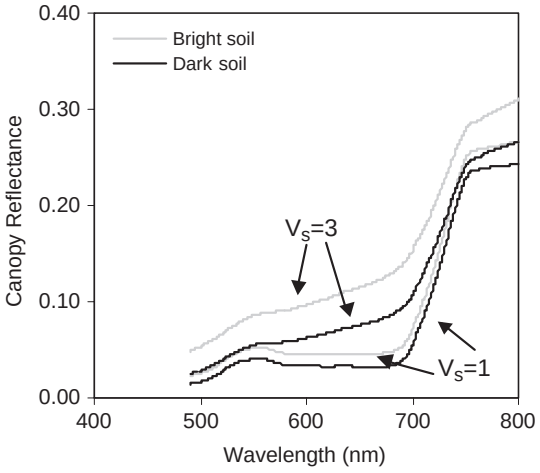

Fig. 5. Canopy reflectance simulation conducted with PROSPECT–rowMCRM as function of soil background (ρ_s) and visible soil strip (V_s).

for Agriculture project (CROMA), with a goal to successfully simulate different scene component proportions, as a function of row orientations and crop dimensions, and soil background and shadow effects as function of viewing geometry in *row-structured* crop canopies. Therefore the rowMCRM canopy reflectance model was considered an optimum candidate for the *scaling-up* of narrow-band indices in row-structured vineyard canopies. The inputs required to the link PROSPECT–rowMCRM used in this study are shown in Table 5: i) leaf parameters for simulating the leaf optical properties, such as chlorophyll a+b (C_{ab}), dry matter (C_m), water content (C_w), and structural parameter (N); ii) canopy layer and structure parameters such as the row leaf area index (LAI), leaf angle distribution function (LADF), relative leaf size (h_s), Markov parameter (λ_z), leaf transmittance coefficient (t), leaf hair index (l_h), canopy height (C_H), crown width (C_W), visible soil strip length (V_s), and the angular difference between sun azimuth and row direction (ψ); and iii) background and viewing geometry parameters such as soil reflectance (ρ_s), Angstrom turbidity factor (β), and the viewing geometry (θ_s, θ_v, ϕ).

Without an intention to provide an *in-depth* sensitivity analysis for rowMCRM (work conducted as part of CROMA project), an exploratory analysis was carried out to study the effects of the different input parameters for PROSPECT–rowMCRM on the canopy reflectance and selected optical indices. The soil background and distance between rows (visible soil strip) input for this row-structured canopy are shown to have large effects on the canopy reflectance (Fig. 5). As expected, soil brightness effects are greater as function of the visible soil strip, suggesting the importance of the vineyard architecture for successful simulation of the canopy reflectance. Typical vineyard canopies are planted in grids with a distance between rows of around 2 m (1.7 to 2.3 m range in the 103 study sites in this study), resulting in reflectance differences of

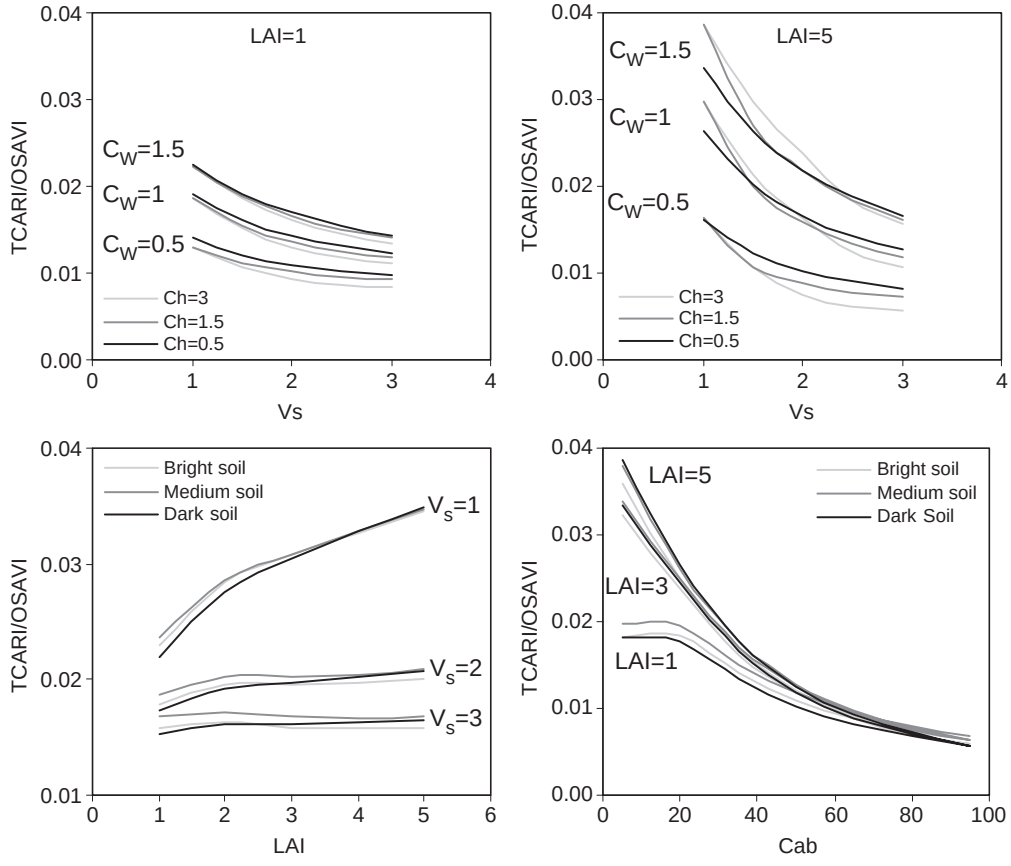

Fig. 6. Effects on TCARI/OSAVI for: i) vine width (C_w) and height (C_H) as function of visible soil strip (V_s) and row LAI (top left and right); ii) visible soil strip (V_s) as function of row LAI and soil background (ρ_s) (bottom left); and iii) row LAI and soil background (ρ_s) on TCARI/OSAVI as function of C_{ab} (bottom right).

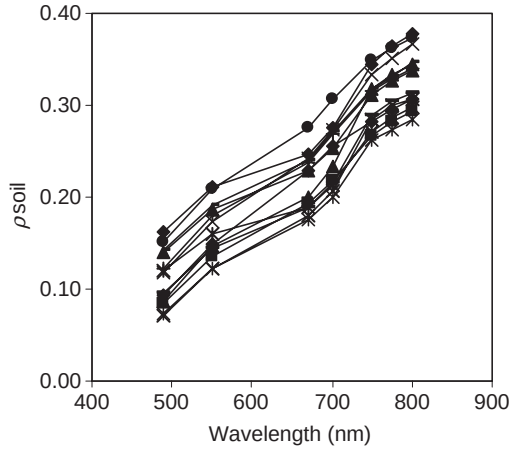

Fig. 7. CASI soil spectra extracted from vineyard study sites and used as input for the simulation methods.

5–7% at 700 nm as function of the soil brightness levels. The effects of row LAI, vineyard row width and height, visible soil strip, and chlorophyll content were then studied for the TCARI/OSAVI index, a combined ratio that has previously proven successful in minimizing background effects for C_{ab} retrieval. The study of vine width and height on TCARI/OSAVI as function of visible soil strip and row LAI (Fig. 6, top left and right) indicates that larger effects are expected due to vine width than to vine height, with larger effects on TCARI/OSAVI as LAI increases. As the visible soil strip increases, vine width effects decrease due to the greater contribution effects of soil reflectance, with lower contribution of vegetation. As LAI increases, large effects on TCARI/OSAVI are found when the visible soil strip is small, i.e. close to 1 m (Fig. 6, bottom left). Nevertheless, for visible soil strips greater than 1 m, i.e. 2 or 3 m (an average of 2 m in the vine sites of this study) simulations suggest a small effect of LAI variation. These simulations indicate that larger effects are found on the index as function of the visible soil strip (background effects) than due to the LAI variation, suggesting the importance for properly describing the vineyard architecture and soil characteristics. When LAI is greater than 1, i.e. 3 or 5 (Fig. 6, bottom right) simulation results suggest the low effects of LAI on TCARI/OSAVI as function of C_{ab} in vineyards with average dimensions (height = 1.5 m; width = 1 m; visible soil strip = 2 m). In addition, in low LAI and low C_{ab} sites (Fig. 6, bottom left and right) soil backgrounds are shown to be important, decreasing the effects on TCARI/OSAVI as row LAI and C_{ab} increase.

These simulations indicate the importance of properly describing the vineyard architecture and dimensions, and the soil background for accurate estimates of chlorophyll concentration. Therefore, in this study vineyard structural parameters and airborne-sun viewing geometry angles that varied between fields were taken into account as inputs for *scaling-up* methods with the rowMCRM canopy model for simulation on each one of the 103 study plots. Vineyard planting grids ranged between 2.5×1 and 3×1.5 m, vine height between 1.2 and 1.8 m, vine width between 0.6 and 1.3 m, visible soil strip between 1.7 and 2.3 m, difference between sun azimuth and row direction between 11° and 95°, and sun zenith angle between 31.5° and 46.7° for all images collected on the airborne campaigns for the 2 years and 103 sites. In addition, simulation methods for C_{ab} estimation employed the input of soil reflectance spectra obtained directly from the imagery on areas of canopy openings or missing vines within the field. Fig. 7 shows a range of soil spectra extracted from the CASI imagery from each of the 14 fields acquired in the 2003 campaign, illustrating the gradient in soil brightness and differences greater than 10% reflectance.

Predictive relationships were calculated for each field study site between C_{ab} and optical indices, using image and field-measured parameters for the vineyard structure, soil background and viewing geometry. *Scaling-up* methods used here are similar to the ones described in Zarco-Tejada et al. (2001) for forest canopies, Haboudane et al. (2002, 2004) for corn crops using PROSPECT-SAILH, and Zarco-Tejada et al. (2004) for open tree canopy crops using PROSPECT-SAILH-FLIM models. *Scaling-up* relationships were developed for each study site using a range of LAI values between 1 and 5, and between 5 and 95 μg/cm^2 for C_{ab}, fixing the remaining leaf

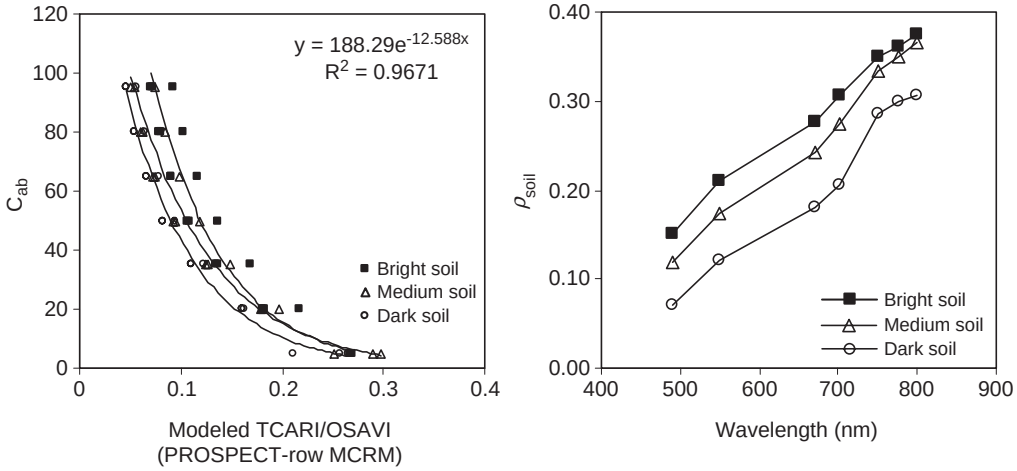

Fig. 8. Example of 3 predictive relationships (left) developed for study sites with extreme soil backgrounds (right). Relationships were developed using a range of row LAI values between 1 and 5, C_{ab} ranging between 5 and 95 μg/cm^2 and structural parameters measured in the field. The remaining parameters were fixed to the values shown in Table 5.

parameters to the values estimated by model inversion from the leaf samples previously described, with the field structural measurements describing the vineyard canopy structure on each study site (Table 5; Fig. 8). Estimated C_{ab} for each of the 103 study sites was then compared with the field-measured values of pigment content obtained by destructive sampling and described in the previous section.

5. Results

Analysis conducted on the 605 leaves where optical properties and leaf biochemical constituents C_a, C_b, C_{ab}, C_{x+c} and ratios C_a/C_b, C_a/C_{x+c}, C_b/C_{x+c}, C_{ab}/C_{x+c} were measured are presented in this section. Results for the regression analysis between leaf reflectance indices and biochemical constituents, leaf model inversion with PROSPECT on vine leaves, and C_{ab} estimation at canopy level with PROSPECT–rowMCRM models through *scaling-up* methods are described.

5.1. Relationships between optical indices and C_{ab} for V. vinifera L. leaves

Results of the relationships found between 45 narrow-band optical indices calculated from leaf reflectance spectra (Table 4), and biochemical constituents C_a, C_b, C_{ab}, C_{x+c} and ratios

Table 6
Determination coefficients (r^2) found for linear relationships (left on each cell), exponential (center) and 3rd order polynomial (right) between leaf optical indices and biochemical constituents ($n=605$)

	C_a	C_b	C_{ab}	C_{x+c}	C_a/C_b	C_a/C_{x+c}	C_b/C_{x+c}	C_{ab}/C_{x+c}
NDVI	0.26 0.52 0.37	0.23 0.43 0.35	0.26 0.50 0.37	0.25 0.41 0.31	0.05 0.09 0.08	0.37 0.48 0.48	0.18 0.22 0.31	0.33 0.41 0.45
RDVI	0.34 0.60 0.56	0.31 0.50 0.54	0.33 0.58 0.57	0.33 0.50 0.51	0.05 0.09 0.08	0.40 0.50 0.53	0.20 0.24 0.35	0.36 0.44 0.50
SR	0.36 0.56 0.37	0.34 0.52 0.35	0.36 0.56 0.37	0.31 0.42 0.31	0.01 0.02 0.07	0.46 0.53 0.49	0.29 0.33 0.31	0.44 0.50 0.46
MSR	0.34 0.58 0.36	0.32 0.52 0.35	0.34 0.57 0.36	0.30 0.44 0.31	0.02 0.04 0.08	0.46 0.54 0.48	0.26 0.31 0.31	0.42 0.50 0.45
G	0.53 0.32 0.60	0.50 0.36 0.57	0.53 0.34 0.60	0.44 0.32 0.51	0.00 0.00 0.04	0.27 0.20 0.39	0.23 0.20 0.26	0.28 0.21 0.37
ZM	**0.89 0.83 0.89**	**0.84 0.82 0.84**	**0.89 0.84 0.89**	**0.76 0.74 0.76**	0.00 0.00 0.04	0.68 0.64 **0.75**	0.45 0.46 0.47	0.65 0.62 **0.71**
VOG_1	**0.89 0.84 0.89**	**0.84 0.82 0.84**	**0.89 0.85 0.89**	**0.76 0.74 0.76**	0.00 0.01 0.05	0.69 0.65 **0.75**	0.46 0.46 0.47	0.66 0.63 **0.71**
VOG_2	**0.87 0.76 0.87**	**0.82 0.76 0.82**	**0.87 0.78 0.87**	**0.73** 0.69 **0.73**	0.00 0.00 0.03	0.63 0.57 **0.74**	0.43 0.43 0.46	0.60 0.56 0.69
VOG_3	**0.86 0.75 0.87**	**0.82 0.75 0.83**	**0.87 0.76 0.87**	**0.73** 0.68 **0.74**	0.00 0.00 0.03	0.62 0.56 **0.74**	0.42 0.42 0.47	0.59 0.55 0.69
GM_1	**0.87 0.82 0.88**	**0.84 0.82 0.84**	**0.88 0.84 0.88**	**0.76 0.74 0.76**	0.00 0.00 0.05	0.66 0.62 **0.73**	0.45 0.45 0.47	0.63 0.61 0.69
GM_2	**0.81 0.85 0.82**	**0.77 0.82 0.78**	**0.81 0.85 0.82**	0.69 **0.73 0.70**	0.00 0.01 0.05	**0.70** 0.68 **0.73**	0.46 0.48 0.46	0.66 0.66 0.69
CTR_1	0.16 0.25 0.22	0.14 0.22 0.20	0.16 0.25 0.22	0.15 0.20 0.20	0.01 0.02 0.02	0.19 0.22 0.25	0.09 0.12 0.14	0.17 0.20 0.23
CTR_2	0.41 **0.71** 0.65	0.37 0.61 0.61	0.41 0.69 0.65	0.38 0.56 0.55	0.05 0.09 0.09	0.52 0.64 0.66	0.27 0.33 0.42	0.47 0.57 0.62
RGI	0.35 0.12 0.54	0.35 0.17 0.53	0.35 0.14 0.55	0.27 0.14 0.48	0.02 0.03 0.06	0.12 0.06 0.29	0.14 0.11 0.20	0.14 0.08 0.28
BGI_1	0.10 0.10 0.14	0.09 0.09 0.13	0.09 0.10 0.14	0.08 0.08 0.13	0.00 0.000 0.00	0.08 0.08 0.10	0.05 0.05 0.06	0.07 0.07 0.10
BGI_2	**0.77** 0.64 **0.77**	**0.72** 0.64 **0.72**	**0.77** 0.65 **0.77**	0.66 0.59 0.66	0.00 0.00 0.00	0.51 0.46 0.58	0.35 0.35 0.39	0.49 0.45 0.56
BRI_1	0.01 0.02 0.02	0.00 0.02 0.01	0.01 0.02 0.02	0.00 0.01 0.01	0.00 0.00 0.00	0.02 0.03 0.03	0.01 0.01 0.01	0.02 0.02 0.02
BRI_2	0.35 0.53 0.36	0.31 0.46 0.31	0.35 0.52 0.35	0.33 0.42 0.33	0.03 0.05 0.05	0.40 0.46 0.44	0.21 0.25 0.23	0.36 0.42 0.39
CUR	0.33 0.41 0.33	0.30 0.40 0.30	0.33 0.41 0.33	0.27 0.31 0.28	0.00 0.00 0.01	0.36 0.39 0.38	0.24 0.28 0.24	0.35 0.38 0.36
LIC_1	0.23 0.48 0.33	0.21 0.38 0.31	0.23 0.46 0.33	0.23 0.38 0.29	0.05 0.10 0.08	0.32 0.42 0.43	0.15 0.18 0.27	0.28 0.36 0.41
LIC_2	0.25 0.39 0.28	0.22 0.34 0.24	0.25 0.38 0.27	0.23 0.31 0.26	0.02 0.04 0.06	0.30 0.35 0.37	0.15 0.19 0.19	0.27 0.32 0.33
LIC_3	0.08 0.21 0.10	0.08 0.17 0.09	0.08 0.20 0.10	0.08 0.17 0.10	0.02 0.04 0.08	0.14 0.19 0.17	0.06 0.08 0.08	0.12 0.16 0.15
SIPI	0.36 0.62 0.43	0.34 0.54 0.42	0.36 0.61 0.44	0.33 0.48 0.37	0.03 0.06 0.08	0.47 0.56 0.51	0.26 0.31 0.34	0.43 0.51 0.49
PRI_1	0.41 0.34 0.44	0.40 0.37 0.42	0.41 0.36 0.44	0.25 0.22 0.29	0.01 0.01 0.00	0.43 0.39 0.43	0.32 0.34 0.32	0.43 0.40 0.43
PRI_2	0.13 0.02 0.17	0.13 0.04 0.16	0.13 0.03 0.17	0.06 0.01 0.11	0.01 0.01 0.05	0.07 0.03 0.13	0.07 0.06 0.09	0.07 0.04 0.12
PRI_3	0.35 0.44 0.36	0.34 0.44 0.34	0.36 0.45 0.36	0.23 0.27 0.23	0.01 0.00 0.01	0.49 0.51 0.50	0.34 0.38 0.34	0.48 0.50 0.48
NPCI	0.04 0.11 0.05	0.03 0.08 0.04	0.03 0.11 0.05	0.03 0.08 0.06	0.03 0.04 0.05	0.09 0.12 0.11	0.02 0.04 0.03	0.07 0.09 0.08
SRPI	0.03 0.09 0.05	0.02 0.06 0.04	0.03 0.08 0.05	0.02 0.06 0.06	0.02 0.03 0.05	0.07 0.10 0.11	0.02 0.03 0.03	0.06 0.08 0.08
NPQI	0.01 0.01 0.01	0.00 0.01 0.01	0.01 0.01 0.00	0.01 0.01 0.00	0.01 0.00 0.01	0.01 0.01 0.01	0.01 0.01 0.01	0.01 0.01 0.01
MCARI	0.66 0.66 **0.79**	0.61 0.67 **0.74**	0.65 0.68 **0.79**	0.54 0.54 0.66	0.00 0.00 0.02	0.60 0.57 0.61	0.40 0.43 0.43	0.57 0.57 0.59
TCARI	**0.74 0.73 0.83**	0.69 **0.74 0.78**	**0.74 0.75 0.83**	0.61 0.60 **0.70**	0.01 0.00 0.01	0.65 0.61 0.65	0.45 0.48 0.45	0.62 0.62 0.62
OSAVI	0.29 0.56 0.47	0.27 0.46 0.45	0.29 0.54 0.47	0.29 0.45 0.41	0.05 0.09 0.08	0.38 0.49 0.52	0.19 0.23 0.34	0.34 0.43 0.49
$MCARI_1$	0.23 0.44 0.31	0.20 0.35 0.29	0.22 0.41 0.31	0.25 0.39 0.32	0.05 0.09 0.08	0.25 0.33 0.28	0.10 0.13 0.16	0.21 0.28 0.25
$MCARI_2$	0.23 0.46 0.34	0.20 0.37 0.31	0.22 0.44 0.34	0.25 0.39 0.34	0.05 0.09 0.08	0.27 0.37 0.32	0.12 0.15 0.19	0.24 0.31 0.30
$MTVI_1$	0.02 0.12 0.09	0.01 0.07 0.07	0.02 0.11 0.08	0.04 0.11 0.10	0.05 0.09 0.08	0.04 0.09 0.11	0.00 0.01 0.03	0.03 0.06 0.09
$MTVI_2$	0.00 0.02 0.01	0.00 0.00 0.08	0.00 0.01 0.02	0.01 0.02 0.07	0.05 0.08 0.08	0.00 0.02 0.06	0.00 0.01 0.04	0.01 0.001 0.03
TVI	0.01 0.04 0.21	0.01 0.01 0.19	0.01 0.03 0.20	0.00 0.03 0.19	0.05 0.09 0.08	0.00 0.03 0.18	0.01 0.01 0.09	0.00 0.01 0.16
MSAVI	0.36 0.62 0.54	0.33 0.53 0.52	0.36 0.61 0.54	0.35 0.51 0.48	0.04 0.08 0.08	0.43 0.53 0.53	0.22 0.27 0.35	0.39 0.47 0.50
MCARI/OSAVI	0.68 **0.82 0.87**	0.62 **0.78 0.81**	0.68 **0.82 0.86**	0.58 0.65 **0.74**	0.01 0.02 0.02	**0.70 0.73 0.72**	0.44 0.49 0.46	0.66 **0.70** 0.68
TCARI/OSAVI	**0.70 0.90 0.89**	0.64 **0.83 0.83**	0.69 **0.90 0.89**	0.62 **0.73 0.77**	0.02 0.04 0.06	**0.72 0.78 0.74**	0.43 0.49 0.47	0.67 **0.74 0.70**
$MCARI_1$/OSAVI	0.16 0.36 0.18	0.14 0.29 0.16	0.15 0.34 0.18	0.13 0.24 0.17	0.03 0.06 0.07	0.30 0.38 0.31	0.15 0.18 0.17	0.27 0.33 0.28
$MCARI_2$/OSAVI	0.09 0.15 0.12	0.09 0.14 0.11	0.10 0.15 0.12	0.06 0.08 0.09	0.00 0.00 0.01	0.18 0.18 0.19	0.12 0.12 0.12	0.17 0.18 0.18
$MTVI_1$/OSAVI	0.44 0.66 0.50	0.41 0.60 0.48	0.44 0.65 0.50	0.37 0.50 0.40	0.02 0.04 0.05	0.56 0.63 0.59	0.33 0.38 0.38	0.52 0.58 0.56
$MTVI_2$/OSAVI	0.60 **0.70** 0.67	0.56 0.69 0.64	0.60 **0.71** 0.67	0.49 0.55 0.53	0.00 0.01 0.03	0.62 0.64 0.64	0.42 0.46 0.44	0.60 0.63 0.62
TVI/OSAVI	0.53 **0.70** 0.62	0.49 0.66 0.60	0.53 **0.70** 0.62	0.45 0.54 0.50	0.01 0.02 0.04	0.59 0.64 0.63	0.37 0.42 0.42	0.56 0.61 0.60

Highlighted are results for $r^2>0.7$.

are shown in Table 6. The determination coefficients obtained for regression analysis using linear, exponential and 3rd order polynomials demonstrate the non-linearity between specific indices and the biochemical constituents. Red edge ratio indices are generally linear, such as the Vogelmann (VOG_2) or ZM index, yielding $r^2=0.87$ and $r^2=0.89$, respectively for C_{ab} (Fig. 9, top). Other indices showed a clear non-linear relationship with C_{ab}, such as those calculated from visible bands only or in addition to red edge wavelengths (OSAVI, $MCARI_1$, $MCARI_2$, MSAVI, PRI_3), and those indices calculated as combined with OSAVI (MCARI/OSAVI, TCARI/OSAVI, etc) (Fig. 9, center for PRI3 and TCARI/OSAVI). The best optical indices for correlation with C_{ab} in *V. vinifera* L. leaves were ZM ($r^2=0.89$, linear), VOG_1 ($r^2=0.89$, linear), VOG_2 ($r^2=0.87$, linear), VOG_3 ($r^2=0.87$, linear), GM_1 ($r^2=0.88$, linear), GM_2 ($r^2=0.85$, exponential), BGI_2 ($r^2=0.77$, linear), MCARI ($r^2=0.79$, 3rd order polynomial), TCARI ($r^2=0.83$, 3rd order polynomial), MCARI/OSAVI ($r^2=0.86$, 3rd order polynomial), and TCARI/OSAVI ($r^2=0.9$, exponential). As expected, indices traditionally used for vegetation monitoring, such as NDVI, SR or MSR did not obtain as good results as red edge and combined indices,

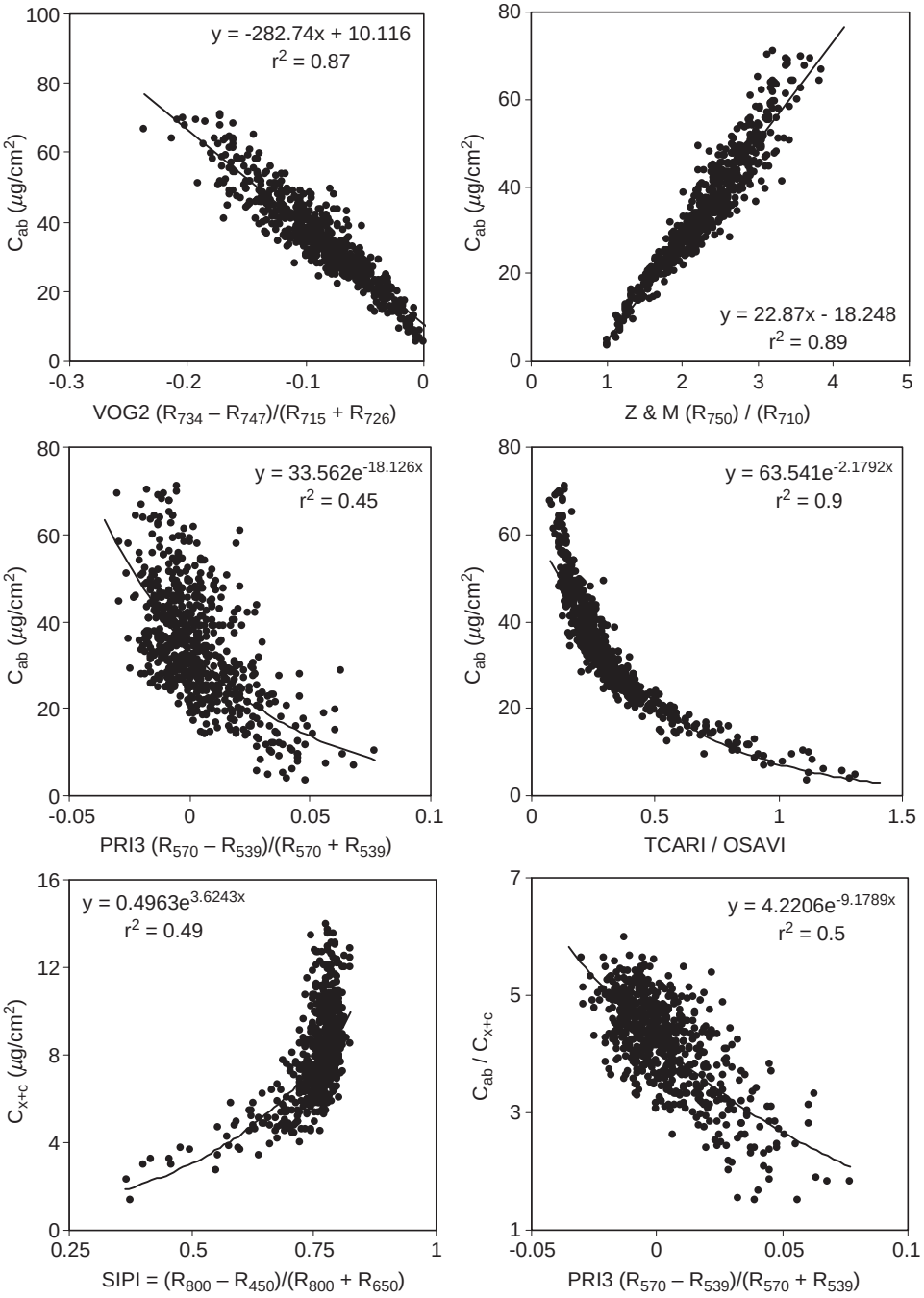

Fig. 9. Relationships obtained between C_{ab} and optical indices calculated from leaf reflectance spectra VOG_2 (upper left) and ZM (upper right), showing a non-linear behavior with PRI_3 (center left) and TCARI/OSAVI (center right), SIPI with C_{x+c} (bottom left) and PRI_3 with C_{ab}/C_{x+c} (bottom right).

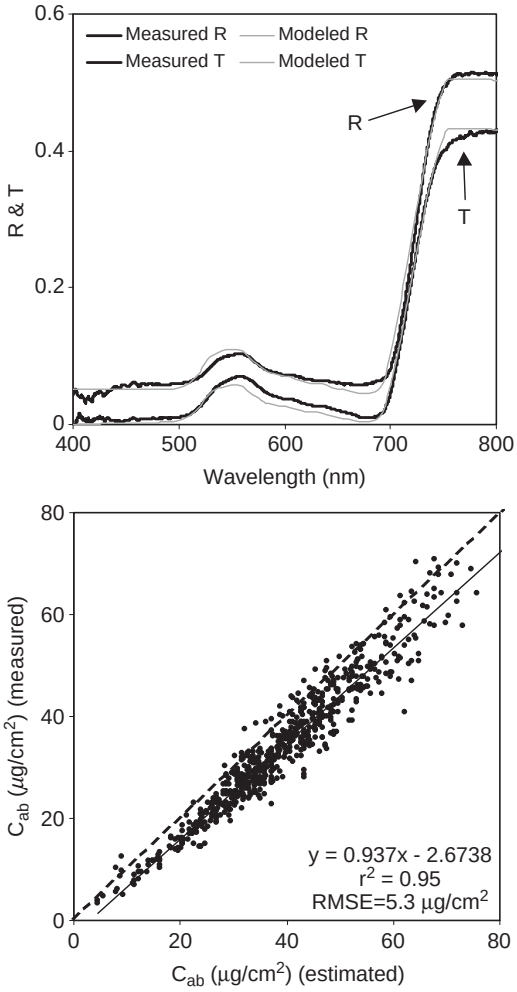

Fig. 10. Leaf reflectance and transmittance spectra measured with the Li-Cor 1800-12 integrating sphere and simulated with PROSPECT (top). Relationship obtained between the C_{ab} measured by destructive sampling and estimated by PROSPECT inversion using the leaf optical properties (bottom).

yielding $r^2=0.5$ (NDVI, exponential), $r^2=0.56$ (SR, exponential), and $r^2=0.57$ (MSR, exponential). Indices developed for maximizing its sensitivity to LAI while decreasing C_{ab} effects, such as $MCARI_2$ and $MTVI_2$ (Haboudane et al., 2004), demonstrated a low relationship with C_{ab}, as expected. Among these structural indices that are demonstrated to be highly related to LAI, $MTVI_2$ was shown in this study to be less affected by C_{ab} variations ($r^2=0.02$) than the $MCARI_2$ index ($r^2=0.44$, exponential).

Regression results for indices and C_{x+c} and ratios C_{ab}/C_{x+c} generally showed poorer relationships, obtaining $r^2=0.49$ for C_{x+c} with SIPI, and $r^2=0.5$ for C_{ab}/C_{x+c} with PRI_3 (Fig. 9, bottom). The PRI index developed for xanthophyll cycle pigment change detection (Gamon et al., 1992) was shown to be more related to the C_{ab}/C_{x+c} ratio ($r^2=0.5$, exponential) than to C_{ab} alone ($r^2=0.45$) and C_{x+c} ($r^2=0.27$). This result agrees with Sims and Gamon (2002) who suggested PRI as a potential indicator for carotenoid/chlorophyll ratio monitoring. With respect to chlorophyll a and b ratios, none of the indices proposed were related to the chlorophyll ratio C_a/C_b, all yielding poor results.

5.2. Estimation of C_{ab} by PROSPECT inversion in *V. vinifera* L. leaves

The *V. vinifera* L. leaf reflectance and transmittance database used for inversion with PROSPECT yielded a good agreement with the modeled spectra, obtaining an average RMSE=0.025 for the 605 leaves (Fig. 10, top). The input variables N, C_{ab} and C_m for PROSPECT, estimated for each leaf spectra by inversion using the iterative optimization method between 400 and 800 nm, yielded average values for the 605 leaves for N ($\mu=1.62$, $\sigma=0.14$), C_{ab} ($\mu=39.4$, $\sigma=13.4$), and C_m ($\mu=0.0035$, $\sigma=0.0012$). The relationship between the measured C_{ab} for each vine leaf, and the PROSPECT-inverted C_{ab} from the optical measurements on the same leaves yielded a determination coefficient of $r^2=0.95$ and RMSE=5.3 µg/cm^2 (Fig. 10, bottom). The PROSPECT model was shown to be valid for simulating the leaf optical properties of *V. vinifera* L. leaves, although a slight overestimation of C_{ab} was found when compared to the 1:1 relationship (yielding the RMSE=5.3 µg/cm^2 mentioned). The RMSE obtained is within the normal range of variation found in similar studies with other species that, in conjunction with the high determination coefficient obtained for this large database, demonstrates the applicability of PROSPECT to simulate the optical properties of *V. vinifera* L. leaves.

5.3. Estimation of C_{ab} by PROSPECT–rowMCRM in *V. vinifera* L. fields

The narrow-band indices that obtained the best relationships in the leaf-level study for C_{ab} estimation, plus the traditional index NDVI (Table 6), were calculated from the 103 sites of 10×10 m imaged by ROSIS and CASI sensors. Relationships were obtained between field-measured C_{ab} and the indices calculated from the airborne reflectance for all pixels falling within the 10×10 m site (pure vine+soil+shadows) and for

Table 7
Determination coefficients (r^2) obtained between ROSIS and CASI airborne optical indices and C_{ab} for the 103 study sites imaged

Indices calculated from ROSIS and CASI images	Chlorophyll content (C_{ab})	
	All pixels (soil+vegetation)	Pure vegetation pixels
NDVI	0.00	0.36
ZM	0.00	0.24
VOG_1	0.00	0.25
VOG_2	0.03	0.31
VOG_3	0.03	0.30
GM_1	0.11	0.07
GM_2	0.00	0.21
CTR_2	0.21	0.14
MCARI	0.40	**0.54**
TCARI	0.43	**0.58**
MCARI/OSAVI	**0.61**	**0.53**
TCARI/OSAVI	**0.59**	**0.55**
$MTVI_2$/OSAVI	0.25	**0.51**
TVI/OSAVI	0.23	0.49

Highlighted are results for $r^2>0.5$.

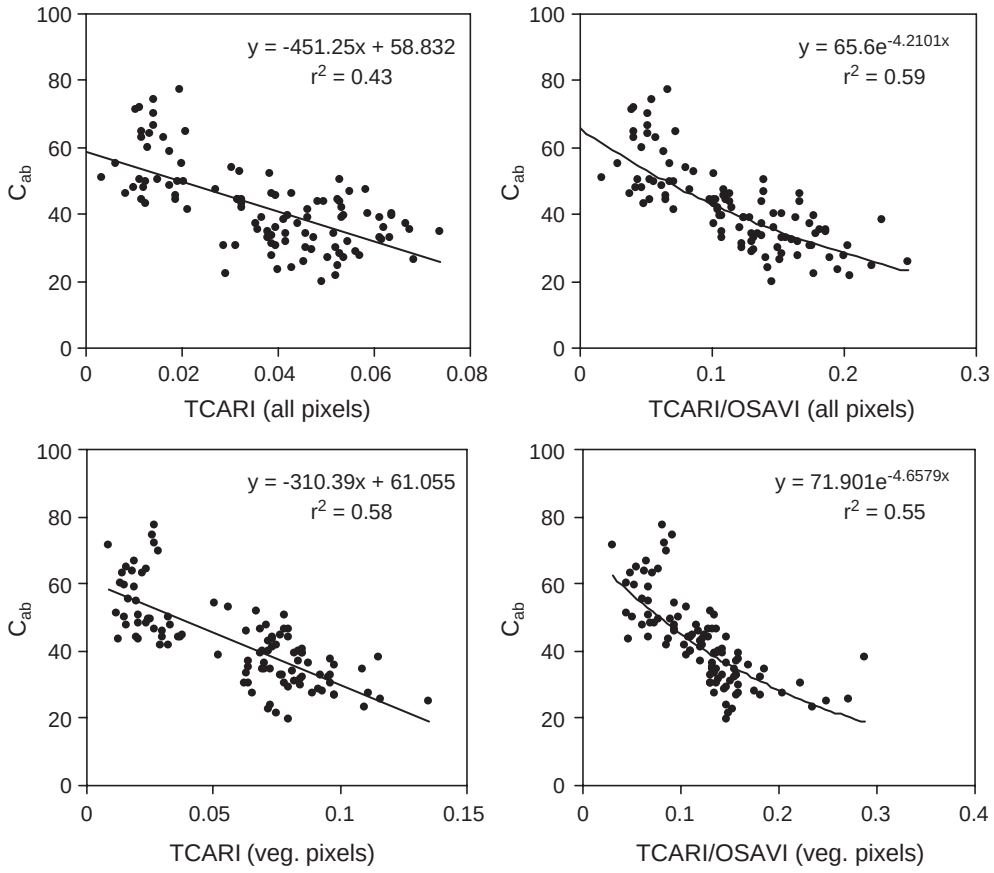

Fig. 11. Relationships obtained between C_{ab} and ROSIS and CASI indices TCARI (top and bottom left), and TCARI/OSAVI (top and bottom right) for aggregated pixels (top left and right) and pure vine pixels (bottom left and right).

the pure vine reflectance only at each study site as extracted with the high-resolution imagery (Table 7). Consistent with previous studies in non-homogeneous crop canopies (Zarco-Tejada et al., 2004), MCARI, TCARI, and combined indices MCARI/OSAVI and TCARI/OSAVI indices yielded the best relationships for both aggregated and pure vegetation pixels. MCARI (TCARI) yielded $r^2=0.40$ ($r^2=0.43$) for aggregated pixels, and $r^2=0.54$ ($r^2=0.58$) for pure vine pixels, showing the effects of soil and shadows on both indices (Fig. 11, top and bottom left for TCARI). Combined indices MCARI/OSAVI and TCARI/OSAVI showed less sensitivity to background effects, as expected, yielding $r^2=0.61$ and $r^2=0.59$ for aggregated pixels, respectively (Fig. 11 top and bottom right for TCARI/OSAVI). The TCARI/OSAVI index showed the greatest consistency when calculated for aggregated and pure vine pixels ($r^2=0.59$ for aggregated pixels; $r^2=0.55$ for pure vine pixels), suggesting this as the most robust narrow-band index for vineyard pigment content monitoring. Other vegetation indices that show significant results at the leaf-level, such as ZM ($r^2=0.89$ at leaf-level), $VOG_{1,\ 2,\ 3}$ ($r^2=0.8$), $GM_{1,\ 2}$ ($r^2=0.8$), and CTR_2 ($r^2=0.69$), were shown to be totally unsuccessful when applied to image-level aggregated pixels due to their high sensitivity to soil background ($r^2\sim0.1$), generating a maximum of $r^2\sim0.3$ when applied to pure vine pixels. The traditional NDVI index, generally used for vegetation biomass and vigor monitoring, yielded $r^2\sim0$ on aggregated pixels and $r^2=0.36$ on pure vine pixels, demonstrating that it is not appropriate for vineyard condition monitoring on non-homogeneous canopies imaged with spatial resolutions lower than 1 m pixel size due to the large background effects and low sensitivity to pigment concentration as indicator of physiological status.

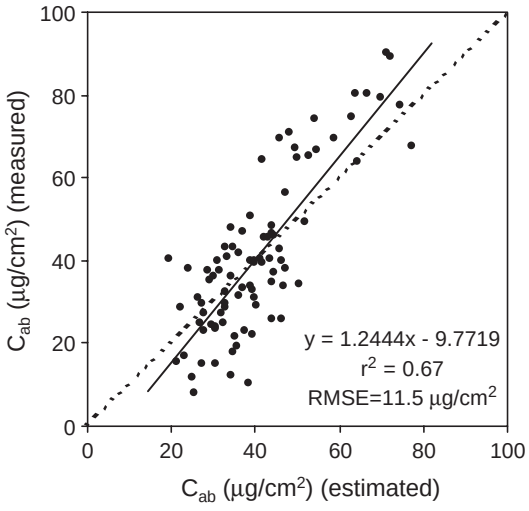

Fig. 12. Estimation of vine C_{ab} at the canopy level by scaling-up TCARI/OSAVI through PROSPECT linked to rowMCRM model.

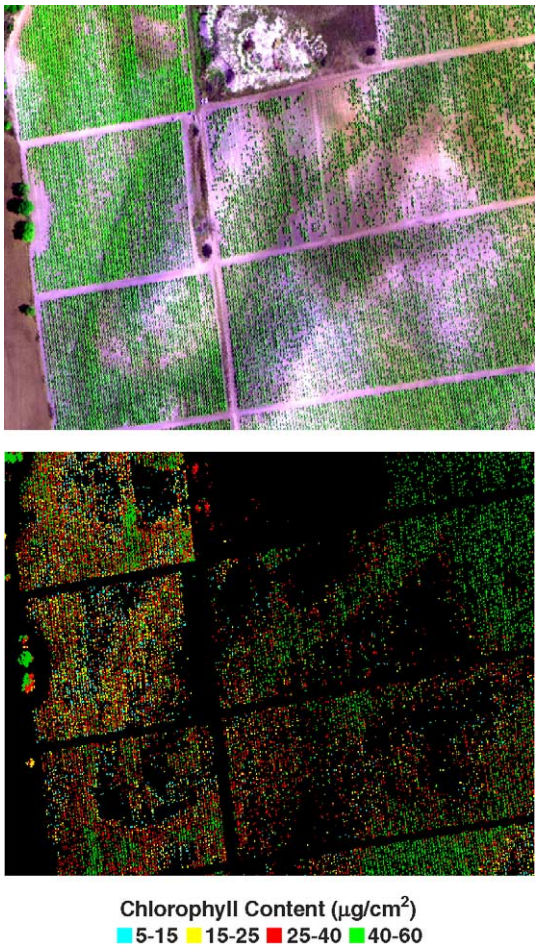

Fig. 13. Airborne CASI image of 1 m spatial resolution and 8 spectral bands (top) showing C_{ab} estimated with TCARI/OSAVI index through PROSPECT–rowMCRM linked models (bottom).

Prediction relationships obtained with PROSPECT–rowMCRM models as explained in the Methods section (Table 5; Fig. 8) when applied to the 103 study sites imaged by ROSIS and CASI airborne sensors yielded $r^2=0.67$ (RMSE=11.5 µg/cm^2) for C_{ab} estimation (Fig. 12). These results at leaf, canopy level for specific indices, and through *scaling-up* methods, suggest the successful retrieval capability of C_{ab} in row-structured vineyard canopies. An example of the natural variability detected in C_{ab} at the vine level in different fields imaged by the CASI sensor in July 2003 can be seen in Fig. 13, illustrating the C_{ab} product in 5 ranges of chlorophyll concentration. The provision of a C_{ab} product map in 5 steps is considered consistent with the RMSE=11.5 µg/cm^2 retrieval accuracy expected.

6. Conclusions

This study investigated the optical properties of *V. vinifera* L. leaves through reflectance and transmittance measurements, optical index calculation, and destructive determination of pigments using a large database of 1467 leaves collected in summer 2002 and 2003. Airborne campaigns imaged a total of 103 study sites from 24 vineyard fields with the ROSIS and CASI hyperspectral sensors at 1 m spatial resolution, studying the validity of optical indices generally used with success in other species at leaf and canopy levels through *scaling-up* simulation with PROSPECT and rowMCRM row-structured canopy reflectance model.

A measurement protocol using a Li-Cor 1800-12 integrating sphere attached to an Ocean Optics model USB2000 fiber spectrometer for stray-light corrected reflectance and transmittance measurements was presented. The measurement protocol consisted of a total of five measurements modifying the position of the collimated light, dark and white plugs of the integrating sphere to measure the reflectance and transmittance signals, reflectance internal standard, reflectance ambient, and dark measurement. The best optical indices for correlation with C_{ab} in *V. vinifera* L. leaves were ZM, VOG_1, VOG_2, VOG_3, GM_1, GM_2, BGI_2, MCARI, TCARI, MCARI/OSAVI, and TCARI/OSAVI (r^2 ranging between 0.8 and 0.9), with poor performance of traditional indices NDVI, SR or MSR. Linear relationships were found between red edge ratio indices such as ZM and VOG indices, whereas generally non-linear relationships were derived with combined indices and ratio indices with visible bands. Results for C_{x+c} and C_{ab}/C_{x+c} ratios yielded $r^2=0.49$ for C_{x+c} with SIPI, and $r^2=0.5$ for C_{ab}/C_{x+c} with PRI_3. The PRI index was shown as a potential indicator for carotenoid/chlorophyll ratio monitoring.

The inversion of PROSPECT model for N, C_{ab}, C_m and C_w estimation, using the large subset database of 605 vine leaf spectra, obtained an averaged RMSE of 0.025, yielding mean values of $N=1.62$, $C_{ab}=39.4$, $C_w=0.02$, and $C_m=0.0035$ ($r^2=0.95$ and RMSE=5.3 µg/cm^2 for C_{ab} estimation by inversion). Therefore these results demonstrate that the PROSPECT leaf model is valid for simulation of the optical properties of vine leaves as function of different pigment levels.

The leaf-level indices that produced the best correlations with C_{ab} were tested at the canopy level on vineyard reflectance spectra extracted from CASI and ROSIS hyperspectral images collected from 103 sites in 24 fields over 2 years. Results at the canopy level demonstrated that MCARI, TCARI, and combined indices MCARI/OSAVI and TCARI/OSAVI indices generated the best relationships for both aggregated and pure vegetation pixels. Combined indices MCARI/OSAVI and TCARI/OSAVI showed less sensitivity to background effects, yielding $r^2=0.61$ and $r^2=0.59$ for aggregated pixels containing pure vine, soil and shadow components. TCARI/OSAVI was the most consistent index for estimating C_{ab} on aggregated and pure vine pixels, yielding $r^2=0.59$ for aggregated pixels and $r^2=0.55$ for pure vine pixels. Physical methods based on PROSPECT linked to rowMCRM model enabled accounting for vineyard structure, row orientation, viewing geometry and background effects, indicating the large effects of the background and vine dimensions on the canopy reflectance. Predictive relationships were developed using PROSPECT–rowMCRM model between C_{ab} and TCARI/OSAVI as function of LAI, using field-measured vine dimensions and image-extracted soil background, row-orientation and viewing geometry. Model-based prediction relationships for C_{ab} content were successfully

applied to the 103 study sites imaged by ROSIS and CASI airborne sensors, yielding $r^2=0.67$ (RMSE=11.5 μg/cm^2).

Results presented in this manuscript indicate the validity of narrow-band indices for C_{ab} estimation and chlorosis detection at the leaf and canopy levels in *V. vinifera* L., demonstrating the validity of PROSPECT and rowMCRM models for leaf and canopy level estimations. This methodology for *scaling-up* leaf-level sensitive indices enabled conclusions to be reached on the effectiveness of biochemical constituent retrievals in canopies where model inversions are complex due to the large number of input parameters required to feed the linked leaf-canopy model.

Acknowledgments

The authors gratefully acknowledge the HySens HS2002-E1 project support provided through the *Access to Research Infrastructures* EU Program. Financial support from the Spanish Ministry of Science and Technology (MCyT) for the project AGL2002-04407-C03, and financial support to P.J. Zarco-Tejada under the *Ramón y Cajal* and *Averroes* Programs are also acknowledged. Financial support from the Natural Sciences and Engineering Research Council (NSERC) of Canada to permit contributions by J.R. Miller is gratefully acknowledged. We thank S. Holzwarth, A. Müeller and the rest of the DLR group, L. Gray and J. Freemantle from York University, and the INTA group for efficient airborne field campaigns with CASI, ROSIS, and DAIS sensors, providing coordination with field data collection. Fertiberia S.A. is acknowledged for providing determinations of foliar nutrients. A. Kuusk and J. Praks are gratefully acknowledged for sharing the rowMCRM code, and E. Vera-Toscano for providing valuable suggestions.

References

Allen, W. A., Gayle, & Richarson, A. J. (1970). Plant canopy irradiance specified by the Duntley equations. *Journal of the Optical Society of America*, *60*(3), 372–376.

Allen, W. A., Gausman, H. W., Richarson, A. J., & Thomas, J. R. (1969). Interaction of isotropic light with compact plan leaf. *Journal of the Optical Society of America*, *59*(10), 1376–1379.

Barnes, J. D. (1992). A reappraisal of the use of DMSO for the extraction and determination of chlorophylls a and b in lichens and higher plants. *Environmental Experimental Botany*, *2*, 85–100.

Ben-Dor, E., & Levin, N. (2000). Determination of surface reflectance from raw hyperspectral data without simultaneous ground data measurements: A case study of the GER 63-channel sensor data acquired over Naan, Israel. *International Journal of Remote Sensing*, *21*, 2053–2074.

Broge, N. H., & Leblanc, E. (2000). Comparing prediction power and stability of broadband and hyperspectral vegetation indices for estimation of green leaf area index and canopy chlorophyll density. *Remote Sensing of Environment*, *76*, 156–172.

Carter, G. A. (1991). Primary and secondary effects of water content of the spectral reflectance of leaves. *American Journal of Botany*, *78*, 916–924.

Carter, G. A. (1994). Ratios of leaf reflectances in narrow wavebands as indicators of plant stress. *International Journal of Remote Sensing*, *15*, 697–704.

Carter, G. A., Dell, T. R., & Cibula, W. G. (1996). Spectral reflectance characteristics and digital imagery of a pine needle blight in the southeastern United States. *Canadian Journal of Forest Research*, *26*, 402–407.

Carter, G. A., & Spiering, B. A. (2002). Optical properties of intact leaves for estimating chlorophyll concentration. *Journal of Environmental Quality*, *31*(5), 1424–1432.

Ceccato, P., Flasse, S., Tarantola, S., Jacquemoud, S., & Gregoire, J. M. (2001). Detecting vegetation leaf water content using reflectance in the optical domain. *Remote Sensing of Environment*, *77*, 22–33.

Chen, J. (1996). Evaluation of vegetation indices and modified simple ratio for boreal applications. *Canadian Journal of Remote Sensing*, *22*, 229–242.

Danson, F. M., Steven, M. D., Malthus, T. J., & Clarck, J. A. (1992). High-spectral resolution data for determining leaf water content. *International Journal of Remote Sensing*, *13*, 461–470.

Daughtry, C. S. T., Walthall, C. L., Kim, M. S., Brown de Colstoun, E., & McMurtrey, J. E. III (2000). Estimating corn leaf chlorophyll concentration from leaf and canopy reflectance. *Remote Sensing of the Environment*, *74*, 229–239.

Dobrowski, S. Z., Ustin, S. L., & Wolpert, J. A. (2002). Remote estimation of vine canopy density in vertically shoot-positioned vineyards: determining optimal vegetation indices. *Australian Journal of Grape and Wine Research*, *8*(2), 117–125.

Dobrowski, S. Z., Ustin, S. L., & Wolpert, J. A. (2003). Grapevine dormant pruning weight prediction using remotely sensed data. *Australian Journal of Grape and Wine Research*, *9*(3), 177–182.

Fernandez-Escobar, R., Moreno, R., & Garcia-Creus, M. (1999). Seasonal changes of mineral nutrients in olive leaves during the alternate-bearing cycle. *Scientia Horticulturae*, *82*, 24–45.

Fourty, T., & Baret, F. (1997). Vegetation water and dry matter contents estimated from top-of-the-atmosphere reflectance data: A simulation study. *Remote Sensing of Environment*, *61*(1), 34–45.

Fuentes, D. A., Gamon, J. A., Qiu, H., Sims, D. A., & Roberts, D. A. (2001). Mapping Canadian boreal forest vegetation using pigment and water absorption features derived from AVIRIS sensor. *Journal of Geophysical Research*, *106*, 33565–33577.

Gamon, J. A., Peñuelas, J., & Field, C. B. (1992). A narrow-waveband spectral index that tracks diurnal changes in photosynthetic efficiency. *Remote Sensing of Environment*, *41*, 35–44.

Gamon, J. A., & Surfus, J. S. (1999). Assessing leaf pigment content and activity with a reflectometer. *New Phytologist*, *143*, 105–117.

Gao, B.-C. (1996). NDWI — a normalized difference water index for remote sensing of vegetation liquid water from space. *Remote Sensing of Environment*, *58*, 257–266.

Gitelson, A. A., Gritz, Y., & Merzlyak, M. N. (2003). Relationships between leaf chlorophyll content and spectral reflectance and algorithms for non-destructive chlorophyll assessment in higher plants. *Journal of Plant Physiology*, *160*(3), 271–282.

Gitelson, A. A., & Merzlyak, M. N. (1996). Signature analysis of leaf reflectance spectra: Algorithm development for remote sensing of chlorophyll. *Journal of Plant Physiology*, *148*, 494–500.

Gitelson, A. A., & Merzlyak, M. N. (1997). Remote estimation of chlorophyll content in higher plant leaves. *International Journal of Remote Sensing*, *18*, 2691–2697.

Haboudane, D., Miller, J. R., Pattey, E., Zarco-Tejada, P. J., & Strachan, I. (2004). Hyperspectral vegetation indices and novel algorithms for predicting green LAI of crop canopies: Modeling and validation in the context of precision agriculture. *Remote Sensing of Environment*, *90*(3), 337–352.

Haboudane, D., Miller, J. R., Tremblay, N., Zarco-Tejada, P. J., & Dextraze, L. (2002). Integration of hyperspectral vegetation indices for prediction of crop chlorophyll content for application to precision agriculture. *Remote Sensing of Environment*, *81*(2–3), 416–426.

Hall, A., Lamb, D. W., Holzapfel, B., & Louis, J. (2002). Optical remote sensing applications in viticulture — A review. *Australian Journal of Grape and Wine Research*, *8*(1), 36–47.

Hall, A., Louis, J., & Lamb, D. (2003). Characterising and mapping vineyard canopy using high-spatial-resolution aerial multispectral images. *Computers and Geosciences*, *29*, 813–822.

Harron, J. (2000). Optical properties of phytoelements in conifers. MSc. Thesis, York University, Toronto, Canada.

Horler, D. N. H., Dockray, M., & Barber, J. (1983). The red edge of plant leaf reflectance. *International Journal of Remote Sensing*, *4*(2), 273–288.

Huete, A. R. (1988). A soil-adjusted vegetation index (SAVI). *Remote Sensing of the Environment*, *25*, 295–309.

Jacquemoud, S., & Baret, F. (1990). Prospect: A model of leaf optical properties spectra. *Remote Sensing of Environment*, *34*, 75–91.

Jacquemoud, S., Ustin, S. L., Verdebout, J., Schmuck, G., Andreoli, G., & Hosgood, B. (1996). Estimating leaf biochemistry using the PROSPECT leaf optical properties model. *Remote Sensing of Environment*, *56*, 194–202.

Johnson, L. F. (2003). Temporal stability of an NDVI–LAI relationship in a Napa Valley vineyard. *Australian Journal of Grape and Wine Research*, *9*(2), 96–101.

Johnson, L. F., Bosch, D. F., Williams, D. C., & Lobitz, B. M. (2001). Remote sensing of vineyard management zones: Implications for wine quality. *Applied Engineering in Agriculture*, *17*(4), 557–560.

Johnson, L. F., Roczen, D. E., Youkhana, S. K., Nemani, R. R., & Bosch, D. F. (2003). Mapping vineyard leaf area with multispectral satellite imagery. *Computers and Electronics in Agriculture*, *38*, 33–44.

Jolley, V. D, & Brown, J. C. (1994). Genetically controlled uptake and use of iron by plants. In J. A. Manthey, D. E. Crowley, & D. G. Luster (Eds.), *Biochemistry of metal micronutrients in the rhizosphere* (pp. 251–266). Boca Raton: Lewis Publishers.

Jordan, C. F. (1969). Derivation of leaf area index from quality of light on the forest floor. *Ecology*, *50*, 663–666.

Kim, M. S., Daughtry, C. S. T., Chappelle, E. W., McMurtrey III, J. E., & Walthall, C. L. (1994). *The use of high spectral resolution bands for estimating absorbed photosynthetically active radiation (Apar)*. 6th symp. on physical measurements and signatures in remote sensing. Jan. 17–21, 1994, Val D'Isere, France.

Kuusk, A. (1995). A Markov chain model of canopy reflectance. *Agricultural and Forest Meteorology*, *76*, 221–236.

Kuusk, A. (1995). A fast, invertible canopy reflectance model. *Remote Sensing of Environment*, *51*, 342–350.

Lagacherie, P., Collin-Bellier, C., & Goma-Fortin, N. (2001). Analysing rate and spatial variability of vinestock mortality in a Languedocian vineyard from high resolution aerial photographs. *Journal International des Sciences de la Vigne et du Vin*, *35*(3), 141–148.

Lamb, D. W., Weedon, M. M., & Bramley, R. G. V. (2004). Using remote sensing to predict grape phenolics and colour at harvest in a Cabernet Sauvignon vineyard: Timing observations against vine phenology and optimising resolution. *Australian Journal of Grape and Wine Research*, *10*(1), 46–54.

Lanjeri, S., Melia, J., & Segarra, D. (2001). A multi-temporal masking classification method for vineyard monitoring in central Spain. *International Journal of Remote Sensing*, *16*, 3167–3186.

le Maire, G., François, C., & Dufrêne, E. (2004). Towards universal broad leaf chlorophyll indices using PROSPECT simulated database and hyperspectral reflectance measurements. *Remote Sensing of Environment*, *89*, 1–28.

Lichtenhaler, H. K., Lang, M., Sowinska, M., Heisel, F., & Mieh, J. A. (1996). Detection of vegetation stress via a new high resolution fluorescence imaging system. *Journal of Plant Physiology*, *148*, 599–612.

Li-Cor Inc. (1984), *Li-Cor model 1800-12 integrating sphere instruction manual* (Revision 1984). Li-Cor Incorporated, 4421 Superior Street, PO Box 4425 Lincoln Nebraska, USA, Publication No. 8305-0034.

Marschner, H., Romheld, V., & Kissel, M. (1986). Different strategies in higher plants in mobilization and uptake of iron. *Journal of Plant Nutrition*, *9*, 695–713.

Montero, F. J., Meliá, J., Brasa, A., Segarra, D., Cuesta, A., & Lanjeri, S. (1999). Assessment of vine development according to available water resources by using remote sensing in La Mancha, Spain. *Agricultural Water Management*, *40*, 363–375.

O'Neill, N. T., Zagolski, F., Bergeron, M., Royer, A., Miller, J. R., & Freemantle, J. (1997). Atmospheric correction validation of CASI images acquired over the BOREAS southern study area. *Canadian Journal of Remote Sensing*, *23*, 143–162.

Peñuelas, J., Filella, I., Lloret, P., Muñoz, F., & Vilajeliu, M. (1995). Reflectance assessment of mite effects on apple trees. *International Journal of Remote Sensing*, *Vol. 16–14*, 2727–2733.

Peñuelas, J., Gamon, J. A., Fredeen, A. L., Merino, J., & Field, C. B. (1994). Reflectance indices associated with physiological changes in nitrogen- and water-limited sunflower leaves. *Remote Sensing of Environment*, *48*, 135–146.

Peñuelas, J., Piñol, J., Ogaya, R., & Filella, I. (1997). Estimation of plant water concentration by the reflectance water index (R900/R970). *International Journal of Remote Sensing*, *18*, 2869–2875.

Qi, J., Chehbouni, A., Huete, A. R., Keer, Y. H., & Sorooshian, S. (1994). A modified soil vegetation adjusted index. *Remote Sensing of Environment*, *48*, 119–126.

Rondeaux, G., Steven, M., & Baret, F. (1996). Optimization of soil-adjusted vegetation indices. *Remote Sensing of Environment*, *55*, 95–107.

Rougean, J. -L., & Breon, F. M. (1995). Estimating PAR absorbed by vegetation from bidirectional reflectance measurements. *Remote Sensing of Environment*, *51*, 375–384.

Rouse, J. W., Haas, R. H., Schell, J. A., Deering, D. W., & Harlan, J. C. (1974). Monitoring the vernal advancements and retrogradation of natural vegetation. *NASA/GSFC final report*. MD, USA: Greenbelt 371 pp.

Schultz, H. R. (1996). Leaf absorptance of visible radiation in *Vitis vinifera* L.: Estimates of age and shade effects with a simple field method. *Scientia Horticulturae*, *66*(1-2), 93–102.

Sims, D. A., & Gamon, J. A. (2002). Relationships between leaf pigment content and spectral reflectance across a wide range of species, leaf structures and developmental stages. *Remote Sensing of Environment*, *81*, 337–354.

Tagliavini, M., & Rombolà, A. D. (2001). Iron deficiency and chlorosis in orchard and vineyard ecosystems. *European Journal of Agronomy*, *15*, 71–92.

Vogelmann, J. E., Rock, B. N., & Moss, D. M. (1993). Red edge spectral measurements from sugar maple leaves. *International Journal of Remote Sensing*, *14*, 1563–1575.

Wallace, A. (1991). Rational approaches to control of iron deficiency other than plant breeding and choice of resistant cultivars. *Plant Soil*, *130*, 281–288.

Wellburn, A. R. (1994). The spectral determination of chlorophylls a and b, as well as total carotenoids using various solvents with spectrophotometers of different resolutions. *Journal of Plant Physiology*, *144*, 307–313.

Zarco-Tejada, P. J., Berjón, A., Morales, A., Miller, J. R., Agüera, J., Cachorro, V., et al. (2003). Leaf biochemistry estimation on EU high-value crops with ROSIS and DAIS hyperspectral data and radiative transfer simulation. *3rd EARSeL workshop on imaging spectroscopy* (pp. 597–602). Germany: Munich.

Zarco-Tejada, P. J., Miller, J. R., Mohammed, G. H., & Noland, T. L. (2000). Chlorophyll fluorescence effects on vegetation apparent reflectance: I. Leaf-level measurements and simulation of reflectance and transmittance spectra. *Remote Sensing of Environment*, *74*(3), 582–595.

Zarco-Tejada, P. J., Miller, J. R., Mohammed, G. H., Noland, T. L., & Sampson, P. H. (2001). Scaling-up and model inversion methods with narrow-band optical indices for chlorophyll content estimation in closed forest canopies with hyperspectral data. *IEEE Transactions on Geoscience and Remote Sensing*, *39*(7), 1491–1507.

Zarco-Tejada, P. J., Miller, J. R., Morales, A., Berjón, A., & Agüera, J. (2004). Hyperspectral indices and model simulation for chlorophyll estimation in open-canopy tree crops. *Remote Sensing of Environment*, *90*(4), 463–476.

Zarco-Tejada, P. J., Whiting, M., & Ustin, S. L. (2005). Temporal and spatial relationships between within-field yield variability in cotton and high-spatial hyperspectral remote sensing imagery. *Agronomy Journal*, *Vol. 97*(No. 3), 641–653.

Radiometría de Campo para calibración de Imágenes Aeroportadas

Marcos Jiménez
Área de Teledetección del INTA
jimenezmm@inta.es

Introducción

La adquisición de firmas espectrales de superficies naturales y artificiales en campo tiene dos objetivos importantes para la teledetección **(**Curtiss y Goetz, 1994**)**: (a) análisis e interpretación de la imagen mediante librerías espectrales de materiales con escalas espaciales que no tienen que ser iguales a las de la imagen; (b) calibración y validación de imágenes donde las escalas espaciales entre imagen y firma espectral tienen si deben ser equiparables.

La imagen hiperespectral aeroportada es una de las técnicas de teledetección con mayor capacidad de estudio y seguimiento de la superficies terrestres, al elevado muestreo espectral de los sensores hiperespectrales se suma la flexibilidad y control mediante la adquisición desde plataformas aéreas. Una gran exactitud de las reflectancias en el terreno a partir de este tipo de sensores es un requisito ya indispensable, para ello se aplican métodos físicos basados en códigos de transferencia radiativa o métodos empíricos normalmente basados en la adquisición de firmas espectrales de campo. Esta parte del seminario "avances en espectro-radiometría" repasa las características de estos métodos empíricos que permiten una calibración de la imagen a reflectancia en el terreno, pero antes algo de terminología en calibración de imágenes **(**Glosarios CEOS y Landsat):

- Calibración: es el conjunto de procesos que definen la respuesta de un sensor frente a una señal controlada.
- Calibración radiometrica de laboratorio: coeficientes de calibración a radiancia en el sensor en instalaciones de condiciones ambientales controladas (temperatura y humedad) frente a un estándar (ej: esferas de calibración).
- Calibración a reflectancia: transformación a reflectancia en el terreno en base a superficies de reflectancia conocida.
- Calibración Vicaria: calibración radiométrica de un sensor en vuelo/orbita mediante medidas externas a la calibración de laboratorio. Puede ser en base a radiancias en el sensor o a reflectancias en el terreno.

1. Imagen hiperespectral Aeroportada

Las condiciones de vuelo y alturas sobre el terreno con las que son adquiridas las imágenes hiperespectrales aeroportadas imponen determinados aspectos radiométricos y geométricos que es necesario compensar. Desde el punto de vista de la radiometría, y como se puede ver en la Figura 1, la interferencia atmosférica en la región espectral de 350 a 2500 nm es muy similar a la sufrida desde satélites muy por encima de la atmósfera.

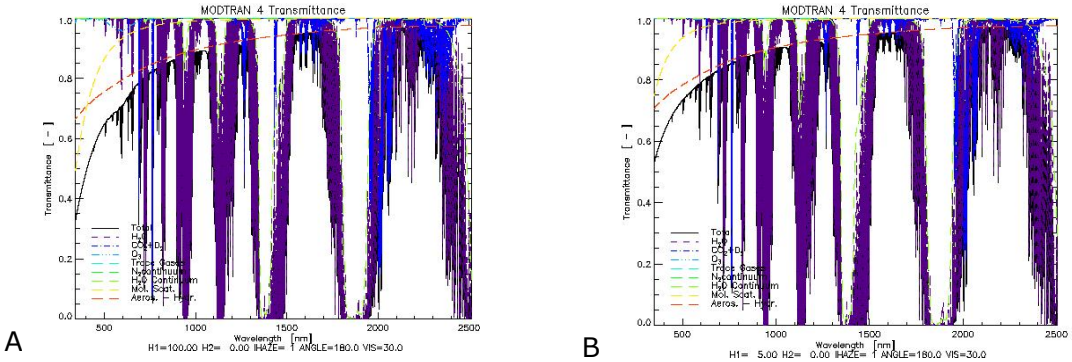

A B

Figura 1: Transmisividad atmosférica [350-2500 nm] a 100 Km sobre el nivel del mar (A) y a 5 km sobre el nivel del mar (B)

Los métodos de corrección geométrica y radiométrica de imágenes hiperespectrales se han desarrollado mucho en los últimos años para conseguir precisiones y exactitudes muy exigentes. Una de las mayores particularidades de las imágenes aeroportadas frente a las adquiridas desde plataformas espaciales, es que muchas veces el estudio de una zona de escala local o regional comprende la adquisición de varias pasadas que alargan el tiempo de adquisición (1 hora de media) que hace que la variabilidad en atmósfera pero sobre todo iluminación sea importante.

Es importante evaluar la aplicación de calibración a reflectancia en la caso de una única imagen sobre una zona elegida con superficies idóneas como es el caso de la calibración vicaria, el caso de una única imagen de una zona concreta de estudio donde las superficies de calibración no sean las idóneas y un último caso para la corrección atmosférica aplicada a un conjunto de las imágenes que forman un mosaico de salida.

2. Protocolo de Radiometría de Campo para Calibración

La calibración de imágenes a reflectancia en el terreno requiere de la adquisición de firmas espectrales de campo sobre superficies homogéneas a la escala de la imagen y del equipo de campo. La caracterización y fiabilidad de la reflectancia espectral de estas superficies requieren de un protocolo de selección de sitios y toma de medidas.

El Área de Teledetección del INTA aplica un protocolo de radiometría de campo para la calibración y validación de sus sensores hipererspectrales basado en los protocolos existentes: (1) para la a la selección, tipo y número de sitios se basa en CSTARS [Universidad de California]; (2) para la el método de adquisición se basa en el del la Universidad de Valencia para las campañas de calibración/validación de la ESA **(**www.uv.es/leo/sen2flex/). En este caso la toma de firmas espectrales se realiza con un seguimiento continuo de las radiancias del blanco de referencia y de la superficie a lo largo de la campaña, este seguimiento asegura la evaluación de la calidad de las reflectancias ya que los cambios de iluminación debidos al cambio de posición solar o a cirros puede ser en determinadas ocasiones muy importantes.

Así mismo para asegurar la aplicación de estas medidas con diversos objetivos se requiere de la incorporación de metadatos sobre las reflectancia medidas en cuanto a: instrumentación, superficie y condiciones meteorológicas (Huni)**.**

3. Calibración a Reflectancia

La corrección del efecto atmosférico tiene que tener en cuanta lo siguientes factores: la influencia de la atmósfera, la iluminación solar y sus variaciones, adyacencia la geometría de observación y la rugosidad del terreno. Las condiciones atmosféricas mas variables son sobre todo el contenido de vapor de agua, el tipo de aerosoles y la visibilidad.

Los métodos de corrección atmosférica se pueden dividir en: (1) modelos físicos basados en códigos de transferencia radiativa y a datos del estado atmosférico, actualmente MODTRAN4 (Berk et al, 2000) y 6S (Vermote et al., 1997). Para la corrección de imágenes aeroportadas hiperespectrales se han desarrollado diversas aplicaciones, a partir de estos códigos, que automatizan las variaciones en imágenes aeroporadas ATREM, ACORN, FLASH, HATCH ATCOR4; (2) métodos empíricos que a su vez se dividen en dos tipos según obtengan la información directamente de la imagen o de espectros de campo tomados por espectrorradiometría de campo.

En teledetección hiperespectral el método mas utilizado es Empirical line (Roberts, 1985), basado en la reflectancia espectral de superficies "oscuras" y "brillantes" que estiman mediante regresión lineal la transformación de nivel digital o radiancia en el sensor a reflectancia en el terreno. Este método asume una atmósfera constante en toda la imagen/imágenes y que las superficies son de respuesta lambertiana. En esta parte se muestra la comparación de la corrección atmosférica con ATCOR4 (www.rese.ch/atcor/atcor4/index.html) y de calibración a reflectancia mediante firmas de un ASD FieldSpec 3 (www.asdi.com/products/fieldspec-3) aplicadas a varias imágenes de los sensores hiperespectales aerportados que opera el Área de Teledección del INTA AHS y CASI1500i.

Referencias

Curtiss, B., & Goetz, A.F.H. (1994). Field spectrometry: techniques and instrumentation. *Proceedings of an International Symposium on Spectral Sensing Research.*

HYRESSA AM8 Report 2007 .FP6 - Research Infrastructures - Accompanying Measure Instrument: SSA.

Ground-Truth Data Collection Protocol For Hyperspectral Remote Sensing. Robert Zomer and Susan Ustin. University of California Davis.
http://www.cstars.ucdavis.edu/classes/hsgrdtutorial.html

A. Hüni, J. Nieke, J. Schopfer, M. Kneubühler and K. I. Itten*. The spectral database SPECCHIO for improved long term usability and data sharing.* Remote Sensing Laboratories, University of Zurich, Winterthurerstrasse 190, 8057 Zurich, Switzerland.

SVC Spectra Vista Corporation www.spectravista.com

FAMILY OF FIELD PORTABLE SPECTRORADIOMETERS							
INSTRUMENT	**GER 1500**	**GER 2600**	**GER 3700**	**SVC MR-768**	**SVC HR-768S**	**SVC HR-768**	**SVC HR-1024**
Spectral Range	350 nm-1050 nm	350 nm-2500 nm	350 nm-2500 nm	350 nm-2500 nm	350 nm-1900 nm	350 nm-2500 nm	350 nm-2500 nm
Spectral Resolution FWHM	3.1 nm @700 nm	3.2 nm @ 700 nm 30 nm @1500/2100 nm	3.2 nm @700 nm 19 nm @1500 nm 28 nm @2100 nm	3.5 nm @ 700 nm 22 nm @1500 nm 22 nm @2100 nm	3.5 nm @ 700 nm 9.5 nm @1500 nm	3.5 nm @ 700 nm 16 nm @1500 nm 14 nm @2100 nm	3.5 nm @ 700 nm 9.5 nm @1500 nm 6.5 nm @2100 nm
Bandwidth	1.5 nm @700	1.5 nm @700 11.5 nm @ 1500	1.5 nm @700 nm 6.5 nm @1500 nm 9.5 nm @2100 nm	1.5 nm @700 nm 5.8 nm @1500 nm 5.8 nm @2100 nm	1.5 nm @700 nm 3.5 nm @1500 nm	1.5 nm @700 nm 7.5 nm @1500 nm 5.0 nm @2100 nm	1.5 nm @700 nm 3.8 nm @1500 nm 2.5 nm @2100 nm
Integration Times	5 ms & up	5-50 ms & up	5-50 ms & up	1-10 ms & up	1-10 ms & up	1-10 ms & up	1-10 ms & up
Detectors	512 Si Array	512 Si Array 128 PbS Array	512 Si Array 128 PbS Array 64 PbS Array	512 Si Array 256 InGaAs Array	512 Si Array 256 InGaAs Array	512 Si Array (2) 128 InGaAs Arrays	512 Si Array 256 InGaAs Array 256 Ext. InGaAs Array
Foreoptics Available	4° & 8° FO	3° & 10°	3° & 10°	4° std., 8° and 14° foreoptics, irradiance spheres, reflectance probes are optioinal			
Fiber Optic Light Guide	.25° Field Replaceable	.25° Field Replaceable	.25° Field Replaceable	25° fiber optic light guides are available in various lengths (Field replaceable)			
Instrument Weight	4 lbs or 2 kg	11.5 lbs or 5.3 kg	13.8 lbs or 6.3 kg	7.3 lbs or 3.3 kg			
Battery Weight	0.5 lbs or 0.23 kg	5 lbs or 2.3 kg	5 lbs or 2.3 kg	1lb or 0.45 kg			
Stand Alone Measurements	Standard	Not Available	Not Available	Stand Alone Capability is Standard-No Field Computer is Required			
Rugged PDA	Optional	Not Available	Not Available	A Rugged PDA with Internal GPS and Bluetooth is Supplied with the System			
Noise Equivalent Radiance w/cm^2/nm/sr at 1 sec.	0.5 x 10^{-3} @ 700 nm	1.6 x 10^{-5} @ 700 nm 9.0x 10^{-5} @ 1500 nm 9.0x 10^{-5} @ 2100 nm	1.6 x 10^{-5} @ 700 nm 1.1x 10^{-5} @ 1500 nm 1.1x 10^{-5} @ 2100 nm	1.2 x 10^{-5} @ 700 nm 2.2 x 10^{-5} @ 1500 nm 2.2 x 10^{-5} @ 2100 nm	1.2 x 10^{-5} @ 700 nm 1.5 x 10^{-5} @ 1500 nm	1.2 x 10^{-5} @ 700 nm 2.2 x 10^{-5} @ 1500 nm 2.2 x 10^{-5} @ 2100 nm	0.8 x 10^{-5} @ 700 nm 1.5x 10^{-5} @ 1500 nm 3.0x 10^{-5} @ 2100 nm
Notebook Computer SW	Supplied	Supplied	Supplied	Supplied	Supplied	Supplied	Supplied

Instrumentos disponibles en el mercado. Análisis comparativo

Ángela De Santis
INSA
angela.de.santis@insa.org

www.asdi.com

FieldSpec® 3

Designed by researchers, for researchers to perform solar spectral reflectance, radiance, and irradiance measurements.

Spectral Range	350-2500 nm
Spectral Resolution	3 nm @ 700 nm 10 nm @ 1400/2100 nm
Sampling Interval	1.4 nm @ 350-1050 nm 2 nm @ 1000-2500 nm
Scanning Time	100 milliseconds
Detectors	One 512 element Si photodiode array 350-1000 nm Two separate, TE cooled, graded index InGaAs photodiodes 1000-2500 nm
Input	1.5 m fiber optic (25° field of view) Optional foreoptics available
Noise Equivalent Radiance (NEdL)	UV/VNIR 1.1 x 10^{-9} W/cm^2/nm/sr @700 nm NIR 2.4 x 10^{-9} W/cm^2/nm/sr @ 1400 nm NIR 4.7 x 10^{-9} W/cm^2/nm/sr @ 2100 nm
Weight	12 lbs (5.2 kg)
Calibrations	Wavelength, reflectance, radiance*, irradiance* All calibrations are NIST traceable (*radiometric calibrations are optional)

FieldSpec® 3 Hi-Res

Higher resolution in the SWIR1 and 2 regions for greater definition of hard-to-resolve features often found in minerals and soils.

Spectral Range	350-2500 nm
Spectral Resolution	3 nm @ 700 nm 8.5 nm @ 1400 nm 6.5 nm @ 2100 nm
Sampling Interval	1.4 nm @ 350-1050 nm 2 nm @ 1000-2500 nm
Scanning Time	100 milliseconds
Detectors	One 512 element Si photodiode array 350-1000 nm Two separate, TE cooled, graded index InGaAs photodiodes 1000-2500 nm
Input	1.5 m fiber optic (25° field of view) Optional foreoptics available
Noise Equivalent Radiance (NEdL)	UV/VNIR 1.1 x 10^{-9} W/cm^2/nm/sr @700 nm NIR 2.2 x 10^{-9} W/cm^2/nm/sr @ 1400 nm NIR 4.0 x 10^{-9} W/cm^2/nm/sr @ 2100 nm
Weight	12 lbs (5.2 kg)
Calibrations	Wavelength, reflectance, radiance*, irradiance* All calibrations are NIST traceable (*radiometric calibrations are optional*)

FieldSpec® 3 Max

Maximum Signal-to-Noise ratios for Maximum performance in the SWIR2 region.

Spectral Range	350-2500 nm
Spectral Resolution	3 nm @ 700 nm 10 nm @ 1400/2100 nm
Sampling Interval	1.4 nm @ 350-1050 nm 2 nm @ 1000-2500 nm
Scanning Time	100 milliseconds
Detectors	One 512 element Si photodiode array 350-1000 nm Two separate, TE cooled, graded index InGaAs photodiodes 1000-2500 nm
Input	1.5 m fiber optic (25° field of view) Optional foreoptics available
Noise Equivalent Radiance (NEdL)	UV/VNIR 1.1 x 10^{-9} W/cm^2/nm/sr @700 nm NIR 2.2 x 10^{-9} W/cm^2/nm/sr @ 1400 nm NIR 4.0 x 10^{-9} W/cm^2/nm/sr @ 2100 nm
Weight	12 lbs (5.2 kg)
Calibrations	Wavelength, reflectance, radiance*, irradiance* All calibrations are NIST traceable (*radiometric calibrations are optional*)

Ocean Optics
inventors of the world's first miniature spectrometer
www.oceanoptics.com

USB2000+ Miniature Fiber Optic Spectrometer

Physical	
Dimensions:	89.1 mm x 63.3 mm x 34.4 mm
Weight:	190 grams
Detector	
Detector:	Sony ILX511B linear silicon CCD array
Detector range:	200-1100 nm
Pixels:	2048 pixels
Pixel size:	14 µm x 200 µm
Pixel well depth:	~62,500 electrons
Sensitivity:	75 photons/count at 400 nm; 41 photons/count at 600 nm
Optical Bench	
Design:	f/4, Symmetrical crossed Czerny-Turner
Focal length:	42 mm input; 68 mm output
Entrance aperture:	5, 10, 25, 50, 100 or 200 µm wide slits or fiber (no slit)
Grating options:	14 different gratings, UV through Shortwave NIR
HC-1 grating option:	No
Detector collection lens option:	Yes, L2
OFLV filter options:	OFLV-200-850; OFLV-350-1000
Other bench filter options:	Longpass OF-1 filters
Collimating and focusing mirrors:	Standard or SAG+
UV enhanced window:	Yes, UV2
Fiber optic connector:	SMA 905 to 0.22 numerical aperture single-strand optical fiber
Spectroscopic	
Wavelength range:	Grating dependent
Optical resolution:	~0.3-10.0 nm FWHM
Signal-to-noise ratio:	250:1 (at full signal)
A/D resolution:	16 bit
Dark noise:	50 RMS counts
Dynamic range:	2 x 10^8 (system); 1300:1 for a single acquisition
Integration time:	1 ms to 65 seconds
Stray light:	<0.05% at 600 nm; <0.10% at 435 nm
Corrected linearity:	>99.8%
Electronics	
Power consumption:	250 mA @ 5 VDC
Data transfer speed:	Full scans to memory every 1 ms with USB 2.0 or 1.1 port, 300 ms with serial port
Inputs/Outputs:	No
Analog channels:	No
Auto nulling:	No
Breakout box compatibility:	No
Trigger modes:	3 modes
Strobe functions:	Yes
Gated delay feature:	Yes
Connector:	22-pin connector
Computer	
Operating systems:	Windows 98/Me/2000/XP, Mac OS X and Linux with USB port; Any 32-bit Windows OS with serial port
Computer interfaces:	USB 2.0 @ 480 Mbps; RS-232 (2-wire) @ 57.6 K baud
Peripheral interfaces:	I2C inter-integrated circuit

USB4000 Miniature Fiber Optic Spectrometer

Physical	
Dimensions:	89.1 mm x 63.3 mm x 34.4 mm
Weight:	190 grams
Detector Specifications	
Detector:	Toshiba TCD1304AP Linear CCD array
Detector range:	200-1100 nm
Pixels:	3648 pixels
Pixel size:	8 µm x 200 µm
Pixel well depth:	100,000 electrons
Signal-to-noise ratio:	300:1 (at full signal)
A/D resolution:	16 bit
Dark noise:	50 RMS counts
Corrected linearity:	>99.8%
Sensitivity:	130 photons/count at 400 nm; 60 photons/count at 600 nm
Optical Bench	
Design:	f/4, Asymmetrical crossed Czerny-Turner
Focal length:	42 mm input; 68 mm output
Entrance aperture:	5, 10, 25, 50, 100 or 200 µm wide slits or fiber (no slit)
Grating options:	14 different grating options, UV through Shortwave NIR
HC-1 grating option:	No
Detector collection lens option:	Yes, L4
DET4 filter options:	DET4-200-850; DET4-350-1000
Other bench filter options:	Longpass OF-1 filters
Collimating and focusing mirrors:	Standard or SAG+UPG
UV enhanced window:	Yes, UV4
Fiber optic connector:	SMA 905 to 0.22 numerical aperture single-strand optical fiber
Spectroscopic	
Wavelength range:	Grating dependent
Optical resolution:	~0.3-10.0 nm FWHM (grating dependent)
Signal-to-noise ratio:	300:1 (at full signal)
A/D resolution:	16 bit
Dark noise:	50 RMS counts
Integration time:	3.8 ms - 10 seconds
Dynamic range:	2 x 10^8 (system), 1300:1 for a single acquisition
Stray light:	<0.05% at 600 nm; 0.10% at 435 nm
Electronics	
Power consumption:	250 mA @ 5 VDC
Data transfer speed:	Full spectrum to memory every 4 ms with USB 2.0 port
Inputs/Outputs:	Yes, 8 onboard digital user-programmable GPIOs
Analog channels:	No
Auto nulling:	Yes
Breakout box compatible:	Yes, with the USB-ADP-BB adapter
Trigger modes:	4 modes
Strobe functions:	Yes
Connector:	22-pin connector
Computer	
Operating systems:	Windows 98/Me/2000/XP, Mac OS X and Linux with USB port; Any 32-bit Windows OS with serial port
Computer interfaces:	USB 2.0 @ 480 Mbps (USB1.1 compatible); RS-232 (2-wire) @ 115.2 K baud

HR4000 High-Resolution Spectrometer

Physical	
Dimensions:	148.6 mm x 104.8 mm x 45.1 mm
Weight:	570 grams
Detector	
Detector:	Toshiba TCD1304AP linear CCD array
Detector range:	200-1100 nm
Pixels:	3636 pixels
Pixel size:	8 µm x 200 µm
Pixel well depth:	~100,000 electrons
Sensitivity:	130 photons/count at 400 nm; 60 photons/count at 600 nm
Optical Bench	
Design:	f/4, Symmetrical crossed Czerny-Turner
Focal length:	101.6 mm input and output
Entrance aperture:	5, 10, 25, 50, 100 or 200 µm wide slits or fiber (no slit)
Grating options:	14 different gratings, UV through Shortwave NIR
HC-1 grating option:	provides 200-1050 nm range (best efficiency)
Detector collection lens option:	Yes, L4
OFLV filter options:	OFLV-200-1100
Other bench filter options:	Longpass OF-1 filters
Collimating and focusing mirrors:	Standard or SAG+UPG-HR
UV enhanced window:	Yes, UV4
Fiber optic connector:	SMA 905 to 0.22 numerical aperture single-strand optical fiber
Spectroscopic	
Wavelength range:	Grating dependent
Optical resolution:	~0.02-8.4 nm FWHM
Signal-to-noise ratio:	300:1 (at full signal)
A/D resolution:	14 bit
Dark noise:	12 RMS counts
Dynamic range:	2 x 10^8 (system); 1300:1 for a single acquisition
Integration time:	3.8 ms to 10 seconds
Stray light:	<0.05% at 600 nm; <0.10% at 435 nm
Corrected linearity:	>99.8%
Electronics	
Power consumption:	450 mA @ 5 VDC
Data transfer speed:	Full scans to memory every 4 ms with USB 2.0 port
Inputs/Outputs:	Yes, 10 onboard digital user-programmable GPIOs
Analog channels:	One 13-bit analog input; one 9-bit analog output
Auto nulling:	No
Breakout box compatibility:	Yes, HR4-BREAKOUT
Trigger modes:	4 modes
Strobe functions:	Yes
Gated delay feature:	No
Connector:	30-pin connector
Computer	
Operating systems:	Windows 98/Me/2000/XP, Mac OS X and Linux with USB port; Any 32-bit Windows OS with serial port
Network Access:	Remora's USB interface adapts for Ethernet Connectivity
Computer interfaces:	USB 2.0 @ 480 Mbps; RS-232 (2-wire) @ 115.2 K baud
Peripheral interfaces:	SPI (3-wire); I2C inter-integrated circuit

Ocean Optics

inventors of the world's first miniature spectrometer

HR2000+ High-resolution Spectrometer

Physical	
Dimensions:	148.6 mm x 104.8 mm x 45.1 mm
Weight:	570 grams
Detector	
Detector:	Sony ILX511B linear silicon CCD-array
Detector range:	200-1100 nm
Pixels:	2048 pixels
Pixel size:	14 µm x 200 µm
Pixel well depth:	~62,500 electrons
Sensitivity:	75 photons/count at 400 nm; 41 photons/count at 600 nm
Optical Bench	
Design:	f/4, Symmetrical crossed Czerny-Turner
Focal length:	101.6 mm input and output
Entrance aperture:	5, 10, 25, 50, 100 or 200 µm wide slits or fiber (no slit)
Grating options:	14 different gratings, UV through Shortwave NIR
HC-1 grating option:	provides 200-1100 nm range
Detector collection lens option:	Yes, L2
OFLV filter options:	OFLV 200-1100 nm
Other bench filter options:	Longpass OF-1 filters
Collimating and focusing mirrors:	Standard or SAG+UPG-HR
UV enhanced window:	Yes, UV2
Fiber optic connector:	SMA 905 to 0.22 numerical aperture single-strand optical fiber
Spectroscopic	
Wavelength range:	Grating dependent
Optical resolution:	~0.035-6.8 nm FWHM
Signal-to-noise ratio:	250:1 (at full signal)
A/D resolution:	14 bit
Dark noise:	12 RMS counts
Dynamic range:	2 x 10^8 (system); 1300:1 for a single acquisition
Integration time:	1 ms to 65 s (20 s typical max.)
Stray light:	<0.05% at 600 nm; <0.10% at 435 nm
Corrected linearity:	>99.8%
Electronics	
Power consumption:	220 mA @ 5 VDC
Data transfer speed:	Full scans to memory every 1 ms with USB 2.0 port, 15 ms with USB 1.1 port
Inputs/Outputs:	Yes, 10 onboard digital user-programmable GPIOs
Analog channels:	One 13-bit analog input; one 9-bit analog output
Auto nulling:	No
Breakout box compatibility:	Yes, HR4-BREAKOUT
Trigger modes:	4 modes
Strobe functions:	Yes
Gated delay feature:	No
Connector:	30-pin connector
Computer	
Operating systems:	Windows 98/Me/2000/XP, Mac OS X and Linux with USB port; Any 32-bit Windows OS with serial port
Network Access:	Remora's USB interface adapts for Ethernet Connectivity
Computer interfaces:	USB 2.0 @ 480 Mbps; RS-232 (2-wire) @ 115.2 K baud
Peripheral interfaces:	SPI (3-wire); I2C inter-integrated circuit

QE65000-FL Scientific-grade Spectrometer

Physical	
Dimensions:	182 mm x 110 mm x 47 mm
Weight:	1.18 kg (without power supply)
Detector	
Detector:	Hamamatsu S7031-1006
Detector range:	200-1100 nm
Pixels:	1024 x 58 (1044 x 64 total pixels)
Pixel size:	24.576 μm^2
Pixel well depth:	1000 Ke-
Sensitivity:	~0.065 counts / e-
Quantum efficiency:	90% peak; 65% at 250 nm
Optical Bench	
Design:	f/4, Symmetrical crossed Czerny-Turner
Focal length:	101.6 mm input and output
Entrance aperture:	5, 10, 25, 50, 100 or 200 µm wide slits or fiber (no slit)
Grating options:	14 different grating options, UV through Shortwave NIR
HC1-QE grating option:	provides UV-Shortwave NIR coverage
Detector collection lens option:	None
OFLV filter options:	OFLV-QE (200-950 nm); OFLV-QE-250 (250-1000 nm); OFLV-QE-300 (300-1050 nm); OFLV-QE-350 (350-1100 nm); OFLV-QE-400 (400-1150 nm)
Other bench filter options:	Longpass OF-1 filters
Collimating and focusing mirrors:	Standard only
UV enhanced window:	No
Fiber optic connector:	SMA 905 to 0.22 numerical aperture single-strand optical fiber
Spectroscopic	
Wavelength range:	Grating dependent
Optical resolution:	~0.14-7.7 nm FWHM
Signal-to-noise ratio:	1000:1 (at full signal)
A/D resolution:	16 bit
Dark noise:	3 RMS counts
Dynamic range:	7.5 x 10^9 (system), 25000:1 for a single acquisition
Integration time:	8 ms to 15 minutes
Stray light:	<0.08% at 600 nm; 0.4% at 435 nm
Corrected linearity:	>99.8%
Electronics	
Power consumption:	500 mA @ 5 VDC (no TE cooling); 3.5 A @ 5 VDC (with TE cooling)
Data transfer speed:	Full scans to memory every 7 ms with USB 2.0 port, 18 ms with USB1.1 port, 300 ms with serial port
Inputs/Outputs:	10 onboard digital user-programmable GPIOs (general purpose inputs/outputs)
Analog channels:	No
Auto nulling:	Yes
Breakout box compatibility:	Yes, HR4-BREAKOUT
Trigger modes:	4 modes
Strobe functions:	No
Gated delay feature:	Yes
Connector:	30-pin connector
Power-up time:	<5 seconds
Dark current:	4000 e-/pixel/sec @ 25 °C; 200 e-/pixel/sec @ 0 °C

Computer	
Operating systems:	Windows 98/Me/2000/XP, Mac OS X and Linux with USB port; Any 32-bit Windows OS with serial port
Computer interfaces:	USB 2.0 @ 480 Mbps; RS-232 (2-wire) @ 115.2 K baud
Network Access:	Remora's USB interface adapts for Ethernet Connectivity
Peripheral interfaces:	SPI (3-wire); I2C inter-integrated circuit
Temperature and Thermoelectric (TE) Cooling	
Temperature limits:	0 °C to 50.0 °C; no condensation
Set point:	Software controlled; lowest set point is 40 °C below ambient
Stability	+/-0.1 °C of set temperature in <2 minutes

Measurement and analysis of bidirectional reflectance data

Juha Suomalainen, Jouni Peltoniemi, and Teemu Hakala
Finnish Geodetic Institute, Box 15, 02431 Masala, Finland
E-Mail: juha.suomalainen@fgi.fi; Tel. +358-9-47-890-410; Fax: +358-9-29555211

1. Reflectance factors

Reflectance factor (RF) is defined as a ratio of radiances reflected from a target and from a Lambertian surface, while illumination and observer are held constant. [1] RF equals zero for completely black surface, and equals one for an ideal white isotropic surface. However, unity is not the maximum value for RF, if the reflectance distribution is anisotropic. However, when RF is averaged over all view directions, the result is always smaller than unity.
This anisotropy in reflectance is described with concepts such as Bidirectional Reflectance Factor (BRF) and Hemispherical-Directional Reflectance Factor (HDRF). BRF is a reflectance factor where both illumination and observation are assumed to unidirectional. By definition, HDRF assumes isotropic hemispherical illumination and directional observation. The first one is a good approximation for a reflectance factor measured in laboratory. In natural sunlight, sample is illuminated, for some part, from all directions and thus term HDRF is commonly used for sunlit reflectance factor.

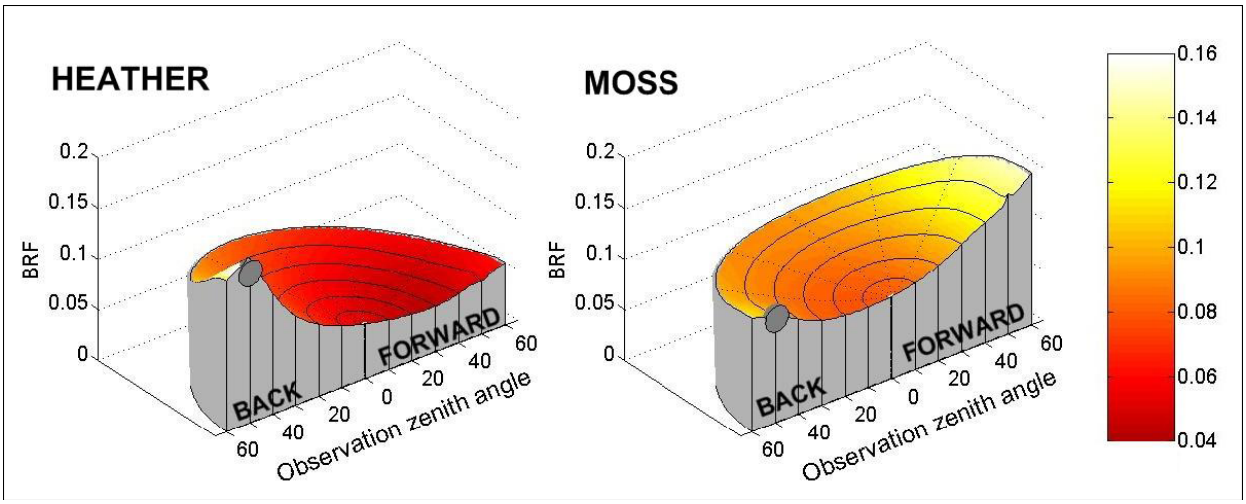

Figure 1 Smoothed BRFs of two different types of samples plotted as a function of view direction. The wavelength is 550 nm (green). The height in the center depicts BRF at nadir view. Heather is a strong backscatterer, while moss scatters strongly forward. The direction of illumination, at 50° zenith angle, is marked with a gray ball.

2. Bidirectional reflectance effects

Bidirectional reflectance behavior of natural surfaces is affected by numerous properties of the surface; most clearly single scattering spectrum and 3D structure both in macroscopic and microscopic scale. In nature, targets have wide variations in BRFs (Figure 1): some are backscatterers; some scatter mostly forward; some are darkest to nadir and brighten to lower view angles; some have a clear specular glare; etc. [2-7] As natural surfaces are complex in structure, there are no general models to accurately predict BRF/HDRF behavior.

Generally, the most distinct BRF distributions are result of single scattering processes. In single scattering, shadows of 3D structure and individual shining surfaces create distinct scattering features. Single scattering is dominant on dark objects where multiple scattering is diminished by the absorptions. Multiply scattered light is generally more isotropic due to higher randomization of directions. Thus bright objects usually

have more isotropic BRFs than dark ones. Due to the varying single scattering spectrum, which is common in e.g. vegetation and snow, BRF behavior is not constant over wavelength. However, usually the general trend of forward or backward scattering holds.

3. Measuring BRF/HDRF on ground

BRF and HDRF are measured similarly as any reflectance factor. Reflected radiance is measured first from a reference target, most commonly Spectralon panel, and then from the sample of interest. To form a BRF/HDRF dataset, the measurement is repeated multiple times from various directions using a goniometer setup. Some well known goniometers are EGO [8], FIGOS/LAGOS [9], Automated spectro-goniometer [10], CLabSpeG [11], and FIGIFIGO [12, 13]; of which the last one is discussed here more precisely.

Finnish Geodetic Institute Field Goniospectrometer (FIGIFIGO) can measure BRF/HDRF of a sample, 5–25 cm in diameter, in 10–20 minutes. FIGIFIGO exploits ASD FieldSpec PRO FR spectrometer and has a spectral range from 350–2500 nm. The system fits inside an estate car and it is operational within 5–15 minutes after arriving to the site. Optionally, FIGIFIGO can also measure linearly polarized reflectance factors. If diffuse light measurements are taken, it is also possible to estimate BRF from sunlit HDRF measurements.
FIGIFIGO has been developed mostly for field use and it has various built in features to enable easy and reliable use on field: battery powered operation; a pyranometer to record variation in illumination; a Sun compass for orientation; a GPS-receiver to give input for exact Sun position calculation; and two inclinometers to measure tilt of goniometer body and arm.

Figure 2. Finnish Geodetic Institute Field Goniospectrometer (FIGIFIGO) measuring asphalt reflectance. FIGIFIGO has automated zenith turn sequence, but it is manually rotated around the sample.

A BRF/HDRF dataset typically consist of a number of datapoints each containing a reflectance factor spectrum, view direction (as zenith and azimuth angles), and illumination direction. The FIGIFIGO data are stored to *Finnish Geodetic Institute (FGI) Reflectance Library* and they can be accessed using *FGI Reflectance Toolbox for Matlab.*

Currently, FGI Reflectance Library contains BRFs and HDRFs of more than 150 samples, mostly concentrating on snow, boreal forest understorey vegetation, and manmade surfaces observable in remote sensing. These data and tools can be inquired from the author.

4. An application on empirical line method

A common need for goniometer measurements is in the production of aerial reflectance factor images with empirical line method. In empirical line method, two (or more) objects of known reflectance are selected from images. A linear conversion model is fitted on the object pixel radiances and the known reflectances, allowing calculation of a

reflectance image. Results of best accuracy can be reached by measuring the reflectance factors of the reference objects in-situ, concurrent to the aerial images. Preferably, these measurements are taken with a goniometer to take image view direction into account.

FGI has utilized a MD4-200 (Microdrones GmbH, Germany) unmanned aerial vehicle (UAV) for close range aerial photography. (Figure 3) The UAV is mounted with a small consumer camera (Ricoh GR II). Despite the radiometrically low quality camera, by applying various calibrations and an empirical line method, accurate reflectance images can be calculated.

In spring 2009, the UAV setup was tested on capability to measure a HDRF map of a small snow covered area. HDRF calibrated reflectance reference targets were placed on around the area and the UAV was programmed to take 31 images from all directions. The images were georeferenced and converted to reflectances to form a HDRF map of the area. The preliminary results show that the UAV acquired HDRF map is in very close agreement with simultaneous FIGIFIGO measurement.

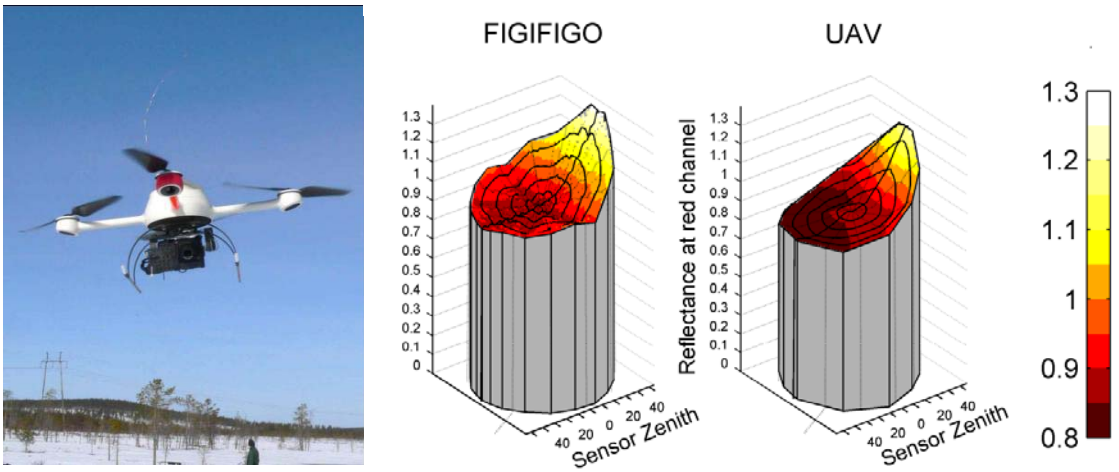

Figure 3. (Left) MD4-200 unmanned aerial vehicle (UAV) carrying a small consumer camera. (Middle and right) HDRFs of snow pack, at green band, as measured using FIGIFIGO and as combined from empirical line calibrated UAV images.

5. Conclusions

Bidirectional reflectance effects affect all passive remote sensing, working as source of both error and information. Thus BRF and HDRF measurements, using goniometers, are needed in various applications, including testing and development of light scattering models and calibration and validation sensors. In operational stage, bidirectional reflectances data are produced by e.g. MISR, POLDER, and CHRIS/PROBA satellites. These multiangular data are used to improve classification results and to retrieve surface albedo, forest parameters, etc.

References

1. NICODEMUS, F.E.; RICHMOND, J.C.; HSIA, J.J.; GINSBERG, I.W.; LIMPERIS, T. IN *GEOMETRICAL CONSIDERATIONS AND NOMENCLATURE FOR REFLECTANCE,* INSTITUTE FOR BASIC STANDARDS, NATIONAL BUREAU OF STANDARDS: WASHINGTON D.C., USA, 1977.

2. PELTONIEMI, J.I.; NÄRÄNEN, J.; KAASALAINEN, S.; MATIKAINEN, L.; PIIRONEN, J. MEASUREMENTS OF SNOW BRDF. *REMOTE SENS. ENVIRON.* **2003**.

3. PELTONIEMI, J.I.; KAASALAINEN, S.; NÄRÄNEN, J.; RAUTIAINEN, M.; STENBERG, P.; SMOLANDER, H.; SMOLANDER, S.; VOIPIO, P. BRDF MEASUREMENT OF UNDERSTORY VEGETATION IN PINE FORESTS: DWARF SHRUBS, LICHEN AND MOSS. *REMOTE SENS. ENVIRON.* **2005**, *94*, 343-354.

4. PELTONIEMI, J.I.; KAASALAINEN, S.; NÄRÄNEN, J.; MATIKAINEN, L.; PIIRONEN, J. MEASUREMENT OF DIRECTIONAL AND SPECTRAL SIGNATURES OF LIGHT REFLECTANCE BY SNOW*. IEEE TRANS. GEOSCI. REMOTE SENS.* **2005***, 43*, 2294-2304.

5. PELTONIEMI, J.I.; PIIRONEN, J.; NÄRÄNEN, J.; SUOMALAINEN, J.; KUITTINEN, R.; MARKELIN, L.; HONKAVAARA, E. BIDIRECTIONAL REFLECTANCE SPECTROMETRY OF GRAVEL AT THE SJÖKULLA TEST FIELD*. J. PHOTOGRAM. REMOTE SENS.* **2007***, 62*, 434-446.

6. SUOMALAINEN, J.; HAKALA, T.; PUTTONEN, E.; PELTONIEMI, J.I. POLARISED BIDIRECTIONAL REFLECTANCE FACTOR MEASUREMENTS FROM VEGETATED LAND SURFACES*. J. QUANT. SPECTROSC. RADIAT. TRANSF.* **2009**.

7. PUTTONEN, E.; SUOMALAINEN, J.; HAKALA, T.; PELTONIEMI, J.I. MEASUREMENT OF REFLECTANCE PROPERTIES OF ASPHALT SURFACES AND THEIR USABILITY AS REFERENCE TARGETS FOR AERIAL PHOTOS*. IEEE TRANS. GEOSCI. REMOTE SENS.* **2009**.

8. MEISTER, G.; ROTHKIRCH, A.; HOSGOOD, B.; SPITZER, H.; BIENLEIN, J. ERROR ANALYSIS FOR BRDF MEASUREMENTS AT THE EUROPEAN GONIOMETER FACILITY*. REMOTE SENS. REV.* **2000***, 19*, 111-131.

9. SCHOPFER, J.; DANGEL, S.; KNEUBÜHLER, M.; ITTEN, K.I. THE IMPROVED DUAL-VIEW FIELD GONIOMETER SYSTEM FIGOS*. SENSORS* **2008***, 8*, 5120-5140.

10. PAINTER, T.H.; PADEN, B.; DOZIER, J. AUTOMATED SPECTRO-GONIOMETER: A SPHERICAL ROBOT FOR THE FIELD MEASUREMENT OF THE DIRECTIONAL REFLECTANCE OF SNOW*. REV. SCI. INSTR.* **2003***, 74*, 5179-5188.

11. BILIOURIS, D.; VERSTRAETEN, W.W.; DUTRÉ, P.; VAN AARDT, J.A.; MUYS, B.; COPPIN, P. A COMPACT LABORATORY SPECTRO-GONIOMETER (CLABSPEG) TO ASSESS THE BRDF OF MATERIALS. PRESENTATION, CALIBRATION AND IMPLEMENTATION ON FAGUS SYLVATICA L. LEAVES*. SENSORS* **2007***, 7*, 1846-1870.

12. SUOMALAINEN, J.; HAKALA, T.; PELTONIEMI, J.I.; PUTTONEN, E. POLARISED MULTIANGULAR REFLECTANCE MEASUREMENTS USING THE FINNISH GEODETIC INSTITUTE FIELD GONIOSPECTROMETER*. SENSORS* **2009***, 9*, 3891-3907.

13. HAKALA, T. IMPROVEMENTS, CALIBRATION AND ACCURACY OF THE FINNISH GEODETIC INSTITUTE FIELD GONIOSPECTROMETER **2009**.

Sensores Infrarrojos. Instrumentación, Protocolos de medidas y Aplicaciones

José A. Sobrino, Juan C. Jiménez, Guillem Sòria, Juan Cuenca, Belén Franch, Victoria Hidalgo, Rosa Oltra, Yves Julien, Cristian Mattar
Unidad de Cambio Global, Laboratorio de Procesado de Imágenes, Universidad de Valencia

Resumen

En esta charla se presenta un resumen de las actividades realizadas por la Unidad de Cambio Global de la Universidad de Valencia con respecto a las medidas de campo relacionadas con la teledetección térmica, que es aquella que utiliza sensores que registran la radiancia emitida por las superficies en la región del infarrojo térmico, generalmente entre los 8 y 13 micrómetros. En esta región espectral las principales variables a medir son la temperatura y la emisividad espectral de la superficie terrestre, por lo que este trabajo se centra en las técnicas de medida y obtención de dichos parámetros.

Para presentar los distintos sensores térmicos utilizados en los últimos años por nuestra unidad de investigación, se distinguen tres niveles: i) instrumentación de campo (a nivel de superficie), ii) sensores aerotransportados (por tanto instalados a bordo de un avión volando a baja altura) y iii) sensores a bordo de satélites (y por tanto orbitando a gran altura por encima de la atmósfera). Las medidas de temperatura y emisividad realizadas con la instrumentación de campo se utilizan para calibrar y validar las estimaciones de estas variables a partir de imágenes de teledetección obtenidas tanto a partir de sensores aerotransportados como de sensores a bordo de satélites.

El principal problema a resolver cuando se trabaja en el infrarrojo térmico es la separación entre la temperatura y la emisividad, ya que son dos variables acopladas. En este trabajo se muestran dos técnicas para obtener estas variables a partir de medidas de campo. La primera de ellas es el denominado método de la caja, en el que se utiliza una caja de paredes reflectantes con dos tapas, una fría y otra caliente, lo que permite mediante diferencia obtener directamente el valor de emisividad. La temperatura de la superficie se obtiene corrigiendo la medida directa del radiómetro del efecto de emisividad y radiancia atmosférica descendente. La segunda técnica consiste en la aplicación del algoritmo TES (Temperature and Emissivity Separation) a medidas de campo realizadas con radiómetros multibanda, que proporciona simultáneamente las emisividades espectrales y la temperatura. Se muestran también algunos ejemplos de medidas de la variación angular de estos parámetros utilizando sistemas goniométricos.

Por lo que respecta a la medida de espectros de emisividad en laboratorio, se muestran algunos resultados obtenidos para distintas muestras utilizando la técnica FTIR (Fourier Transform Infra-Red) junto con esferas integradoras.
Tal y como se comentó anteriormente, la principal aplicación de estas medidas de campo es la calibración y validación de los resultados obtenidos a partir de imágenes. Los mapas de temperatura y emisividad generados a partir de las imágenes adquiridas con distintos sensores se utilizan en distintas aplicaciones, desde la detección de los cambios ocurridos en la superficie cuando se trabaja con datos de baja resolución espacial, hasta la estimación de los flujos de energía y evapotranspiración cuando se trabaja con datos de media y alta resolución, o el estudio del efecto de isla térmica.

Spectral Databases. Motivations, State of the Art, Visions

Andreas Hueni
Remote Sensing Laboratories, Institute of Geography,
University of Zurich, Switzerland
ahueni@geo.uzh.ch

Abstract

The interest of the remote sensing user community in spectral databases for the storage of spectral field data has substantially increased over the past few years. Starting with a vision of embedding spectral databases in complete observing systems, this work documents and discusses the current state of the art of spectral databases while giving recommendations regarding further development. Ultimately, the success of spectral database systems will depend on both technical implementations and increased standardisation of spectral field data acquisition techniques by the research community.

1. Introduction

Spectral databases are systems for the organised storage of spectral signatures accompanied by associated metadata (Hueni et al., 2009b). This may seem fairly trivial, but we may better appreciate the potential of spectral databases by putting them into the context of a complete observing system as envisaged by NASA and GEOSS (GEO, 2005, National Research Council, 2007). Such a complete observing system would encompass spacebased, airborne and *in situ* data, offering the possibility of seamless data integration at different scales of observation and thus facilitating data validation processes as standard operations. In such a setup, data will be acquired by spatially and organisationally separated entities and fed into storage components that are all linked up in a scientific data grid. Data grids are essentially frameworks connecting heterogeneous components in a manner that allows presenting users and other systems with a uniform access interface. In such a system, information will be at the scientist's fingertips and comprehensive metadata and automatically derived quality indicators will facilitate the assessment of data quality and hence their suitability for new applications.

Today's spectral databases are not yet at a stage where the presented vision of seamless data sharing has become reality. This fact is not only due to limited research on the topic but may also be attributed to related issues such as missing standardisation of sampling approaches, messing metadata, bad sensor calibrations, operator mistakes, practices regarding data policy and mission based thinking.

In the following, existing approaches will be presented and discussed, highlighting the advantages and disadvantages of spectral databases and finally, some guidelines for future systems will be provided.

2. Methods and Implementations

The current state of the art of spectral databases will be based on four existing database systems:
SPECCHIO (Hueni et al., 2009b), DLR Spectral Archive (Heiden et al.), SSD's Spectral Library Database (Pfitzner et al., 2008) and Hyperspectral.info (Ferwerda et al., 2006). Most concepts and methods are however illustrated using SPECCHIO.

Data Acquisition

Data acquisition under field conditions requires a proper preparation including: (a) a measurement procedure describing the instrument target geometries to be used, the sampling process to be observed (instrument settings, measurement order (White

reference – target sequences), metadata to be noted), a sampling pattern to be applied to each target and an organised storage concept of data in the field, (b) a sampling protocol to be filled in per target, containing fields for all metadata to be recorded and (c) instrument calibration checks before and after each campaign.

Dataflow and Storage
Spectral files holding spectral signatures acquired during data acquisition are read using specialised procedures and the spectral information and metadata are stored in the database.

The reading procedures are dependent on the input file format and thus often instrument specific. Conversion of native formats to standard formats such as comma separated values (CSV) may result in substantial loss of metadata. Tests performed on the SPECCHIO system have shown that parsing metadata from the ASD binary files can provide around 13 parameters in an automated way (Hueni et al., In preparation).

Metadata Editing
Metadata not automatically gleaned from input files need to be entered by the user in manual fashion. This input is a critical function in regards of end user acceptance of the spectral database; it must be as streamlined as possible to minimise the time spent on data input. For this reason, SPECCHIO offers a 'group update' functionality, which allows the definition of common metadata parameters for groups of spectra with a single action (Hueni et al., 2009b).

Retrieval
Data retrieval is the operation of selecting a subset of data from the spectral database for subsequent processing and/or output. Retrieval of data is usually implemented via Interactive browsing or metadata space restrictions (Hueni and Kneubuehler, 2009). In both cases, retrieval is based on metadata content. Examples of the various graphical user interfaces for data retrieval include: (a) browsing via a hierarchical folder structure (Hueni and Kneubuehler, 2009), (b) metadata restriction definition (Hueni and Kneubuehler, 2009) and (c) Google Earth interface (Ferwerda et al., 2006).

Processing and Output
Processing and output operations are applied to data selected by retrieval procedures. Implementing processing modules in spectral database software offers the possibility to perform calculations in the full metadata context of the involved spectra. One example is the correction for Spectralon reference panel non idealness; according correction factors can be selected automatically if appropriate links and data have been entered during metadata editing (Hueni et al., 2009a). The implementation of such modules must be kept generic whenever possible to allow their use with various sensor data.

Data output involves the writing of spectral information and metadata to standardised file formats such as CSV or ENVI spectral libraries. The structure of these files requires a denormalisation of the data, thus, many metadata will be written redundantly.

Data Exchange
Data exchange between spectral databases of identical schemata has been addressed for the SPECCHIO system using XML style files for transmitting data between systems (Hueni et al., In preparation). Data exchanges between heterogeneous databases are even more challenging and would become more feasible if minimal common metadata parameter sets for spectral field data were to be developed and implemented.

Data Access
Physical database access can be treated as a simple technology issue; databases are typically run on dedicated database servers and access is possible via Internet or Intranet, utilising VPN connections where firewall restrictions apply.

Access rights on the data define the read, update and delete rights of the database user. SPECCHIO has been designed as a multi user system with the basic concept that all users can read all data while update and delete operations can only be performed by the owner of the data (Hueni et al., 2009b).

Data Quality

Estimation of data quality is the key to successful data exchange. However, only minimal research has been conducted so far. It mainly involves the linking of quality with the amount of captured metadata, basing on the fact that scarce metadata significantly compromises the long term use of data (Curtiss and Goetz, 2001, Michener, 2000). According efforts have been implemented in SPECCHIO by the measure of the metadata space density (Hueni et al., In preparation) and in the DLR Spectral Archive (Heiden et al.).

3. Advantages and Constraints

The advantages of well ordered and documented storage of spectral data in a spectral database system are most likely only apparent after an initial phase of data input. Typically, this phase is most critical as researchers are forced to change their existing workflow to a database centric one. Graphical user interfaces for data storage and metadata editing must be streamlined or users will be deterred from entering their data. Once a considerable amount of well documented data has accumulated, users will begin to see the advantages and start to get data from the database instead of performing tedious file searches on workstations and servers. Eventually, spectral databases should become the one stop shop for spectral field data in every institution in the remote sensing sector.

The metadata parameters required by the various spectroscopy communities do differ and the definition of database schemata and user interfaces able to deal with all variations is accordingly complex. Work in this direction has been carried out in the context of the Hyperspectral.info system (Ferwerda et al., 2006).

Data sharing ultimately relies on providing data of a known or estimated quality. Spectral data quality estimation and development of according quality indicators is still an area of ongoing research and remains only marginally supported in current systems.

The full potential of spectral databases will only become apparent when the data will be directly accessible by other software packages and storages/processing systems. It is therefore essentials to pursue the integration of spectral database access in existing and future systems by providing according interfaces.

4. Discussion and Outlook

Spectral databases act as data repositories for spectral data and associated metadata. They offer considerable advantages over traditional methods of data storage such as file systems. The active use of spectral databases in the remote sensing community is currently rather scarce but interest has increased considerably over the past couple of years. Critical factors are the user interfaces and the acceptance of the system by the researchers, who face a change in their traditional workflows.

The success of spectral databases will be tied to the combination of efforts in spectral database development and design as well as in further standardisations of data acquisition: spectral databases must be designed in a generic fashion in order to accommodate the needs of the various user communities while users need to homogenise their existing workflows and develop common data capturing techniques, at least within the research groups. Without these combined efforts, data exchange and long term use of data will remain in the realm of visions.

References

Curtiss, B., Goetz, A. F. H., 2001. Field Spectrometry: techniques and instrumentation. Analytical Spectral Devices Inc., 9 pp. http://www.asdi.com/Field%20Spectroscopy_screen.pdf

Ferwerda, J. G., Jones, S. D., Reston, M., 2006. A free online reference library for hyperpectral reflectance signatures. SPIE Newsroom, 1 2, http://newsroom.spie.org/x5275.xml.

GEO, 2005. Global earth observation system of systems GEOSS: 10 Year implementation plan reference document, ESA Publications Division 2200 AG Noordwijk, The Netherlands

Heiden, U., Becvar, M., Hirner, A., Mueller, A. Abstract: QUALITY MANAGEMENT OF A SPECTRAL ARCHIVE. In: Proceedings IGRASS'10.

Hueni, A., Kneubuehler, M., 2009. SPECCHIO: A Free Spectral Data Management and Processing System. In: Proceedings SPIE Optics and Photonics, San Diego, CA.

Hueni, A., Kneubuehler, M., Nieke, J., Itten, K., 2009a. PROCESSING EXTENSION FOR THE SPECTRAL DATABASE SPECCHIO. In: Proceedings EARSeL SIG IS, Tel Aviv, Israel.

Hueni, A., Malthus, T., Kneubuehler, M., Schaepman, M., In preparation. Data Exchange between distributed Spectral Databases. Computers & Geosciences.

Hueni, A., Nieke, J., Schopfer, J., Kneubu hler, M., Itten, K., 2009b. The spectral database SPECCHIO for improved long term usability and data sharing. Computers & Geosciences 35(3), 557 565.

Michener, W. K., 2000. Metadata, In: Michener, W. K., Brunt, J. W. (Eds.), Ecological data: Design, management and processing, Blackwell Science, Oxford, UK, pp. 92 116.

National Research Council, 2007. Earth Science and Applications from Space: National Imperatives for the Next Decade and Beyond, The National Academies Press, Washington, DC, 456 pp.

Pfitzner, K., Esparon, A., Bollhoefer, A., 2008, 29.09. 03.10.2008. SSD's Spectral Library Database. In: Proceedings 14th Australasian Remote Sensing and Photogrammetry Conference, Darwin, AU.

Espectro-Radiometría y Teledetección Hiperespectral

Antonio Plaza
Departamento de Tecnología de los Computadores y de las Comunicaciones
Escuela Politécnica de Cáceres, Universidad de Extremadura
Avda. de la Universidad s/n, E-10071 Cáceres
Teléfono: +34 927 257000 (Ext. 51662)
Fax: +34 927 257203
E-mail: aplaza@unex.es
URL: http://www.umbc.edu/rssipl/people/aplaza

Resumen

En la presente ponencia se abordarán aspectos relacionados con espectro-radiometría y teledetección hiperespectral. La ponencia incluirá aspectos teóricos relacionados con análisis de datos hiperespectrales, así como aspectos prácticos y demostraciones de los algoritmos y técnicas presentadas. En concreto, se abordarán los siguientes aspectos:

1. **Introducción**. Presentación general de aspectos relacionados con teledetección hiperespectral, utilizando una imagen de ejemplo obtenida por el sensor Airborne Visible Infra-Red Imaging Spectrometer (AVIRIS) de NASA/Jet Propulsion Laboratory para ilustrar conceptos básicos acerca del proceso de adquisición y preprocesado de este tipo de imágenes.

2. **Aspectos clave en el diseño de algoritmos de análisis hiperespectral**. En este punto se presentan aspectos relevantes que diferencian el análisis de imágenes hiperespectrales de otros tipos de datos obtenidos en aplicaciones de teledetección, incluyendo la presencia de píxels mezcla y su caracterización, la posibilidad de integrar información espacial y espectral, y los requerimientos computacionales introducidos por diversas aplicaciones que necesitan una respuesta en tiempo real.

3. **Algoritmos de desmezclado para imágenes hiperespectrales**. En este punto se presentan las diferentes aproximaciones existentes para caracterizar píxels mezcla en imágenes hiperespectrales, aprovechando la resolución espectral de los datos para aumentar la resolución espacial disponible mediante técnicas de análisis sub-píxel. Se particulariza en dos modelos para caracterizar píxels mezcla:

    a) *Modelo lineal*. Permite caracterizar mezclas a partir de la identificación de firmas espectrales puras (*endmembers*) que posteriormente se utilizan para estimar la concentración (abundancia) de cada *endmember* en cada píxel mezcla teniendo en cuenta restricciones de no negatividad y suma unitaria de las abundancias estimadas en cada píxel. Durante la ponencia se ilustrará el funcionamiento de diferentes algoritmos (no supervisados) para caracterizar mezclas en imágenes hiperespectrales siguiendo un modelo lineal, tales como el método Pixel Purity Index (PPI) para extracción de *endmembers* en imágenes hiperespectrales.

    b) *Modelo no lineal*. Permite caracterizar mezclas cuyo comportamiento es intrínsicamente no lineal, debido a efectos de dispersión múltiple de la luz en los objetos observados y a otro tipo de fenómenos. En la presente ponencia se ilustra el uso de redes neuronales artificiales para abordar el problema del desmezclado desde un punto de vista no lineal y supervisado, utilizando un caso de estudio centrado en el desmezclado de datos no lineales correspondientes a mezclas de minerales y un juego de imágenes obtenidas a diferentes resoluciones

por los sensores DAIS 7915 y ROSIS sobre una zona de Dehesas en Extremadura.

4. **Otros aspectos presentados en la ponencia**. Con carácter previo a la conclusión de la ponencia con una serie de observaciones generales y anuncios, se presenta brevemente el proyecto Hyper-I-Net financiado por la Comisión Europea dentro del Sexto Programa Marco, con el objetivo de informar a los asistentes sobre el estado actual de dicho proyecto y la posibilidad de acceder a algunos de los resultados derivados del mismo, con idea de buscar posibles sinergias y colaboraciones con los investigadores participantes en el seminario.

Palabras clave

Análisis hiperespectral, diseño de algoritmos, desmezclado lineal, desmezclado no lineal, espectro-radiometría, extracción de *endmembers*, estimación de abundancias.

Resúmenes de los trabajos presentados en la sesión de aplicaciones

Experiencias en Radiometría de Campo

Magalí Odi Lara
Instituto de Desarrollo Regional (IDR), UCLM

1. Seguimiento de cultivos de regadío

El seguimiento de cultivos mediante el uso de la reflectancia de la cubierta se basa en la correlación entre la respuesta espectral y algunos parámetros biofísicos como el índice de área foliar, la fracción de cobertura, la altura de planta, la biomasa seca, además de otros parámetros relacionados con la gestión del riego como el coeficiente de cultivo. Los patrones espectrales asociados al crecimiento del cultivo son utilizados en el desarrollo de índices de vegetación (IV), de manera de sintetizar la información correspondiente a la vegetación y reducir la de otros factores (suelo, condiciones de iluminación solar, atmósfera).

El IDR ha llevado a cabo campañas de monitoreo de cultivos mediante radiometría con el fin de estimar parámetros biofísicos de importancia agronómica y mejorar la eficiencia de uso del agua en la agricultura de regadío. En este sentido, la estimación de la evapotranspiración de los cultivos es un factor crucial. Un método ampliamente usado para su cálculo es el propuesto en FAO-56 en función de un coeficiente de cultivo (Kc) y una evapotranspiración de referencia (ETo). En vista de que los patrones temporales de los IV y los coeficientes del cultivo son similares, se ha propuesto el uso de los IV para estimar Kc (Heilman *et al*., 1982). Así, se han desarrollado relaciones lineales entre el Kc y diferentes IV , para ser usadas en un contexto operacional de la programación de riegos (Bausch and Neale,1987 y 1989; Bausch,1993 y 1995; Choudhury et al., 1994; González-Piqueras *et al*., 2004; González-Piqueras, 2006; López-Urrea *et al*., 2009).

Como casos de estudio podemos citar los cultivos de maíz, trigo y sorgo, en los que se han observado las propiedades espectrales de la cubierta durante el ciclo de crecimiento completo (Figura 1). Estos cultivos fueron sembrados sobre un lisímetro de pesada continua que permite obtener los valores reales de evapotranspiración. Para maíz y trigo se utilizó un radiómetro multiespectral GER 3700 (350-2500 nm, FOV=6.6º), mientras que en sorgo se midió con el HR4000 de Ocean Optics (200-1100 nm, FOV=10º). La información obtenida en campo ha permitido reescalar la relación entre el IV y el Kc para su aplicación a escala regional en el acuífero 08.29 Mancha Oriental utilizando imágenes del satélite Landsat 5 TM.

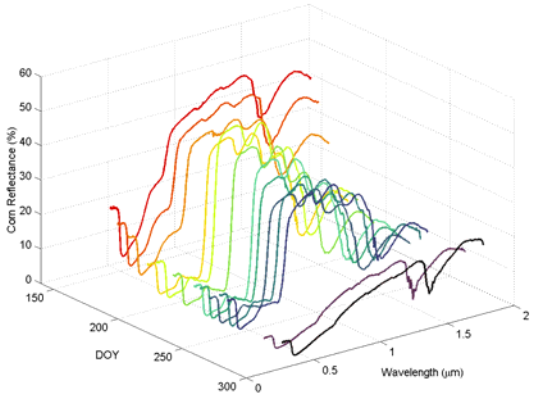

Figura 1. Firma espectral de maíz durante el ciclo de crecimiento.
Las Figuras 2 y 3 muestran algunos resultados de los cultivos analizados.

Las Figuras 2 y 3 muestran algunos resultados de los cultivos analizados.

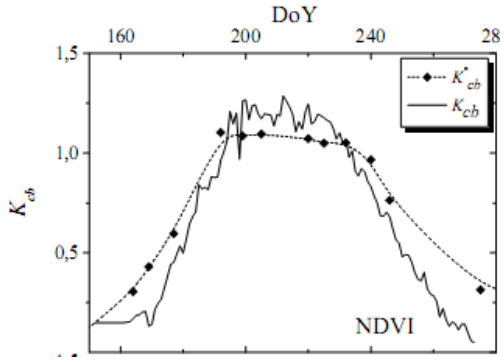

Figura 2. Kcb FAO-56 y Kcb espectral (NDVI) vs. día juliano en maíz.*

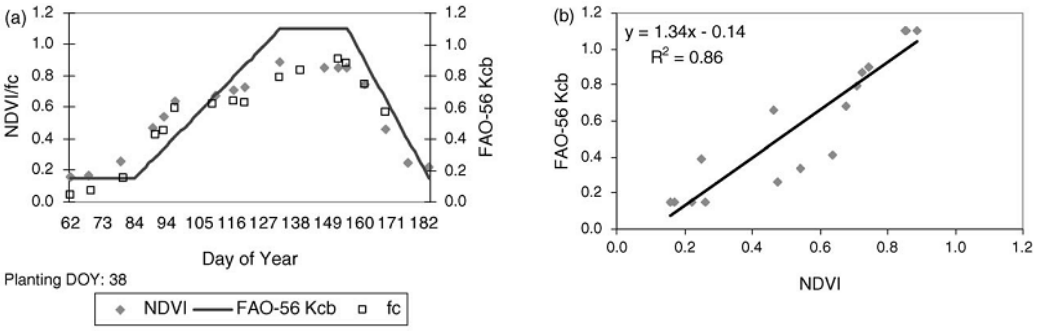

Figura 3. Evolución temporal de FAO-56 Kcb y NDVI y fc en trigo (a). Relación entre FAO-56 Kcb y NDVI en trigo.(b)

2. Calibración radiométrica de cámara digital DMC de Z/I

Una importante incorporación en el paso de la fotografía analógica a la digital es el potencial radiométrico de éstas. Estudios hechos sobre la potencialidad radiométrica de la fotografía digital muestran las limitaciones de su uso cuantitativo debido a una pobre descripción de los sensores, del post-proceso de la información registrada y la calibración de éstos. Existe actualmente, una demanda del uso de la información radiométrica en las imágenes fotogramétricas de alta resolución espacial.

En el marco del convenio de colaboración entre la dirección general del Instituto Geográfico Nacional y el IDR de la Universidad de Castilla La Mancha se ha desarrollado el Proyecto Conjunto para la Aerotriangulación Radiométrica de Imágenes Aéreas. El objetivo del trabajo ha sido estudiar la corrección radiométrica y de anisotropía a partir de los avances logrados hasta el momento dentro del ámbito de la teledetección y adaptarlos de forma operacional a la fotogrametría (Honkavaara *et al*. 2009). La zona de estudio para calibrar la cámara DMC (4 canales azul, verde, rojo, infra-rojo cercano, FOV 42 x 69.3º) mediante radiometría de campo se estableció en la Provincia de Albacete. Se midió la reflectancia (%) de superficies invariantes (asfalto, suelo desnudo, agua, césped, lonas) con un espectroradiómetro Field Spec 3 (350-2500 nm, FOV 25º) simultáneamente a la ejecución del vuelo fotogramétrico. Un elemento clave en esta corrección es la perturbación introducida por la atmósfera y la anisotropía introducida por la BRDF especialmente en sensores fotogramétricos que presentan un ángulo instantáneo de observación grande. Para establecer la corrección absoluta y la homogeneización por BRDF a nivel de cámara (ND), se hace una calibración en vuelo y corrección atmosférica de los fotogramas para obtener la reflectividad a nivel de suelo. Luego, se aplica la corrección por anisotropía obteniendo la reflectividad a nadir a nivel de suelo. Las Figuras 1 y 2 muestran resultados de la corrección atmosférica.

Figura 1. Efecto visual de la corrección atmosférica sobre la imagen D581495. De izquierda a derecha se observa la imagen original, corregida por ATCOR4 y corregida por 6S.

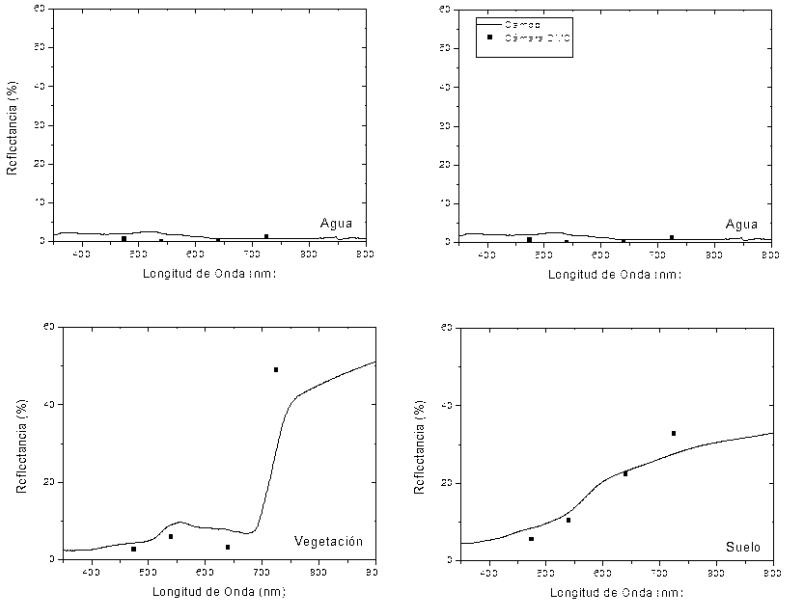

Figura 2: Firma espectral medida en campo (línea continua) de algunas superficies utilizadas en la calibración (vegetación, asfalto, suelo y agua) frente a los valores obtenidos de la imagen corregida (cuadrados negros).

Bibliografía

Bausch, W. 1995. Remote sensing of crop coefficients for improving the irrigation scheduling of corn. Agricultural Water Management 27:55-68.

Bausch, W. 1993. Soil background effects on reflectance-based crop coefficients for corn. Remote Sensing of Environment 46:213-222.

Bausch, W.C. and C.M.U. Neale. 1989. Spectral inputs improve corn crop coefficients and irrigation scheduling, Trans. ASAE, 46: 1901-1908.

Bausch, W.C. and C.M.U. Neale. 1987. Crop coefficients derived from reflected canopy radiation: a concept, Trans. ASAE, 30: 703-709.

Choudhury, B. J., Ahmed, N. U., Idso, S. B., Reginato, R. J. and Daughtry, C. S. 1994. Relations between evaporation coeficients and vegetation indices studied by model simulations, Remote Sensing of Environment 50: 1-17.

Duchemin, B., R. Hadria, S. Erraki, G. Boulet, P. Maisongrande, A. Chehbouni, R. Escadafal, J. Ezzahar, J.C.B. Hoedjes, M.H. Kharrou, S. Khabba, B. Mougenot, A. Olioso, J.C. Rodriguez, V. Simonneaux 2006. Monitoring wheat phenology and irrigation in Central Morocco: On the use of relationships between evapotranspiration, crops coefficients, leaf area index and remotely-sensed vegetation indices. Agricultural Water Management 79: 1–27.

González-Piqueras, J. 2006. Evapotranspiración de la cubierta vegetal mediante la determinación del coeficiente de cultivo por teledetección. Tesis doctoral, Facultat de Físca. Universitat de Valencia, España. 337 pp.

González-Piqueras, J., A. Calera, M.A. Gilabert, A. Cuesta, and F. de la Cruz. 2004. Estimation of crop coefficients by means of optimized vegetation indices for corn. Proceedings SPIE 5232:110-118.

Heilman, J.L., W.E. Heilman and D.G. Moore. 1982. Evaluating the crop coefficient using spectral reflectance, Agronomy Journal, 74: 967-971.

Honkavaara, E., Arbiol, R., Markelin, L., Martínez, L., Cramer, M., Bovet, S., Chandelier, L., Ilves, R., Klonus, S., Marshal, P., Schlapfer, D., Tabor, M., Thom, C. and Veje, N. 2009. Digital air-borne photogrammetry: A new tool for quantitative remote sensing?. A state-of-the-art review on radiometric aspects of digital photogrammetric images. Remote Sensing 1(3): 577-605.

López-Urrea, A. Montoro, J. González-Piqueras, P. López-Fuster, and E. Fereres. 2009. Water use of spring wheat to raise water productivity. Agricultural Water Management, 96: 1305-1310.

Actividades del Laboratorio de Espectro-radiometría y teledetección ambiental (SpecLab)

M. Pilar Martín Isabel
Centro de Ciencias Humanas y Sociales (CCHS-CSIC)
mpilar.martin@cchs.csic.es

El laboratorio de Espectro-radiometría y Teledetección Ambiental (SpecLab) (http://www.investigacion.cchs.csic.es/espectroradiometria/) del Instituto de Economía, Geografía y Demografía fue creado en 2007 en las nuevas instalaciones del Instituto dentro del Centro de Ciencias Humanas y Sociales del CSIC (http://www.cchs.csic.es/). El laboratorio nace con el objetivo desarrollar investigación básica y aplicada en el campo de la teledetección y más concretamente en el de la espectro-radiometría. Una de las actividades fundamentales del laboratorio consiste en la obtención de medidas espectrales y el desarrollo de protocolos y técnicas de análisis que permitan derivar, por si solos, o en combinación con información procedente de sensores aeroportados y/o espaciales, parámetros biofísicos e indicadores relevantes en la gestión medioambiental.

Por otra parte, el laboratorio trata de responder a la demanda de formación en el campo de la espectro-radiometría y sus aplicaciones y contribuir al establecimiento de buenas prácticas mediante la difusión e intercambio de experiencias que pueda ser de utilidad a usuarios actuales y futuros de esta herramienta. Con este interés el Laboratorio organiza actividades docentes y de difusión de la actividad científica como el Seminario "Avances en Espectro-radiometría" y coordina otras iniciativas como el grupo de trabajo de Espectroscopia de campo y laboratorio de la Asociación Española de teledetección (http://www.aet.org.es/).

El laboratorio SpecLab cuenta con un completo equipo de espectro-radiometría de campo y laboratorio que incluye un radiómetro ASD Fieldspec 3 FR con un rango espectral de 350 a 2500 nanómetros con accesorios para mediciones no destructivas de vegetación (*plant probe* y *leaf clif*), un radiómetro ASD Handheld ultraportátil con rango espectral de 325 a 1075 nanómetros y una esfera de integración para mediciones de reflectividad/transmisividad, además de vehículos todoterreno, una grúa remolcable para mediciones sobre dosel arbóreo y licencias de software específico para el tratamiento de datos e imágenes de satélite.

El laboratorio está gestionado por el Grupo de Investigación en Tecnologías de Información Geográfica (GITIG) al que facilita el apoyo técnico e instrumental necesario en el desarrollo de diversas líneas de investigación (incendios forestales, agricultura de precisión, desarrollo rural, cambio global, etc) donde la espectro-radiometría resulta una herramienta de gran relevancia para la calibración y validación de modelos físicos y empíricos. En la actualidad el laboratorio SpecLab participa de las actividades científicas de diversos proyectos liderados por el grupo de investigación GITIG como por ejemplo el proyecto Biospec "Obtención de información espectral a diversas escalas para la estimación de parámetros biofísicos de la vegetación Mediterránea en el contexto del cambio global" (http://www.lineas.cchs.csic.es/biospec/) financiado por el Ministerio de Ciencia e Innovación y en el que participan investigadores del CEAM, INIA, Universidad de Alcalá así como expertos internacionales de las Universidades de Alberta (Canadá), Davis y Míchigan (EE.UU) .

Entre los objetivos de Biospec se plantea contribuir al desarrollo y mejora de productos de teledetección para la estimación de parámetros biofísicos de la vegetación en el contexto de los estudios sobre cambio global. Para ello, se plantea el análisis de las relaciones entre variables biofísicas de la vegetación (área foliar, contenido de agua, clorofila, etc), su variabilidad espacio temporal y las mediciones espectrales en

laboratorio y campo mediante modelos empíricos y modelos de transferencia radiativa, a diversas escalas (de la hoja al dosel).

La apropiada caracterización y estimación de parámetros biofísicos de la vegetación es clave para entender el intercambio de flujos en la biosfera a escala global. Por ello, uno de los objetivos del proyecto consiste en analizar las relaciones entre determinados parámetros biofísicos estimados con teledetección y las mediciones de flujos Tierra-atmósfera realizadas, en el ámbito de la red FLUXNET, sobre determinadas áreas-test seleccionadas en España. Estos puntos se integrarán en la red SpecNet (http://spectralnetwork.net/), una asociación internacional de colaboración entre investigadores que desarrollan su actividad en áreas en las que se realizan simultáneamente mediciones espectrales y de flujos con el objetivo de entender mejor los intercambios de carbono y vapor de agua.

Biospec propone una metodología basada en la integración multi-escala de diversas fuentes de información espectral combinando conjuntos de datos de distinta resolución espectral, obtenidos a diferentes resoluciones desde plataformas espaciales (Landsat/Aster, MERIS, MODIS) y aeroportadas (sensores hiperespectrales) a datos de campo obtenidos con espectro-radiómetros. Simultáneamente se adquiere información en las áreas-test sobre determinados parámetros biofísicos de la vegetación, variables meteorológicas así como medidas de CO2 y H20 y flujos energéticos, a escala de ecosistema. La figura 1 sintetiza el flujo de trabajo que se seguirá en el proyecto.

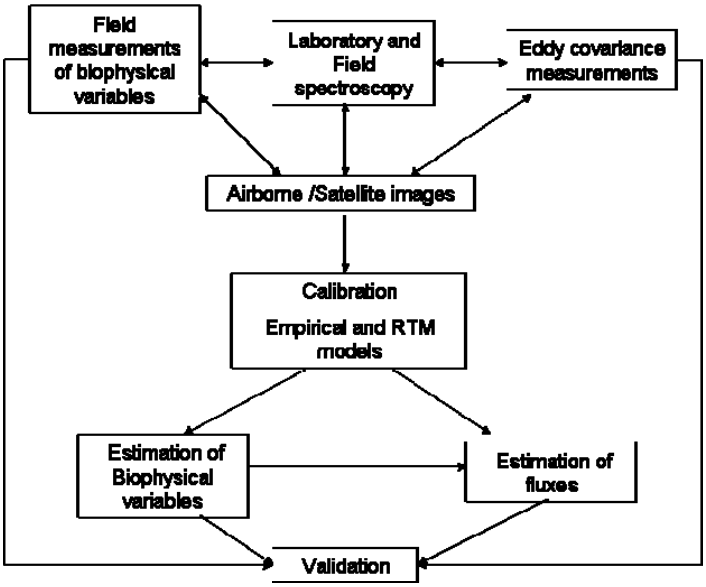

Figura 1. Esquema metodológico del proyecto Biospec

En el ámbito del proyecto Biospec se ha realizado durante 2009 una intensa campaña de campo para la obtención de información espectral y de variables biofísicas de la vegetación en las dos áreas de estudio del proyecto: una dehesa, localizada al NE de la provincia de Cáceres, y un arrozal situado en el municipio de Sueca (Valencia). Ambos ecosistemas presentan una estructura de la vegetación diferente, distinto patrón estacional de los flujos de carbono y de vapor de agua y una gran amplitud de velocidades de intercambio de carbono. Por otra parte, los dos estratos de la vegetación en el ecosistema de dehesa (estrato arbóreo al 20% de fracción cabida cubierta y pastizal) presentan diferente fenología y distintos patrones estacionales de flujos. Estas características son consideradas ideales para ensayar la metodología propuesta en el proyecto.

Desde marzo a diciembre de 2009 se han realizado mediciones quincenales de radiometría sobre la zona de dehesa y mensuales en el caso del arrozal siguiendo el

ciclo estacional de ambos ecosistemas. Las mediciones se han realizado tanto a nivel de parcela como en el caso del pastizal y el cultivo; como a nivel de hoja en el caso de la encina. Adicionalmente se han realizado muestreos simultáneos de parámetros biofísicos de la vegetación (LAI, biomasa, contenido en humedad, clorofila). Una de las actividades más interesantes en esta etapa del proyecto ha sido el diseño espacio-temporal del muestreo en las distintas áreas de estudio y la elaboración de protocolos específicos para la toma de datos sobre terreno y el procesado de los mismos en laboratorio.

Las actividades del laboratorio en el proyecto Biospec forman parte de la *Cost Action* ES0903 "Spectral Sampling Tools for Vegetation Biophysical Parameters and Flux Measurements in Europe" que integra investigadores europeos de más de 10 países con el objetivo de desarrollar protocolos comunes para la obtención de medidas espectrales en relación con la red Europea de medición de flujos de carbono.

La geología espectral: ¿cómo puede ser automática?

RIAZA, A.*, BUZZI. J.*, GARCIA-MELENDEZ. E**
* Instituto Geológico y Minero de España, Madrid
** Facultad de Ciencias Ambientales, Universidad de León

El uso de imágenes como método de exploración geológica se ha asociado de manera preferente a la exploración de yacimientos minerales, su actividad industrial tradicional. De una manera casi natural se ha popularizado el término de "mapas de minerales" o "cartografía de minerales" en el mundo de la teledetección geológica.

Sin embargo, los minerales que se pretende cartografiar en estos trabajos, son indicadores de procesos de enriquecimiento mineral en términos de explotación, o trazadores de concentraciones mayores de ciertas sustancias. Como ejemplo más extendido puede citarse la kaolinita, que revela la posible presencia de alteraciones hidrotermales a las que se asocian sales con metales susceptibles de explotación. O la delimitación de zonas con procesos de dolomitización en rocas carbonatadas, que indica áreas favorables para la movilización de sustancias y la localización de zonas explotables. Las absorciones espectrales de estos minerales orientaron el desarrollo de sensores como el thematic mapper. Estas cartografías se ciñen casi siempre a yacimientos en los que se explotan activamente minerales.

Para detectar la presencia minerales en una imagen hiperespectral se usan espectrotecas de referencia elaboradas en laboratorio. Pero los minerales no aparecen en la superficie de la tierra ni aislados, como en el laboratorio, ni en una extensión suficientemente grande como para ser cartografiable. Los minerales forman parte de rocas, que a su vez están expuestas a la atmósfera y sufren procesos de meteorización. Lo que se cartografía son unidades geológicas, procesos geológicos, y expresiones superficiales de realidades geológicamente muy complejas.

Por ello, hacer cartografía en geología es una tarea que sólo puede aspirar a convertirse en automática si las áreas en las que pueden aparecer los minerales o unidades geológicas a considerar miembros extremos, está suficientemente aislada digitalmente. Y aún cuando el contexto esté suficientemente delimitado digitalmente, los materiales que aparecen en el área seleccionada tienen que cualificarse geológicamente en su complejidad para que el mapa resultante tenga verosimilitud en términos geológicos.

En las imágenes que acompañan, en la mina de Sotiel-Almagrera (Huelva), aparecen varias etapas en el proceso de exploración de áreas para la cartografía de sustancias producto de oxidación de piritas, generadoras de aguas ácidas, y muy inestables ante cambios en las condiciones climáticas del medio.

En la composición en falso color (Rojo Verde Azul) (fig.A) con los canales Hymap 18 (0,7207 µm), 40 (1,0337 µm) y 69 (1,49 µm) se aprecian las áreas con cubierta vegetal más densa.

Las zonas menos vegetadas (fig.B) se cartografían de manera esquemática con una composición de color con Fracciones de Ruido Mínimo calculadas con una máscara para las zonas vegetadas. Incluye tanto las áreas afectadas por las explotaciones mineras como las sujetas a trabajos de repoblación forestal (verdes). Entre las primeras se discriminan las escombreras recubiertas con pátinas muy oxidadas (rojos), las zonas de lodos con costras de sulfatos hidratados en superficie (azules), y las zonas húmedas que se han oxidado más intensamente (magenta), tanto en los bordes de balsas de lodos como en el cauce del río Odiel.

Al analizar solamente las áreas donde se sitúan las balsas de cenizas (amarillos y rojos)

y lodos y la planta de tratamiento (azul, magenta y añil) en las explotaciones mineras (fig.C), empiezan a perfilarse las áreas cubiertas por costras de sulfatos producto de la oxidación de piritas, siguiendo un control geomorfológico claro.

De esta manera, cartografiando selectivamente áreas individualizadas por sus particularidades espectrales, puede elaborarse un mapa detallado de las sustancias que se pretende identificar y evaluar ambientalmente (fig.D). Esta cartografía detallada sería imposible tratando la imagen Hymap sin la compartimentación en subescenas que se describe.

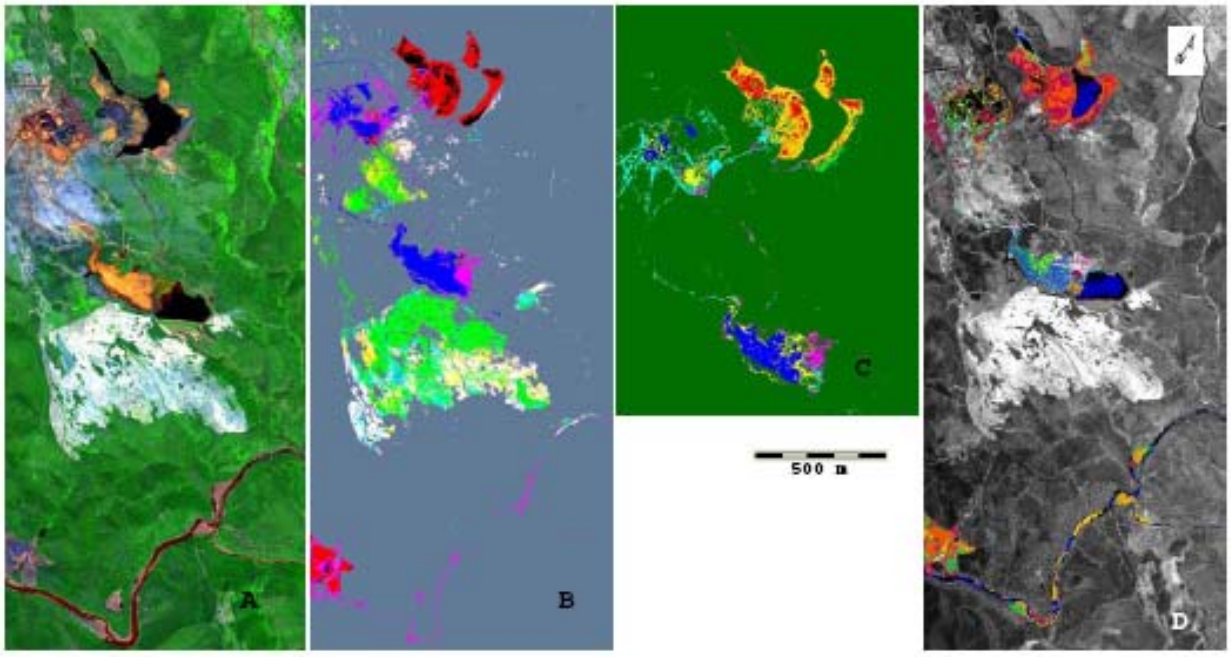

Relaciones entre los productos de combustión y sus propiedades espectrales en matorrales quemados

Raquel Montorio Llovería, Fernando Pérez-Cabello, Alberto García-Martín y Juan de la Riva Fernández
Grupo GEOFOREST (http://geoforest.unizar.es)
Departamento de Geografía y Ordenación del Territorio, Universidad de Zaragoza.
C/ Pedro Cerbuna, 12, 50009, Zaragoza
montorio@unizar.es, fcabello@unizar.es, algarcia@unizar.es, delariva@unizar.es

1. Introducción

El fuego es uno de los factores con mayor influencia en la dinámica general de los espacios forestales (Pérez y Moreno, 1998). De las diferentes variables asociadas con las características del fuego la severidad ha sido comúnmente considerada como una de las más críticas en la evaluación de la dinámica postfuego debido a su importante papel en los procesos de erosión y regeneración vegetal (Miller y Yool, 2002).

La información espectral proporcionada por las imágenes de satélite ha demostrado sobradamente su adecuación y utilidad para detectar y cartografiar esta variable ya que los diferentes intervalos de severidad pueden asociarse con los cambios espectrales experimentados por las cubiertas, especialmente vegetación y suelo.

La evaluación tradicional de la severidad a partir de teledetección se ha basado en el cálculo de índices como el *Normalized Burn Ratio* que proporcionan una estimación general de esta variable. En oposición a esta tendencia las nuevas investigaciones apuntan hacia la utilidad de estimar la presencia de productos de combustión individuales, especialmente de aquellos que normalmente suelen asociarse con niveles de severidad conocidos (Smith *et al.*, 2005; Robichaud *et al.*, 2007). En este nuevo marco de investigación los trabajos a escala de detalle con espectrometría de campo adquieren una gran importancia al convertirse en nexo de unión entre la realidad y las medidas tomadas por sensores a bordo de aviones y satélites permitiendo establecer la validez de las relaciones empíricas antes de trasladar el análisis a escala regional.

En este contexto general esta investigación persigue el cumplimiento de distintos objetivos. Por un lado, se pretende caracterizar las propiedades espectrales de los productos de combustión sólidos a partir de información de reflectividad (R) y de informaciones hiperespectrales derivadas de ésta: primera derivada de la reflectividad (PDR) y profundidad de las bandas de absorción (PB). Por otro lado, se busca evaluar la sensibilidad de los datos espectrales a la presencia superficial de tres productos de combustión – vegetación, carbón y ceniza – representativos de diferentes niveles de severidad – nula, media y alta, respectivamente – comparando, al mismo tiempo, la diferente capacidad de estimación de los tres conjuntos de información espectral – R y PDR y PB –.

2. Área de estudio

El área quemada en la que se han recogido los datos para la presente investigación corresponde con un fuego experimental llevado a cabo en la estación experimental de Peñaflor (EEP), instalada por el grupo de investigación GEOFOREST en las proximidades de la localidad de Zaragoza. La EEP se asienta sobre una ladera de orientación sur con pendiente de 12º. Su vegetación es un matorral mediterráneo poco denso con especies propias de un ambiente semiárido, principalmente *Brachypodium retusum* y *Rosmarinus officinalis*. El fuego experimental se concentró en un sector rectangular de 15x3m

situado en la parte inferior de la ladera, permitiendo que el fuego se extendiera con posterioridad por la ladera de forma natural (Figura 1).

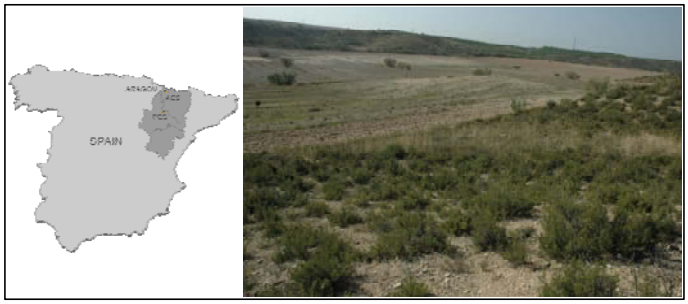

Figura 1. Área de estudio.

3. Metodología

Obtención de los datos de campo

La obtención de datos de campo se realizó mediante la aplicación de dos técnicas de captura diferentes: (1) fotografía de alta resolución espacial por medio de una cámara digital Reflex Nikon D100 y (2) espectrometría de campo con el espectrómetro Avantes AvaSpec que registra reflectividad en el rango espectral entre 400-1800 nm con un intervalo de muestreo de 0.57 nm en el rango VIS-NIR y de 3.5 nm en el rango SWIR.

Para la captura de ambas informaciones se utilizó una estructura metálica de dimensiones 3x3x2m (Figura 2). Esta estructura presenta en la parte superior un travesaño móvil para su desplazamiento en cinco movimientos en el eje vertical. Este travesaño dispone también de cinco puntos de anclaje a los que se sujetan los dos dispositivos de captura permitiendo el registro de información en cinco posiciones en el eje horizontal. Así, en cada una de las cinco diferentes localizaciones de la estructura sobre el área quemada se registraron 25 puntos muestrales generando así un total de 125 muestras que medidas antes y después del fuego permitieron la obtención de la base de datos final de 250 puntos. La utilización de esta estructura metálica ha permitido a esta investigación asegurar, por un lado, el cumplimiento de las condiciones de medida requeridas por la espectrometría de campo y, por otro lado, garantizar la total correspondencia entre las superficies registradas por ambas técnicas y entre los registros antes y después del fuego.

Tanto la fotografía digital como la medida de reflectividad se realizan desde el nadir a una altura aproximada de 2m. En la medida de reflectividad se controló la superficie registrada por el espectrómetro para que ésta recogiera muestras de reducido tamaño y así incrementar el número de puntos muestrales y la pureza de los mismos. Para ello el campo de visión del espectrómetro fue limitado a un ángulo de 10º que, combinado con la altura de medida, generó una superficie de captura circular de 30 cm de diámetro. La superficie recogida en cada una de las fotografías individuales no fue limitada en la captura pero sí en el post-tratamiento de las mismas. De este modo, sólo la superficie circular para la que el espectrómetro registró información fue mantenida en cada fotografía. De este modo se evitaron problemas de distorsión al utilizarse sólo la zona central de las fotografías y los posibles efectos de sombras provocadas por la propia estructura.

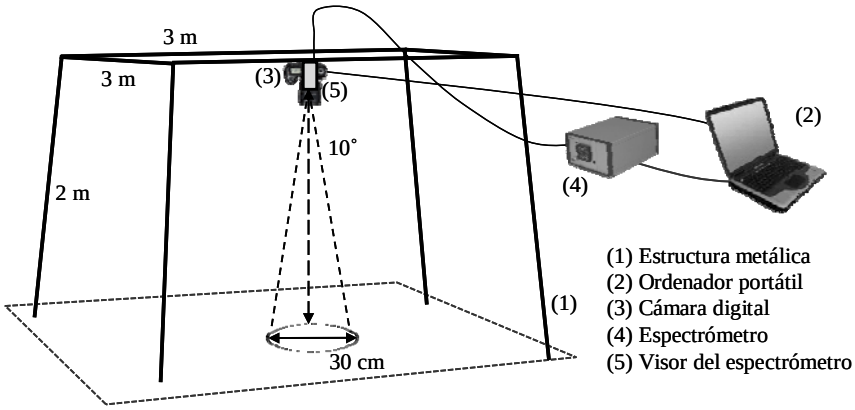

Figura 2. Diseño experimental.

Post-tratamiento de los datos de campo

La cuantificación precisa de los porcentajes de ocupación de los productos de combustión en cada uno de los puntos muestrales se obtuvo a través de un proceso de clasificación supervisada de las fotografías (Figura 3). Para que este proceso de clasificación fuera aplicado de forma homogénea a todos los puntos se contruyó una imagen mosaico a partir de las 250 imágenes circulares. El método de asignación seleccionado fue el de máxima probabilidad. La clasificación supervisada proporcionó una cuantificación de cada una de las cubiertas superficales presentes en el área quemada entre las que se encuentran los tres productos de combustión estudiados en este trabajo: (1) ceniza, indicativa de un proceso de combustión completo; (2) carbón, representativo de áreas donde todavía permanecen restos de combustible aunque muy calcinado; y (3) vegetación, representativa de las áreas no afectadas por el fuego.

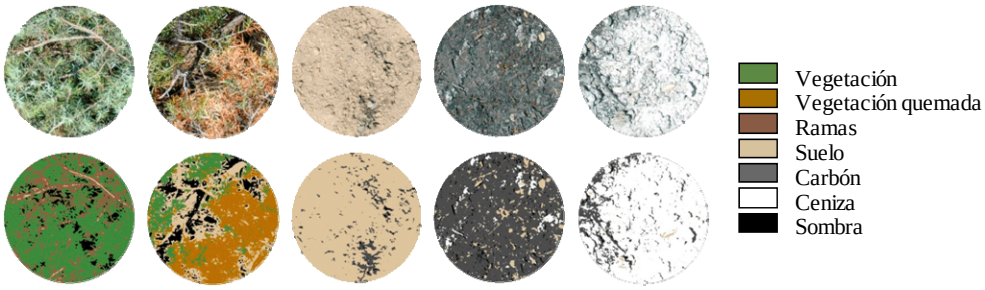

Figura 3. Ejemplo del proceso de clasificación supervisada en puntos muestrales representativos de los diferentes productos de combustión.

La espectrometría de campo proporcionó directamente datos de reflectividad en el rango espectral VIS-SWIR. Con la aplicación de técnicas de tratamiento de datos hiperespectrales se obtuvieron informaciones derivadas: (1) la primera derivada de la reflectividad (PDR) y (2) la profundidad de la banda de absorción (PB).

La transformación de PDR puede definirse como la tasa de cambio de la reflectividad para una distancia espectral específica a lo largo de las diferentes longitudes de onda consideradas (Dawson y Curran, 1998). Esta técnica enfatiza las longitudes de onda donde la curva espectral experimenta cambios bruscos en su forma.

$$FDS_{\lambda(j)} = (R_{\lambda\,(j+1)} - R_{\lambda\,(j)}) / (\lambda\,(j+1) - \lambda\,(j))$$

donde $FDS_{\lambda(j)}$ es la primera derivada de la reflectividad en la longitud de onda j; R es el valor de reflectividad; (j) y (j+1) son las longitudes de onda.

La eliminación de la tendencia o *continuum removal* (CR) es la técnica aplicada para obener los valores de profundidad de la banda de absorción (Mutanga *et al.*, 2004).

$$CR(\lambda i) = R(\lambda i) / Rc(\lambda i)$$

donde $CR(\lambda i)$ es la absorción diferencial en cada longitud de onda (λi), $R(\lambda i)$ es la reflectividad y $Rc(\lambda i)$ es la reflectividad de la tendencia o *continuum*.

A partir de los espectros de reflectividad con la tendencia eliminada se identificaron nueve rasgos de absorción, cinco de ellos a partir de espectros de vegetación y cuatro de ellos a partir de espectros de carbón. Cada uno de estos rasgos de absorción fue caracterizado por sus longitudes de onda inicial y final, su posición y su valor máximo de PB. La PB fue calculada para cada una de las longitudes de onda incluidas en los nueve rasgos de absorción.

$$PB(\lambda i) = 1 - CR(\lambda i)$$

4. Resultados

Las relaciones entre los tres conjuntos de información espectral (R, PDR y PB) y los porcentajes de ocupación de los tres productos de combustión (vegetación, carbón y ceniza) se analizaron a través de los resultados de un análisis de regresión múltiple lineal por pasos sucesivos. El número de puntos disponible (n=250) permitió la selección de hasta seis variables independientes (Tabla 1).

Tabla 1. Resumen de los resultados del análisis de regresión.

	Longitudes de onda	R^2
Reflectividad		
Vegetación	400.24 (-), 755.35 (+), 1427.83 (-)	0.82
Carbón	915.38 (-), 1733.71 (+)	0.585
Ceniza	1110.72 (-), 400.24 (+)	0.671
Primera Derivada de la Reflectividad		
Vegetación	744.59 (+), 592.35 (-), 1543.07 (+), 1330.88 (-), 773.44 (-)	0.864
Carbón	1567.06 (-), 526.82 (-), 862.64 (-), 951 (+), 1587.49 (-), 534.97 (-)	0.753
Ceniza	755.92 (-), 1076.13 (-), 484.23 (-), 1546.51 (-), 438.51 (-), 459.64 (+)	0.746
Profundidad de Absorción		
Vegetación	1459.6 (+), 707.09 (+), 1710.86 (-)	0.82
Carbón	1287.03 (+), 1424.08 (-), 921.06 (+), 444.97 (+)	0.626
Ceniza	1424.28 (-)	0.463

Los resultados muestran la existencia de relaciones estadísticamente significativas entre el porcentaje de ocupación de la vegetación y los tres conjuntos de información espectral. El r^2 ajustado en los tres modelos es superior a 0.8. Los modelos obtenidos para el producto carbón muestran más diferencias entre informaciones espectrales. Así, los valores de ajuste se encuentran en torno a 0.6 en los modelos obtenidos a partir de R y PB destacando el modelo obtenido a partir de PDR con un valor de ajuste de 0.75. El análisis de regresión para el producto ceniza muestra la ausencia de relación con la información espectral de PB (r^2 ajustado = 0.46). Los resultados con las otras dos informaciones son mucho mejores destacando de nuevo el mayor nivel de ajuste registrado por el modelo obtenido a partir de PDR (r^2 ajustado = 0.75).

5. Conclusiones

Este trabajo ha mostrado la validez del uso combinado de la fotografía de alta resolución espacial y la espectrometría de campo para mejorar la comprensión y el estudio de la variable severidad del fuego. De acuerdo con los resultados pueden establecerse algunas conclusiones relacionadas con la sensibilidad de las diferentes informaciones espectrales a la presencia de los productos de combustión. Por un lado, se ha demostrado la utilidad de la obtención de información espectral transformada, especialmente del cálculo de la PDR. Los modelos de regresión obtenidos a partir de esta información registran los mayores valores de ajuste para los tres productos analizados, siendo especialmente importante la mejora aportada para los productos

carbón y ceniza. Considerando los resultados registrados a partir de los valores de PDR puede afirmarse que los productos vegetación, carbón y ceniza pueden ser adecuadamente estimados a partir de datos espectrales. Dado que estos productos son claramente representativos de diferentes niveles de severidad puede afirmarse que a partir de los valores de PDR puede mejorarse la evaluación y estimación de esta variable.

Referencias

Dawson, T.P., Curran, P.J. 1998. Technical note: A new technique for interpolating the reflectance red edge position. *International Journal of Remote Sensing*, 19: 2133-2139.

Miller, J.D., Yool, S.R. 2002. Mapping forest post-fire canopy consumption in several overstory types using multi-temporal Landsat TM and ETM+ data. *Remote Sensing of Environment*, 82: 481-496.

Mutanga, O., Skidmore, A.K. 2004. Hyperspectral band depth analysis for better estimation of grass biomass (Cenchrus ciliaris) measured under controlled laboratory conditions. *International Journal of Applied Earth Observations and Geoinformation*, 5: 87-96.

Pérez, B., Moreno, J.M. 1998. Methods for quantifying fire severity in shrubland-fires, *Plant Ecology*, 139: 91-101.

Robichaud, P.R., Lewis, S.A., Laes, D.Y.M., Hudak, A.T., Kokaly, R.F. y Zamudio, J.A. (2007). Postfire soil burn severity mapping with hyperspectral image unmixing. *Remote Sensing of Environment, 108*, 467-480.

Smith, A.M.S., Wooster, M.J., Drake, N.A., Dipotso, F.M., Falkowski, M.J. and Hudak, H.T. 2005. Testing the potential of multispectral remote sensing for retrospectively estimating fire severity in African Savannahs, *Remote Sensing of Environment*, 97: 92-115.

Evaluación del contenido en ß-carotenos en la harina de cereales mediante técnicas de reflectancia espectral[1]

Díaz-Alguacil, J.M., Martos, V., Aljazairi, S., Garcia del Moral, L.F.
Dpto. Fisiología Vegetal, Facultad de Ciencias, Universidad de Granada, 18071 Granada, España

Introducción

El contenido en pigmentos, que determina el color de la harina y de la sémola, es un carácter muy importante en la evaluación de la calidad de los cereales, sobre todo actualmente cuando los consumidores están demandando panes y galletas con un color más amarillo y mayor calidad nutritiva. De acuerdo a la Asociación Internacional de Ciencia y Tecnología de Cereales, el contenido en pigmentos amarillos se define como la cantidad de carotenoides extraíbles del endospermo, calculados en mg de β-carotenos por 100 g de materia seca. Un alto contenido en β-carotenos en la harina de los cereales es un carácter deseable para la producción de sémolas, pastas y galletas (Gooding and Davies, 1997), no sólo porque mejora sus propiedades organolépticas sino por la acción antioxidante de los carotenoides, lo que los hace beneficiosos para la salud (Cámara, 2000). Por este motivo el aumento del contenido en β-carotenos es uno de los objetivos de los programas de mejora genética para la calidad del trigo y de otros cereales (Carrillo et al., 2006).

La medida directa del contenido en β-carotenos por métodos analíticos resulta laboriosa, ya que hay que triturar el grano, realizar una extracción de pigmentos sobre la harina obtenida y cuantificar el color mediante espectrofotometría con los patrones adecuados. Las técnicas espectrorradiométricas ofrecen la posibilidad de determinaciones rápidas, fiables y no destructivas, por lo que constituyen una excelente alternativa a los métodos basados en el análisis químico (Westerhaus et al., 2004).

2. Material y métodos

En este trabajo, para establecer el modelo de calibración se ha usado harina procedente de varios genotipos de tres cereales, trigo blando, triticale y tritórdeo. Para determinar su contenido en β-carotenos se tomó 1g de harina mantenido durante 3 horas en agitación continua con 5 ml de 1-butanol saturado en agua. La suspensión se centrifugó durante 5 minutos a 6000 rpm y el sobrenadante se evaluó espectrofotométricamente a 448 nm contra una solución de 1-butanol como blanco. Para las medidas de reflectancia espectral se usó un espectrorradiómetro portátil (FieldSpec® Pro JR A 110080 (Analytical Spectral Devices Inc., Boulder, CO), con un rango de reflectancia espectral de 350-2500 nm con un intervalo de muestreo de 1 nm. El sistema incorpora una sonda de contacto de 2 cm. de diámetro FieldSpec Pro FR A111208 (Analytical Spectral Devices Inc.), con luz halógena y una reflectancia especular máxima del 5%. Se calibró el nivel de blanco con un Spectralón de referencia de 9 cm de diámetro, con un 100% de capacidad de reflectancia. Se captaron tres espectros por muestra de harina, previa optimización de los parámetros radioscópicos mediante el software del instrumento.

3. Resultados y discusión

Del análisis de los espectros obtenidos, se deduce que existen diversas zonas de baja reflectancia (y alta absorbancia, por tanto) de las harinas, sobre todo en las bandas correspondientes a alrededor de 1500, 1750, 1800, 2200, 2125 y 2300 nm, todas ellas pertenecientes al infrarrojo cercano (IRC). En la mayoría de esas bandas, los espectros presentaron una buena diferenciación entre las tres especies estudiadas.

[1] Trabajo financiado por Ministerio de Educación y Ciencia, Programa de Infraestructura Científico Tecnológica, Proyecto MEC-JA-FEDER UNGR 05-23-036.

Con los espectros captados se ha elaborado un modelo de predicción para el contenido de β-carotenos, mediante el programa *The Unscrambler*® v.9.8 de la casa CAMO, que permite realizar Análisis Multivariante del conjunto de los 2150 datos de reflectancia contenidos en cada espectro capturado, con su correspondiente variable dependiente (Esbensen, 2004). En la elaboración del modelo se ha usado el método de regresión parcial de mínimos cuadrados (*Partial Least Squares Regression, PLS-R*). Este método utiliza un modelo bilineal donde la información original contenida en las variables independientes (datos de reflectancia para cada λ) es proyectada sobre un pequeño número de variables subyacentes o latentes, llamadas componentes PLS. Los datos de la variable dependiente (β-carotenos en este caso) pueden ser entonces obtenidos desde estas variables latentes, en un proceso de regresión multivariante a partir del espectro de reflectancia. EL PLS-R es un procedimiento ampliamente utilizado en espectroscopía para aplicaciones quimiométricas (Esbensen, 2004; Westerhaus et al., 2004). Para la obtención de los modelos multivariantes se han utilizado, en todos los casos, los valores medios de los tres espectros tomados para cada genotipo.

Tras la aplicación del primer modelo de predicción, el análisis de los valores de la varianza residual permitió establecer que el número de componentes principales (CPs) que mejor explicaba la variación de los datos era de 6 CPs, por lo que se adoptó este valor para el modelo siguiente. Una vez ajustada la PLS-R, la proyección de los valores de las Y-observadas sobre los valores de las Y-calculadas, demostró la existencia de dos datos fuera de rango (*outliers*), que fueron removidos por el programa para calcular un tercer modelo (BETMOD3) cuyos resultados se presentan en la Tabla. Se comprueba que el modelo es capaz de predecir el contenido en ß-carotenos de la harina de los tres cereales a partir de los datos espectrorradiométricos con una seguridad bastante elevada, tal como indican los coeficientes de correlación y determinación, que explican el 98.1% de la variación en ß-carotenos a partir de la huella espectral. Asimismo, el valor de la raíz del cuadrado medio del error de calibración (RMSEC, *Root Mean Square Errof of Calibration*) indica que la precisión del modelo obtenido es de ±1.206 ppm.

Modelo	**BETMOD3**
Analito	ß-carotenos
Elementos	22
Ecuación	ß-carotenos = 0.246 + 0.981 λ
Coeficiente de correlación (r)	0.990 ***
Coeficiente de determinación (R^2)	0.981 (98.1%)
RMSEC	1.206

Puede concluirse, por tanto, que el contenido de ß-carotenos en la harina de estos cereales puede predecirse de una manera rápida, fiable y económica mediante reflectancia espectral, permitiendo su determinación en un gran número de muestras, tal como se requiere en los programas de mejora genética de la calidad en cereales.

Referencias

Cámara, M. 2006. Calidad nutricional y salud. En: *Mejora genética de la calidad en plantas*, G.. Yacer, M.J. Díez, J.M. Carrillo y M.L. Badenes (eds.), Universidad Politécnica de Valencia, pp. 45-65.

Carrillo, J.M.; Vázquez, J.F.; Rodríguez de Quijano, Marta: Ruzi, M. 2006. Mejora de la calidad del trigo. En: *Mejora genética de la calidad en plantas*, G.. Yacer, M.J. Díez, J.M. Carrillo y M.L. Badenes (eds.), Universidad Politécnica de Valencia, pp. 129-164.

Esbensen, K.H. 2004. Multivariate Data Analysis in practice (5th Edition). CAMO Process AS, Oslo.

Gooding, M.J., Davies, W.P., 1997. Wheat Production and Utilization: Systems, Quality and the Environment. CAB International, Wallingford, UK.

Westerhaus, M., Workman, J., Reeves, J.B., Mark, H. 2004. Quantitative analysis. In: *Near-Infrared Spectroscopy in Agriculture*. Roberts, C.A., Workman, J., Reeves, J.B. (eds.), American Society of Agronomy, Madison, Wisconsin, pp. 133-174.

Caracterización espectral de coberturas de vegetación en Costa Rica: misiones aerotransportadas y radiometría de campo

Javier Bonatti ([1]), Maynor Alfaro ([1]), Elena Listo ([2]), Juan Gregorio Rejas ([2]) y Miguel Marchamalo ([2])

([1]) Centro de Investigación en Ciencias Atómicas, Nucleares y Moleculares (CICANUM) la Universidad de Costa Rica
([2]) Laboratorio de Topografía y Geomática. Universidad Politécnica de Madrid

Resumen

Las imágenes aerotransportadas y satelitales son una herramienta importante pues brindan datos espectrales muy valiosos sobre las cubiertas vegetales, facilitando la detección de anomalías presentes en suelos y vegetación (Barret y Curtis, 1992). La utilización de sensores hiperespectrales permite identificar parámetros críticos de la vegetación y de los suelos, que no serían apreciables con los sensores espectrales como Thematic Mapper (TM) y Multispectral Scanner (MSS) de Landsat ó High Resolution Visible (HRV) de SPOT. De igual forma la utilización de sensores hiperespectrales permiten determinar y diferenciar aspectos de la vegetación como son su estado fenológico (Chen *et al*., 1998), estructura de la vegetación (Ustin y Trabucco, 2000), contenido de humedad (Serrano *et al*., 2000, Riaño *et al*., 1999) y cantidad de clorofila (Zarco Tejada *et al*., 2000 y 2001). El presente trabajo confirma la aplicabilidad de la teledetección para la determinación de características espectrales de bosques naturales, plantaciones forestales de teca, pastos y cultivos de musáceas (plátano y banano), por medio de espectroradiometría de campo, en el Pacífico de Costa Rica. Los trabajos fueron realizados con un espectroradiómetro en visible e IRC diseñado por el investigador principal con componentes disponibles en el mercado. Este trabajo forma parte del proyecto "Mejora de la eficiencia de captación y recarga de los sistemas de abastecimiento de agua mediante ordenamiento de los usos de la tierra en Centroamérica" que realizan en conjunto la UCR y la UPM con apoyo de la Agencia Española de Cooperación Internacional para el Desarrollo (PCI-AECID)

1. Objetivos

Objetivo general

Presentar el estado actual de la teledetección en Costa Rica y las aplicaciones más reseñables en estudios ambientales y agronómicos con radiometría de campo.

Objetivos específicos

1. Presentar las misiones aeroportadas realizadas en Costa Rica.
2. Presentar el trabajo de radiometría de campo realizado en Costa Rica en cultivos agronómicos y coberturas naturales
3. Contrastar la respuesta espectral de los cultivos con la respuesta espectral de cultivos afectados con enfermedades o plagas
4. Comparar la respuesta espectral de los cultivos, de las muestras tomadas en el campo, con la respuesta espectral de los cultivos en la imagen hiperespectral, Hymap

2. Conclusiones

En términos generales con el trabajo realizado y los resultados obtenidos se confirma que la teledetección es una herramienta muy poderosa para poder determinar propiedades y discriminar espectralmente los cultivos de Musáceas así como detectar deficiencias en ellos.

Por medio de esta técnica podemos discernir plantas con estrés, como es el caso de las afectadas por la enfermedad de Sigatoka Negra.

Se ha puesto de manifiesto la utilidad de discriminar especies, como en el caso de las Musáceas, con las imágenes Hymap, gracias a que éstas tienen gran resolución espectral. El espectroradiometro utilizado no abarca las longitudes de onda mayores a los 1000nm, disponibles con las imágenes Hymap (hasta 2500 nm) y quizás en estas longitudes de onda es donde mejor podemos discriminar espectralmente las coberturas vegetales. Esto queda claro al observar los datos de reflectancia tomados de la imagen, ya que en la banda IRC es donde mayor diferencias espectrales se detectan entre las plantas de plátano y banano.

Por otro lado es recomendable realizar estudios más a fondo para determinar por qué una planta en ciertas condiciones presenta mayor o menor reflectancia que otras de la misma especie.

También se recomienda realizar mediciones en diferentes épocas del año, periodo seco y periodo lluvioso, para medir el déficit, ganancia y exceso de humedad, ya que esto indudablemente incidirá en la respuesta espectral de las plantas.

NOTAS: